

F/G 20/3

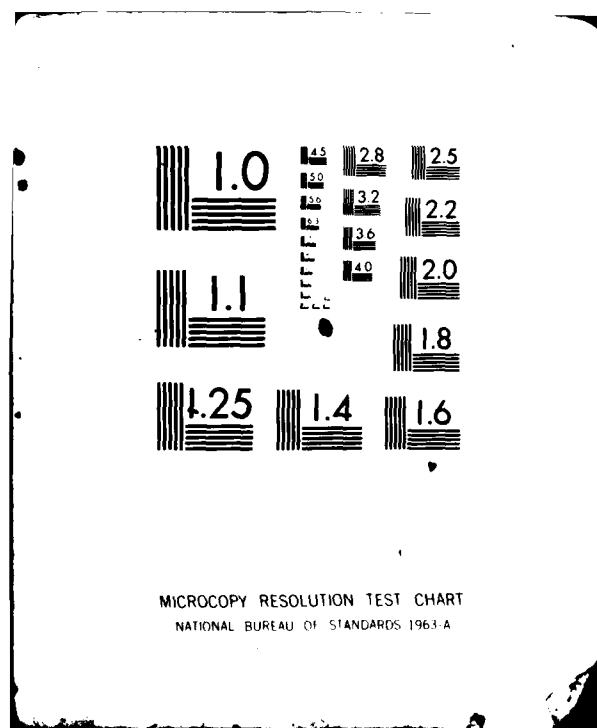
MAXIMAL EW FILE-ETC(07
F29601-70-C-0002

AFWL-TR-81-127

NL

1.2

1995, 1996, 1997, 1998, 1999, 2000, 2001, 2002, 2003, 2004, 2005, 2006, 2007, 2008, 2009, 2010, 2011, 2012, 2013, 2014, 2015, 2016, 2017, 2018, 2019, 2020, 2021, 2022, 2023, 2024, 2025, 2026, 2027, 2028, 2029, 2030, 2031, 2032, 2033, 2034, 2035, 2036, 2037, 2038, 2039, 2040, 2041, 2042, 2043, 2044, 2045, 2046, 2047, 2048, 2049, 2050, 2051, 2052, 2053, 2054, 2055, 2056, 2057, 2058, 2059, 2060, 2061, 2062, 2063, 2064, 2065, 2066, 2067, 2068, 2069, 2070, 2071, 2072, 2073, 2074, 2075, 2076, 2077, 2078, 2079, 2080, 2081, 2082, 2083, 2084, 2085, 2086, 2087, 2088, 2089, 2090, 2091, 2092, 2093, 2094, 2095, 2096, 2097, 2098, 2099, 2100, 2101, 2102, 2103, 2104, 2105, 2106, 2107, 2108, 2109, 2110, 2111, 2112, 2113, 2114, 2115, 2116, 2117, 2118, 2119, 2120, 2121, 2122, 2123, 2124, 2125, 2126, 2127, 2128, 2129, 2130, 2131, 2132, 2133, 2134, 2135, 2136, 2137, 2138, 2139, 2140, 2141, 2142, 2143, 2144, 2145, 2146, 2147, 2148, 2149, 2150, 2151, 2152, 2153, 2154, 2155, 2156, 2157, 2158, 2159, 2160, 2161, 2162, 2163, 2164, 2165, 2166, 2167, 2168, 2169, 2170, 2171, 2172, 2173, 2174, 2175, 2176, 2177, 2178, 2179, 2180, 2181, 2182, 2183, 2184, 2185, 2186, 2187, 2188, 2189, 2190, 2191, 2192, 2193, 2194, 2195, 2196, 2197, 2198, 2199, 2200, 2201, 2202, 2203, 2204, 2205, 2206, 2207, 2208, 2209, 2210, 2211, 2212, 2213, 2214, 2215, 2216, 2217, 2218, 2219, 2220, 2221, 2222, 2223, 2224, 2225, 2226, 2227, 2228, 2229, 2230, 2231, 2232, 2233, 2234, 2235, 2236, 2237, 2238, 2239, 2240, 2241, 2242, 2243, 2244, 2245, 2246, 2247, 2248, 2249, 2250, 2251, 2252, 2253, 2254, 2255, 2256, 2257, 2258, 2259, 2260, 2261, 2262, 2263, 2264, 2265, 2266, 2267, 2268, 2269, 2270, 2271, 2272, 2273, 2274, 2275, 2276, 2277, 2278, 2279, 2280, 2281, 2282, 2283, 2284, 2285, 2286, 2287, 2288, 2289, 2290, 2291, 2292, 2293, 2294, 2295, 2296, 2297, 2298, 2299, 2300, 2301, 2302, 2303, 2304, 2305, 2306, 2307, 2308, 2309, 2310, 2311, 2312, 2313, 2314, 2315, 2316, 2317, 2318, 2319, 2320, 2321, 2322, 2323, 2324, 2325, 2326, 2327, 2328, 2329, 2330, 2331, 2332, 2333, 2334, 2335, 2336, 2337, 2338, 2339, 2340, 2341, 2342, 2343, 2344, 2345, 2346, 2347, 2348, 2349, 2350, 2351, 2352, 2353, 2354, 2355, 2356, 2357, 2358, 2359, 2360, 2361, 2362, 2363, 2364, 2365, 2366, 2367, 2368, 2369, 2370, 2371, 2372, 2373, 2374, 2375, 2376, 2377, 2378, 2379, 2380, 2381, 2382, 2383, 2384, 2385, 2386, 2387, 2388, 2389, 2390, 2391, 2392, 2393, 2394, 2395, 2396, 2397, 2398, 2399, 2400, 2401, 2402, 2403, 2404, 2405, 2406, 2407, 2408, 2409, 2410, 2411, 2412, 2413, 2414, 2415, 2416, 2417, 2418, 2419, 2420, 2421, 2422, 2423, 2424, 2425, 2426, 2427, 2428, 2429, 2430, 2431, 2432, 2433, 2434, 2435, 2436, 2437, 2438, 2439, 2440, 2441, 2442, 2443, 2444, 2445, 2446, 2447, 2448, 2449, 2450, 2451, 2452, 2453, 2454, 2455, 2456, 2457, 2458, 2459, 2460, 2461, 2462, 2463, 2464, 2465, 2466, 2467, 2468, 2469, 2470, 2471, 2472, 2473, 2474, 2475, 2476, 2477, 2478, 2479, 2480, 2481, 2482, 2483, 2484, 2485, 2486, 2487, 2488, 2489, 2490, 2491, 2492, 2493, 2494, 2495, 2496, 2497, 2498, 2499, 2500, 2501, 2502, 2503, 2504, 2505, 2506, 2507, 2508, 2509, 2510, 2511, 2512, 2513, 2514, 2515, 2516, 2517, 2518, 2519, 2520, 2521, 2522, 2523, 2524, 2525, 2526, 2527, 2528, 2529, 2530, 2531, 2532, 2533, 2534, 2535, 2536, 2537, 2538, 2539, 2540, 2541, 2542, 2543, 2544, 2545, 2546, 2547, 2548, 2549, 2550, 2551, 2552, 2553, 2554, 2555, 2556, 2557, 2558, 2559, 2560, 2561, 2562, 2563, 2564, 2565, 2566, 2567, 2568, 2569, 2570, 2571, 2572, 2573, 2574, 2575, 2576, 2577, 2578, 2579, 2580, 2581, 2582, 2583, 2584, 2585, 2586, 2587, 2588, 2589, 2590, 2591, 2592, 2593, 2594, 2595, 2596, 2597, 2598, 2599, 2600, 2601, 2602, 2603, 2604, 2605, 2606, 2607, 2608, 2609, 2610, 2611, 2612, 2613, 2614, 2615, 2616, 2617, 2618, 2619, 2620, 2621, 2622, 2623, 2624, 2625, 2626, 2627, 2628, 2629, 2630, 2631, 2632, 2633, 2634, 2635, 2636, 2637, 2638, 2639, 2640, 2641, 2642, 2643, 2644, 2645, 2646, 2647, 2648, 2649, 2650, 2651, 2652, 2653, 2654, 2655, 2656, 2657, 2658, 2659, 2660, 2661, 2662, 2663, 2664, 2665, 2666, 2667, 2668, 2669, 2670, 2671, 2672, 2673, 2674, 2675, 2676, 26



2

AFWL-TR-81-127

AFWL-TR-
81-127

AD A115187



OPTIMAL APPLICATION OF MULTILAYER SHIELDING FOR MAXIMAL EM FIELD ATTENUATION

F. C. Yang
K. S. H. Lee

Mission Research Corporation
1400 San Mateo Blvd., NE
Albuquerque, NM 87108

April 1982

Final Report

Approved for public release; distribution unlimited.

SUBJECT TO EXPORT CONTROL LAWS: This document contains information for manufacturing or using munitions of war. Exporting this information or releasing it to foreign nationals living in the United States without first obtaining an export license violates the International Traffic in Arms Regulations. Under 22 USC 2778, such a violation is punishable by up to 2 years in prison and by a fine of \$100,000.

AIR FORCE WEAPONS LABORATORY
Air Force Systems Command
Kirtland Air Force Base, NM 87117

DTIC
ELECTE
JUN 7 1982
S B D

DTIC FILE COPY

82 06 07 913

This final report was prepared by the Mission Research Corporation, Albuquerque, New Mexico, under Contract F29601-78-C-0082, Job Order 37630132 with the Air Force Weapons Laboratory, Kirtland Air Force Base, New Mexico. Mr. William S. Kehrer (NTYE) was the Laboratory Project Officer-in-Charge.

When Government drawings, specifications, or other data are used for any purpose other than in connection with a definitely Government-related procurement, the United States Government incurs no responsibility or any obligation whatsoever. The fact that the Government may have formulated or in any way supplied the said drawings, specifications, or other data, is not to be regarded by implication, or otherwise in any manner construed, as licensing the holder, or any other person or corporation; or as conveying any rights or permission to manufacture, use, or sell any patented invention that may in any way be related thereto.

This report has been authored by a contractor of the United States Government. Accordingly, the United States Government retains a nonexclusive, royalty-free license to publish or reproduce the material contained herein, or allow others to do so, for the United States Government purposes.

This report has been reviewed by the Public Affairs Office and is releasable to the National Technical Information Service (NTIS). At NTIS, it will be available to the general public, including foreign nations.

If your address has changed, if you wish to be removed from our mailing list, or if your organization no longer employs the addressee, please notify AFWL/NTYE, Kirtland AFB, NM 87117 to help us maintain a current mailing list.

This technical report has been reviewed and is approved for publication.

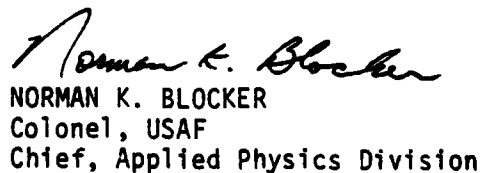


WILLIAM S. KEHRER
Project Officer



J. PHILIP CASTILLO
Chief, Electromagnetics Branch

FOR THE COMMANDER



NORMAN K. BLOCKER
Colonel, USAF
Chief, Applied Physics Division

DO NOT RETURN COPIES OF THIS REPORT UNLESS CONTRACTUAL OBLIGATIONS OR NOTICE ON A SPECIFIC DOCUMENT REQUIRES THAT IT BE RETURNED.

UNCLASSIFIED

SECURITY CLASSIFICATION OF THIS PAGE (When Data Entered)

REPORT DOCUMENTATION PAGE		READ INSTRUCTIONS BEFORE COMPLETING FORM
1. REPORT NUMBER AFWL-TR-81-127	2. GOVT ACCESSION NO. AD-A115187	3. RECIPIENT'S CATALOG NUMBER
4. TITLE (and Subtitle) OPTIMAL APPLICATION OF MULTILAYER SHIELDING FOR MAXIMAL EM FIELD ATTENUATION		5. TYPE OF REPORT & PERIOD COVERED Final Report
		6. PERFORMING ORG. REPORT NUMBER
7. AUTHOR(s) *F. C. Yang (Part I) *K. S. H. Lee (Part II)		8. CONTRACT OR GRANT NUMBER(s) F29601-78-C-0082
9. PERFORMING ORGANIZATION NAME AND ADDRESS Mission Research Corporation 1400 San Mateo Blvd., NE Albuquerque, NM 87108		10. PROGRAM ELEMENT, PROJECT, TASK AREA & WORK UNIT NUMBERS 64711F/37630132
11. CONTROLLING OFFICE NAME AND ADDRESS Air Force Weapons Laboratory (NTYE) Kirtland Air Force Base, NM 87117		12. REPORT DATE April 1982
		13. NUMBER OF PAGES 110
14. MONITORING AGENCY NAME & ADDRESS (if different from Controlling Office)		15. SECURITY CLASS. (of this report) Unclassified
		15a. DECLASSIFICATION DOWNGRADING SCHEDULE
16. DISTRIBUTION STATEMENT (of this Report) Approved for public release; distribution unlimited.		
17. DISTRIBUTION STATEMENT (of the abstract entered in Block 20, if different from Report)		
18. SUPPLEMENTARY NOTES *Dikewood Corporation		
19. KEY WORDS (Continue on reverse side if necessary and identify by block number) Cable Shields Electromagnetic Shielding Periodic Bonding Shielding Topology Multisurface Enclosures Bonding Straps		
20. ABSTRACT (Continue on reverse side if necessary and identify by block number) A two-surface cable shield with periodic bondings and with either discrete or distributed excitation is analyzed. It is found that the bondings improve the overall shielding effectiveness of the cable shield at certain frequencies, but degrade the shielding at others. Certain criteria are established for better shielding. In the case of distributed excitation, the overall effective transfer functions of a two-surface cable shield can be calculated from simple (Over)		

DD FORM 1473
1 JAN 73

EDITION OF 1 NOV 65 IS OBSOLETE

UNCLASSIFIED

SECURITY CLASSIFICATION OF THIS PAGE (When Data Entered)

UNCLASSIFIED

SECURITY CLASSIFICATION OF THIS PAGE(When Data Entered)

20. ABSTRACT (Continued)

circuits. These circuits can be extended for multisurface cable shields. Part II extends the previous work on a single-surface shielded enclosure of arbitrary shape to a multisurface enclosure with or without electrical bonding between the shields. It is found that the inductive mutual interactions among the shields and the bonding straps reduce the effectiveness of a multisurface shielded enclosure against the penetration of external magnetic fields.

UNCLASSIFIED

SECURITY CLASSIFICATION OF THIS PAGE(When Data Entered)

CONTENTS

<u>Part</u>		<u>Page</u>
I	CABLE SHIELDS WITH PERIODIC BONDINGS	2
II	MULTISURFACE SHIELDED ENCLOSURES WITH PARTICULAR REFERENCE TO BONDING BETWEEN SHIELDS	65



Accession For		
NTIS GRA&I	<input checked="" type="checkbox"/>	
DTIC TAB	<input type="checkbox"/>	
Unannounced	<input type="checkbox"/>	
Justification		
By		
Distribution/		
Availability Codes		
Dist	Avail and/or	
A	Special	

PART I

CABLE SHIELDS WITH PERIODIC BONDINGS

PREFACE

The author would like to thank Dr. K.S.H. Lee of The Dikewood Corporation, Dr. C.E. Baum and Mr. W. Kehrler of the Air Force Weapons Laboratory (AFWL) for helpful discussions and suggestions, and Mr. V. Tatoian of Dikewood for numerical computations.

CONTENTS

<u>Section</u>	<u>Page</u>
I INTRODUCTION	9
II DISCRETE EXCITATIONS	12
1. VOLTAGE SOURCE	20
2. CURRENT SOURCE	23
III DISTRIBUTED EXCITATIONS	32
1. SCHELKUNOFF'S CIRCUIT	32
2. CASEY'S CIRCUIT	36
3. GENERAL FORMUALTION	39
IV SUMMARY	56
1. DISCRETE EXCITATIONS	56
2. DISTRIBUTED EXCITATIONS	59
REFERENCES	63

TABLES

<u>Table</u>	<u>Page</u>
1 EXAMPLES OF BONDED COAXIAL-CABLE SHIELDS	59

ILLUSTRATIONS

<u>Figure</u>		<u>Page</u>
1	Discretely excited cable shields with periodic bondings.	10
2	Distributedly excited cable shields with periodic bondings.	11
3	Transmission-line models for discretely excited cable shields with periodic bondings.	13
4	The decomposition of the problem depicted in Figure 3a.	14
5	The resultant transmission-line problem to be solved after decomposition.	15
6	The dispersion relations between ω and k for periodically bonded transmission lines with various $q_S = Z_1' Y_d d$.	17
7	The decaying constants of bonded transmission lines versus frequency for various $q_S = Z_1' Y_d d$.	18
8	Normalized $ \bar{Z}_{TV}' $ (normalized to their values when the cable shields are not bonded) when $z_0 = 0$ versus frequencies for various $q_S = Z_1' Y_d d$.	24
9	Normalized $ \bar{\Omega}_{TV}' $ when $z_0 = 0$ versus frequencies for various $q_S = Z_1' Y_d d$.	25
10	Normalized $ \bar{Z}_{TV}' $ when $z_0 = d/2$ versus frequencies for various $q_S = Z_1' Y_d d$.	26
11	Normalized $ \bar{\Omega}_{TV}' $ when $z_0 = d/2$ versus frequencies for various $q_S = Z_1' Y_d d$.	27
12	Normalized $ \bar{Z}_{TI}' $ when $z_0 = d/2$ versus frequencies for various $q_S = Z_1' Y_d d$.	30
13	Normalized $ \bar{\Omega}_{TI}' $ when $z_0 = d/2$ versus frequencies for various $q_S = Z_1' Y_d d$.	31
14	A theoretical model for a distributed excited double shield with periodic bondings.	33

ILLUSTRATIONS (CONTINUED)

<u>Figure</u>		<u>Page</u>
15	Schelkunoff's circuit for the calculation of Z_T' of a solid tubular double shield with or without periodic bondings.	34
16	Casey's circuit for the calculations of Z_T' and Ω_T of a double shield without periodic bonding.	37
17	Generalized Casey's circuit (constraints $\delta_i \gg \Delta_i$ in Casey's circuit are lifted) for the calculations of Z_T' and Ω_T of a double shield without periodic bonding.	40
18	Normalized \bar{Z}_T' and $\bar{\Omega}_T$ (normalized to their values when the cable shields are not bonded), based on the general Equation 52 and the approximated Equation 43, versus frequencies for $q_S = Z_{cl}' Y_d = 0.1$, $q_Y = Y_{cl}' / Y_{T1}' = 0.004$ and $q_Z = Z_{T1}' / Z_{cl}' = 0.01$.	43
19	Normalized \bar{Z}_T' and $\bar{\Omega}_T$ (normalized to their values when the cable shields are not bonded), based on the general Equation 52 and the approximated Equation 43, versus frequencies for $q_S = Z_{cl}' Y_d = 0.5$, $q_Y = Y_{cl}' / Y_{T1}' = 0.004$ and $q_Z = Z_{T1}' / Z_{cl}' = 0.01$.	44
20	Normalized \bar{Z}_T' and $\bar{\Omega}_T$ (normalized to their values when the cable shields are not bonded), based on the general Equation 52 and the approximated Equation 43, versus frequencies for $q_S = Z_{cl}' Y_d = 1$, $q_Y = Y_{cl}' / Y_{T1}' = 0.004$ and $q_Z = Z_{T1}' / Z_{cl}' = 0.01$.	45
21	Normalized \bar{Z}_T' and $\bar{\Omega}_T$ (normalized to their values when the cable shields are not bonded), based on the general Equation 52 and the approximated Equation 43, versus frequencies for $q_S = Z_{cl}' Y_d = 2$, $q_Y = Y_{cl}' / Y_{T1}' = 0.004$ and $q_Z = Z_{T1}' / Z_{cl}' = 0.01$.	46

ILLUSTRATIONS (CONTINUED)

Figure		Page
22	Normalized \bar{Z}'_T and $\bar{\Omega}'_T$ (normalized to their values when the cable shields are not bonded), based on the general Equation 52 and the approximated Equation 43, versus frequencies for $q_S = Z'_{c1} Y_d d = 0.1$, $q_Y = Y'_{c1} / Y'_{T1} = 0.001$ and $q_Z = Z'_{T1} / Z'_{c1} = 0.002$.	47
23	Normalized \bar{Z}'_T and $\bar{\Omega}'_T$ (normalized to their values when the cable shields are not bonded), based on the general Equation 52 and the approximated Equation 43, versus frequencies for $q_S = Z'_{c1} Y_d d = 0.5$, $q_Y = Y'_{c1} / Y'_{T1} = 0.001$ and $q_Z = Z'_{T1} / Z'_{c1} = 0.002$.	48
24	Normalized \bar{Z}'_T and $\bar{\Omega}'_T$ (normalized to their values when the cable shields are not bonded), based on the general Equation 52 and the approximated Equation 43, versus frequencies for $q_S = Z'_{c1} Y_d d = 1$, $q_Y = Y'_{c1} / Y'_{T1} = 0.001$ and $q_Z = Z'_{T1} / Z'_{c1} = 0.002$.	49
25	Normalized \bar{Z}'_T and $\bar{\Omega}'_T$ (normalized to their values when the cable shields are not bonded), based on the general Equation 52 and the approximated Equation 43, versus frequencies for $q_S = Z'_{c1} Y_d d = 2$, $q_Y = Y'_{c1} / Y'_{T1} = 0.001$ and $q_Z = Z'_{T1} / Z'_{c1} = 0.002$.	50
26	The general circuit for the calculations of \bar{Z}'_T and $\bar{\Omega}'_T$ of a double shield with periodic bondings.	52
27	The values of "q", to be used in the circuit of Figure 26, versus frequencies for $q_Y = Y'_{c1} / Y'_{T1} = 0.004$, $q_Z = Z'_{T1} / Z'_{c1} = 0.01$ and various $q_S = Z'_{c1} Y_d d$.	53
28	The values of "q", to be used in the circuit of Figure 26, versus frequencies for $q_Y = Y'_{c1} / Y'_{T1} = 0.001$, $q_Z = Z'_{T1} / Z'_{c1} = 0.002$ and various $q_S = Z'_{c1} Y_d d$.	54

I. INTRODUCTION

Cable shields and cable conduits have been widely used as part of the integrated electromagnetic pulse (EMP) hardening design for aircraft, missiles, and ground-based systems (Ref. 1). When cable shields are used over a long distance, they are generally periodically grounded to their immediate outer shield through bonding straps, clamps, screws, etc. The periodic grounding provides mechanical rigidity of the shields, reduces the electrostatic hazards, and at the same time might increase the shielding effectiveness against penetration of long-wavelength disturbances. However, for the broad-band EMP, the question arises whether the periodic grounding will improve or degrade the overall shielding effectiveness. In this report, this question will be answered from a rigorous theoretical analysis. The analytical results will help the system engineers to determine the optimum grounding arrangement.

Cable shields generally are not perfect. EMP can penetrate either locally (such as through an aperture, a connector, or one end of the shield, see Fig. 1) or distributedly (such as through diffusion or uniformly distributed apertures, see Fig. 2). These two distinct cases will be separately discussed: discrete excitations in Section II and distributed excitations in Section III. Finally, the results obtained in Sections II and III will be summarized in Section IV, and several practical engineering examples as to how the results can be used will be presented.

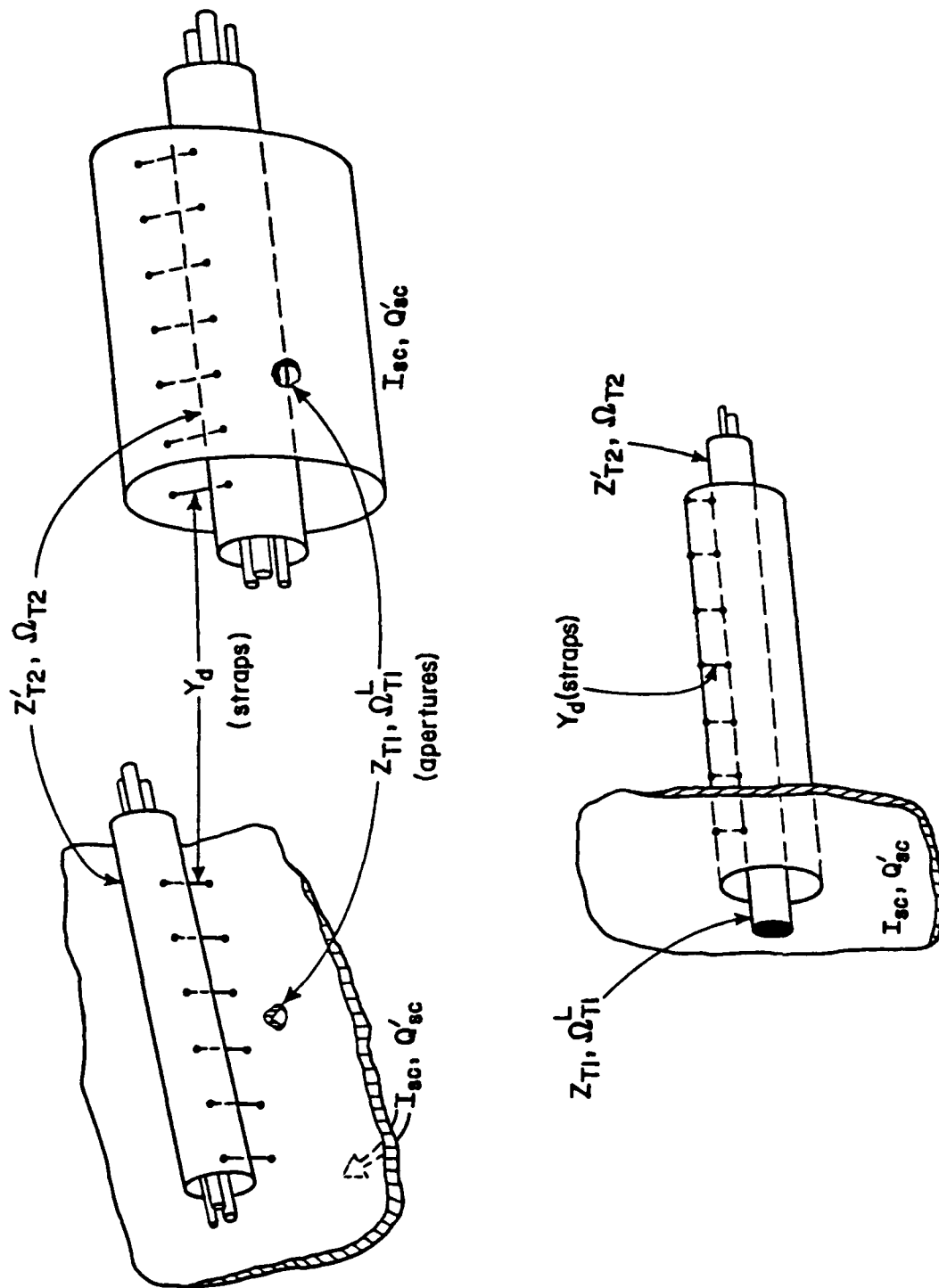


Figure 1. Discretely excited cable shields with periodic bondings.

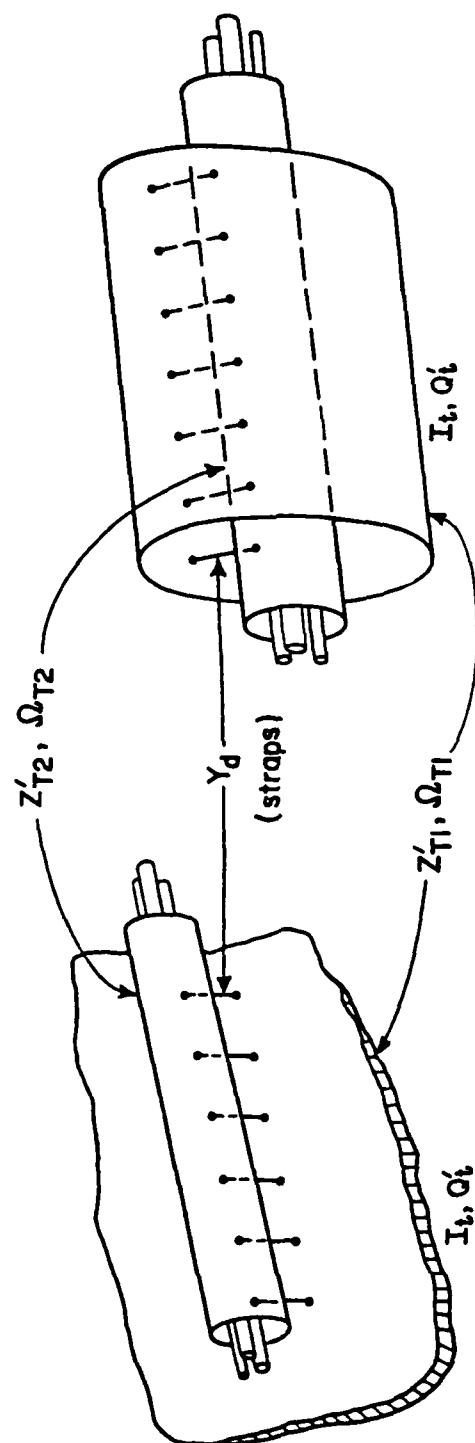


Figure 2. Distributedly excited cable shields with periodic bondings.

II. DISCRETE EXCITATIONS

In this section, the outer shield of a double-shield configuration on Figure 1 is assumed to be perfect, except at some isolated locations where the EMP can penetrate. The current and charge density distributions on the transmission line formed by the two shields due to the penetration from a localized location can be calculated by solving the problem depicted in Figure 3. The distributions due to the voltage and current sources of the localized penetration can be separately considered. The two problems of Figure 3a can be decomposed further (Fig. 4) so that only the problem shown in Figure 3b (which is redrawn as Fig. 5 with $V^s = V_1^s, V_2^s$ or V_0^s and $I^s = I_1^s, I_2^s$ or I_0^s) need be solved. The coupling to the wires inside the inner shield can then be calculated by multiplying the appropriate transfer impedance or charge transfer frequency of the inner shield by the current or charge density distributions. The time variation of $\exp(j\omega t)$ will be assumed and suppressed throughout this report.

At sufficiently low frequencies the TEM mode is dominant and the voltage (V) and current (I) distributions along the line shown in Figure 5 can be calculated by solving the following pair of equations:

$$\frac{dV}{dz} + Z'_1 I = 0 \quad (1)$$

$$\frac{dI}{dz} + \left[Y'_1 + Y_d \sum_{n=-\infty}^{\infty} \delta(z - nd) \right] V = 0, \quad \text{for } z \geq z_0 \quad (2)$$

where Z'_1 and Y'_1 are, respectively, the series impedance and shunt admittance per unit length of the line and Y_d is the admittance of each strap.

From Floquet's theorem, the solution of the periodic Equations 1 and 2 has the following form:

$$V(z) = \sum_{n=-\infty}^{\infty} V_n \exp[-j(k + 2n\pi/d)z] \quad (3)$$

$$I(z) = \sum_{n=-\infty}^{\infty} I_n \exp[-j(k + 2n\pi/d)z] \quad (4)$$

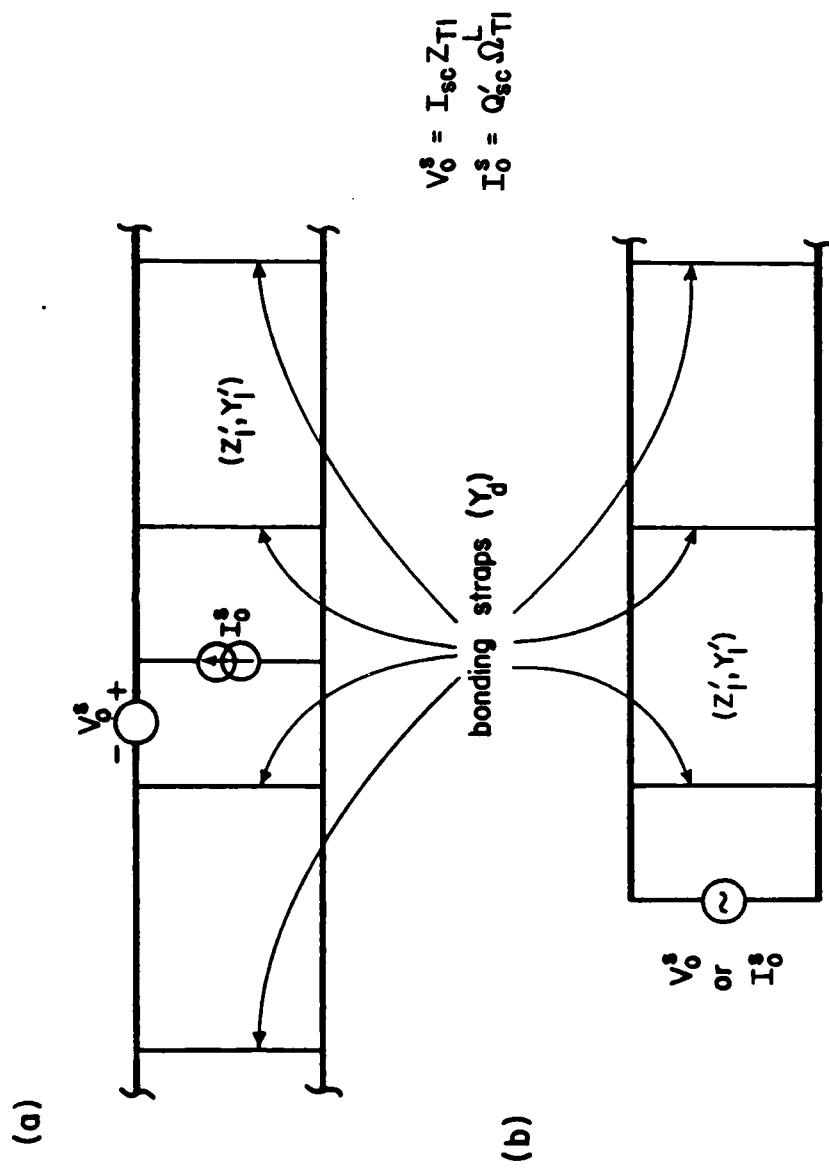
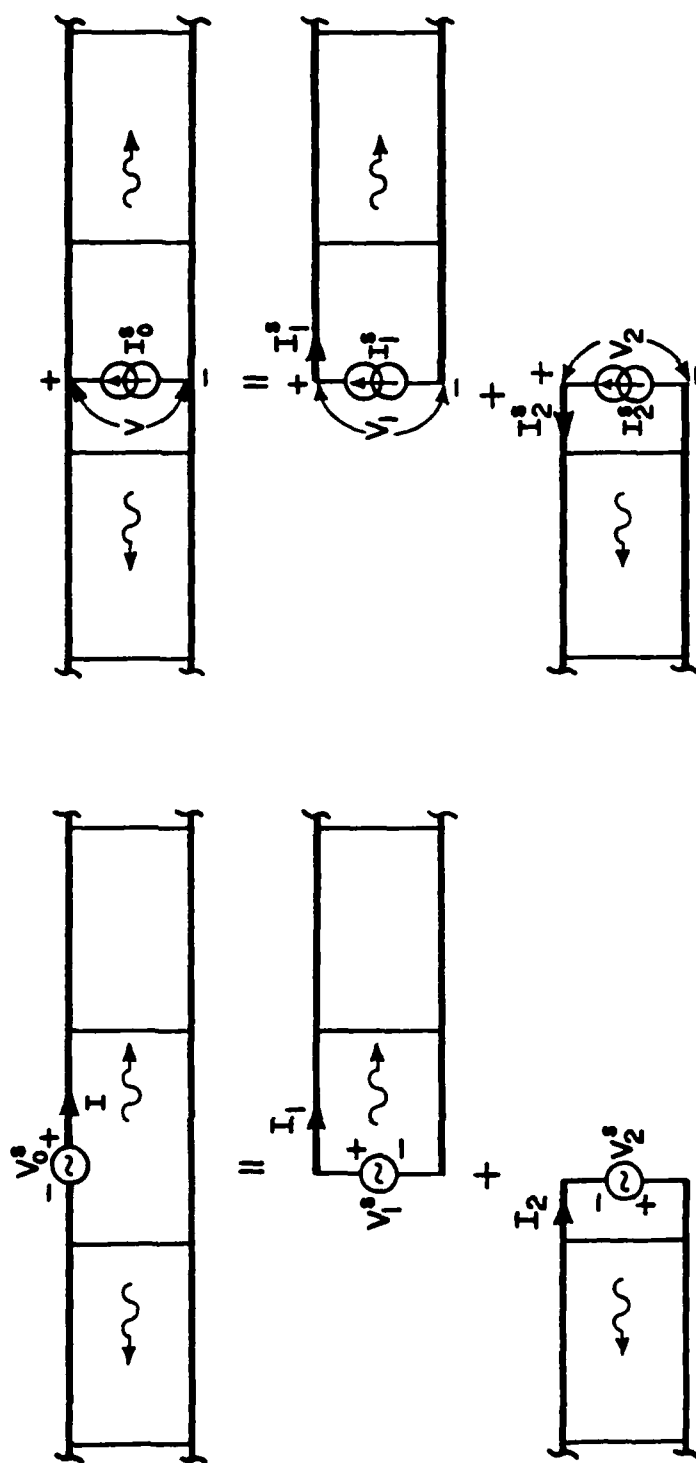


Figure 3. Transmission-line models for discretely excited cable shields with periodic bondings.



$$\begin{aligned} V_1^s + V_2^s &= V_0^s \\ I_1 &= I_2 = I \end{aligned} \quad (a)$$

$$\begin{aligned} I_1^s + I_2^s &= I_0^s \\ V_1 &= V_2 = V \end{aligned} \quad (b)$$

Figure 4. The decomposition of the problem depicted in Figure 3a.

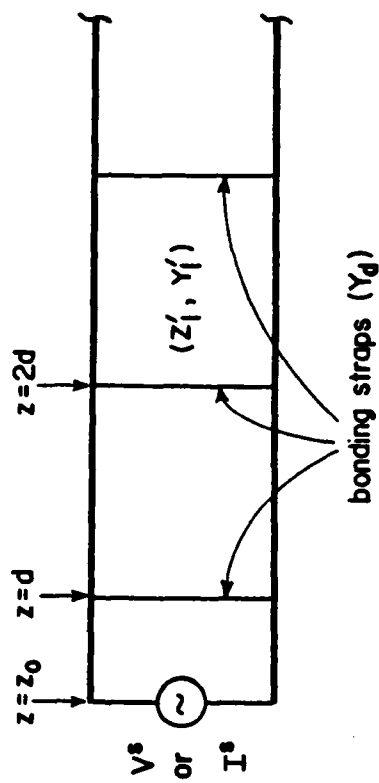


Figure 5. The resultant transmission-line problem to be solved after decomposition.

Substituting Equations 3 and 4 into Equations 1 and 2 one has

$$I_n = j V_n (k + 2n\pi/d) / Z'_1 \quad (5)$$

$$V_n = \frac{-Y'_d Z'_1}{Y'_1 Z'_1 + (k + 2n\pi/d)^2} \frac{V^0}{d} \quad (6)$$

where

$$V^0 = \sum_{n=-\infty}^{\infty} V_n \quad (7)$$

By combining Equations 6 and 7, one finds that the dispersion relation between k and $\sqrt{-Y'_1 Z'_1}$ is (also see Ref. 2)

$$\cos kd = \cos(d\sqrt{-Y'_1 Z'_1}) + \frac{Z'_1 Y'_d d}{2d\sqrt{-Y'_1 Z'_1}} \sin(d\sqrt{-Y'_1 Z'_1}) \quad (8)$$

In Figure 6, $\cos kd$ is plotted versus $d\sqrt{-Y'_1 Z'_1}$ ($\approx \omega d/c$) for various $q_s (= Z'_1 Y'_d d)$. (Generally, Z'_1 , Y'_1 and Y'_d are complex values. To have real and positive $d\sqrt{-Y'_1 Z'_1}$ and $Z'_1 Y'_d d$, one can assume $Z'_1 \approx Z'_{c1}$, $Y'_1 \approx Y'_{c1}$ and $Y'_d \approx (j\omega L_d)^{-1}$, where Z'_{c1} and Y'_{c1} are purely imaginary and are respectively the values of Z'_1 and Y'_1 of a perfect double shield, L_d is the inductance of each bonding strap). In the figure, one clearly sees the passband and stopband structures. The stopbands are generally broader for a larger q_s , especially at the lower $\omega d/c$ region. This is reasonable because a larger q_s means a better grounding. At the higher $\omega d/c$ region, the stopbands become narrower because the high-frequency disturbance does not see the presence of the bonding straps. Also, to have the proper propagation and decaying constants for $z \geq z_0$, one should restrict the k -value to have a positive real part and a negative imaginary part. The imaginary part of k determines how fast the disturbance decays when it propagates away from the penetration point. A plot of $|\text{Im}(kd)|$ versus frequency for various q_s is given in Figure 7. Figure 7 obviously shows that a larger q_s gives a larger $|\text{Im}(kd)|$ (which means

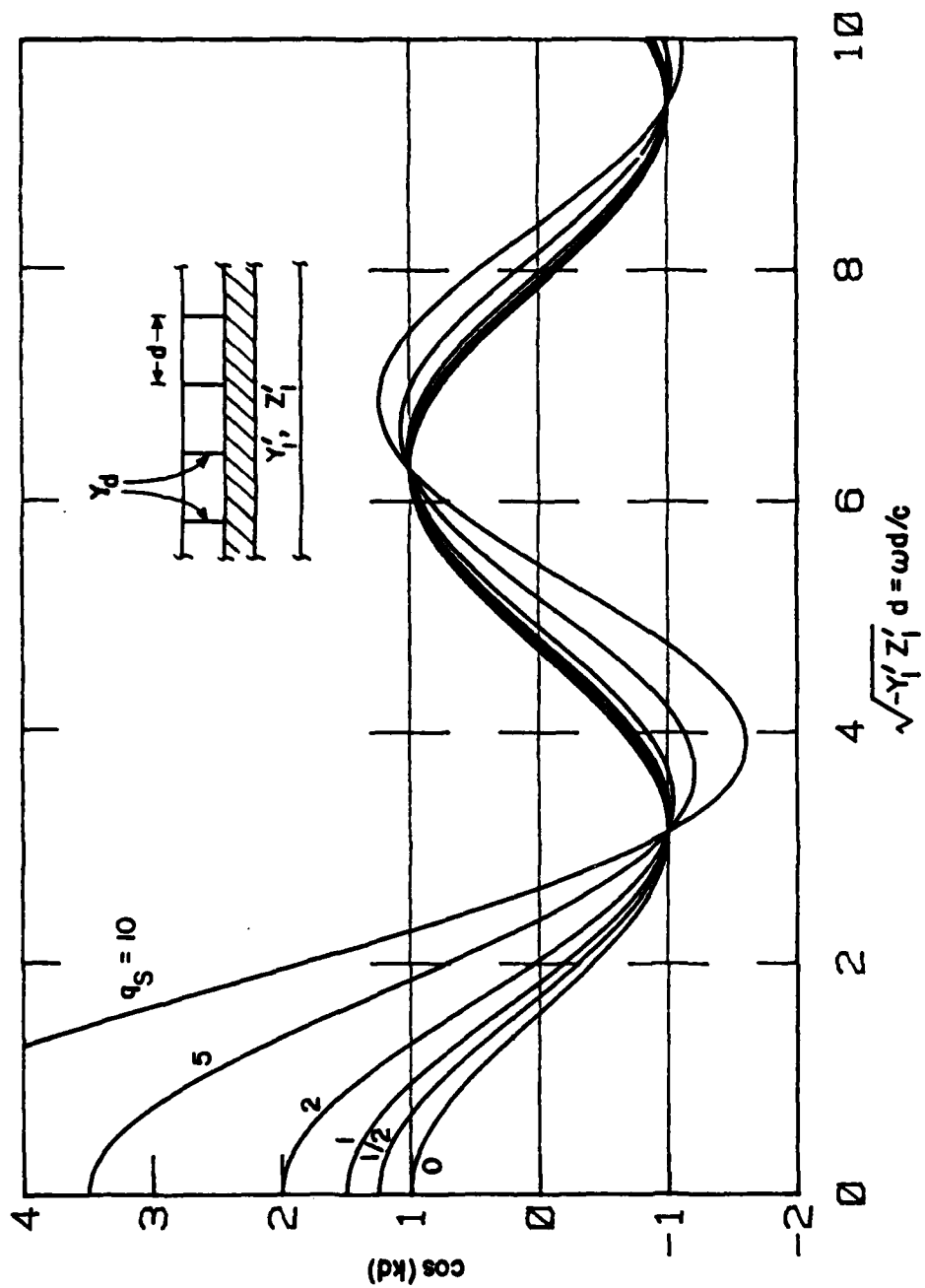


Figure 6. The dispersion relations between ω and k for periodically bonded transmission lines with various $q_S = Z_1' Y_d$.

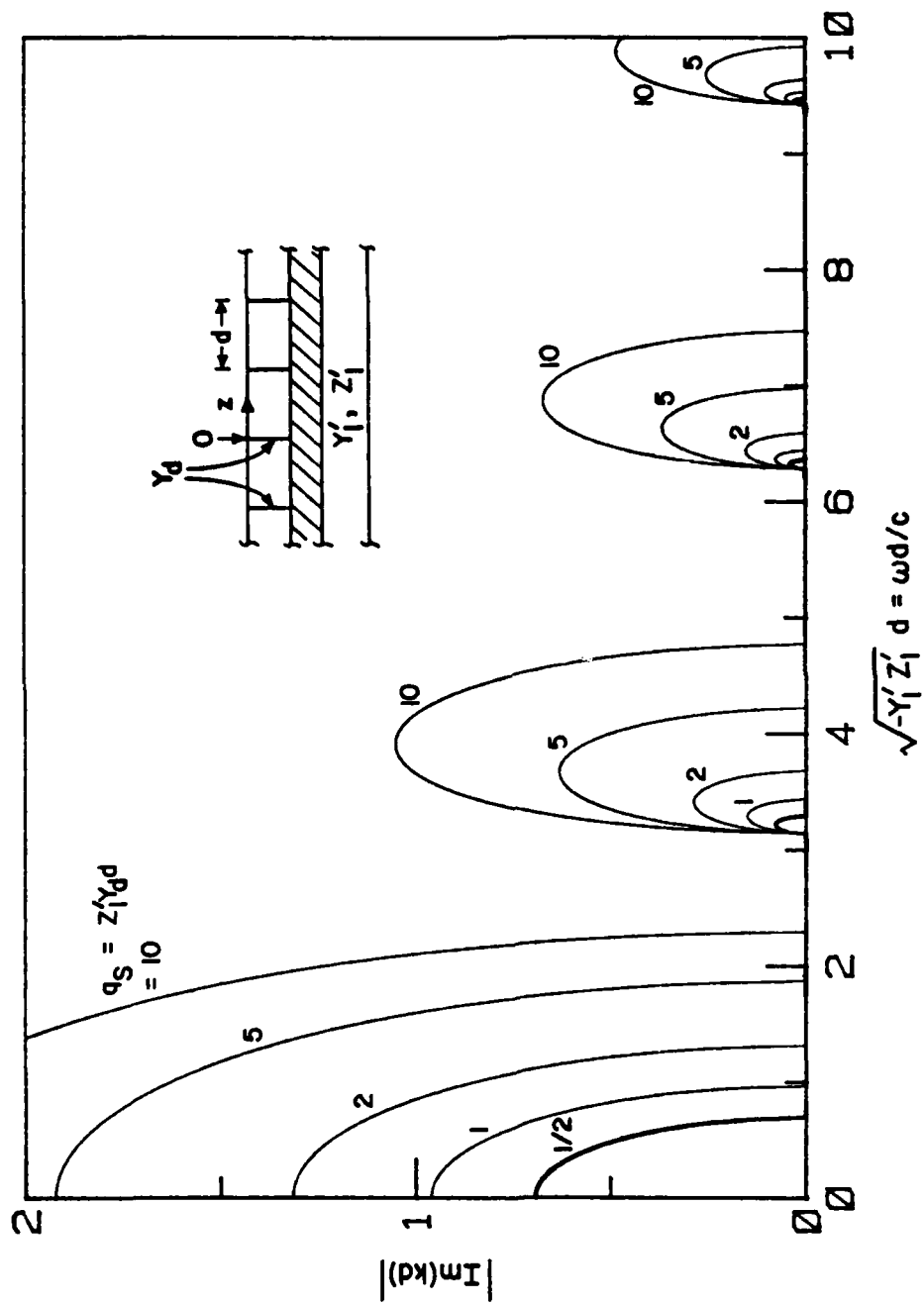


Figure 7. The decaying constants of bonded transmission lines versus frequency for various $q_S = Z'_1 Y_d d$.

that the disturbance decays faster) and thus, is more desirable. Actually, at the low-frequency limit where $\sqrt{-Y_1'Z_1'} d \approx \omega d/c \ll 1$, one can easily show that

$$|\operatorname{Im}(kd)| \approx \cosh^{-1}(1 + q_s/2) \quad (9)$$

$$\approx \cosh^{-1}[1 + L_1' d / (2L_d)] \quad (10)$$

where L_1' is the series inductance per unit length of the double shield.

Using Equations 5 and 6 in Equations 3 and 4, one has

$$\begin{aligned} V(z) &= V_0 \sum_{n=-\infty}^{\infty} \frac{(Y_1'Z_1' + k^2)}{Y_1'Z_1' + (k + 2n\pi/d)^2} e^{-j(k + 2n\pi/d)z} \\ &= \frac{-V_0 (Y_1'Z_1' + k^2) d^2}{Y_d Z_1' d} e^{-jkd(m+1/2)} \times \\ &\quad \times \left\{ \frac{\cos(kd/2) \cos \left[((m+1/2)d - z) \sqrt{-Y_1'Z_1'} \right]}{\cos(d\sqrt{-Y_1'Z_1'}/2)} \right. \\ &\quad \left. + j \frac{\sin(kd/2) \sin \left[((m+1/2)d - z) \sqrt{-Y_1'Z_1'} \right]}{\sin(d\sqrt{-Y_1'Z_1'}/2)} \right\} \quad (11) \\ &\quad \text{for } md \leq z < (m+1)d \end{aligned}$$

$$\begin{aligned} I(z) &= V_0 \sum_{n=-\infty}^{\infty} \frac{j(Y_1'Z_1' + k^2)}{Y_1'Z_1' + (k + 2n\pi/d)^2} \frac{k + 2n\pi/d}{Z_1'} e^{-j(k + 2n\pi/d)z} \\ &= \frac{-j V_0 d \sqrt{-Y_1'Z_1'} (k^2 + Y_1'Z_1') d^2}{(dY_d Z_1') Z_1' d} e^{-jkd(m+1/2)} \times \\ &\quad \times \left\{ \frac{\sin(kd/2) \cos \left[((m+1/2)d - z) \sqrt{-Y_1'Z_1'} \right]}{\sin(d\sqrt{-Y_1'Z_1'}/2)} \right\} \end{aligned}$$

$$\begin{aligned}
& + j \frac{\cos(kd/2) \sin \left[((m+1/2)d - z) \sqrt{-Y'_1 Z'_1} \right]}{\cos(d\sqrt{-Y'_1 Z'_1}/2)} \Bigg\} \quad (12) \\
& \text{for } md \leq z < (m+1)d \\
& = - \frac{1}{Z'_1} \frac{d}{dz} V(z)
\end{aligned}$$

To obtain Equations 11 and 12, one has used the dispersion relation 8 and several series summation formulas in Reference 3. With the expression for $I(z)$, one can calculate the total charge per unit length of the double shield from

$$Q'(z) = - \frac{1}{j\omega} \frac{d}{dz} I(z) \quad (13)$$

As is obvious from Equations 11 and 12, V_0 is yet to be determined from the boundary condition at $z = z_0$. In what follows, the cases with the voltage and current sources will be considered separately.

1. VOLTAGE SOURCE

Applying the condition that $V = V^S$ at $z = z_0$, one immediately obtains from Equation 11 that

$$\begin{aligned}
V_0 = & \frac{-Z'_1 Y_d V^S}{(k^2 + Y'_1 Z'_1) d} e^{jkd/2} \times \\
& \times \left\{ \frac{\cos(kd/2) \cos[(z_0 - d/2) \sqrt{-Y'_1 Z'_1}]}{\cos(d\sqrt{-Y'_1 Z'_1}/2)} \right. \\
& \left. - j \frac{\sin(kd/2) \sin[(z_0 - d/2) \sqrt{-Y'_1 Z'_1}]}{\sin(d\sqrt{-Y'_1 Z'_1}/2)} \right\}^{-1} \quad (14)
\end{aligned}$$

The voltage, current and charge distributions of the double shield can be fully expressed by Equations 8, 11, 12, 13 and 14 provided V^S is known. For the problem of Figure 3b, V^S is simply V_o^S . However, to obtain V^S (Note, one uses $V^S = V_1^S$ for $z > z_o$ and $V^S = V_2^S$ for $z < z_o$) for the problem of Figure 4a, one needs to go through some complicated algebraic manipulations involving Equations 12 and 14 and the relationships given in Figure 4a. For the special cases of $z_o = 0$ and $d/2$ which are the cases to be considered in the following discussions, $V^S = V_1^S = V_2^S = V_o^S/2$. V_o^S can, generally, be obtained from the short-circuit current I_{sc} at the outermost surface of the double shield and the transfer impedance Z_{T1} of the outer shield via

$$V_o^S = I_{sc} Z_{T1} \quad (15)$$

Since $I(z)$ and $Q'(z)$ are now known, one can begin to discuss the coupling to the wires inside the inner shield. The coupling can be completely described by $V'_s(z)$ and $I'_s(z)$ which are, respectively, the voltage and current source terms of the transmission-line equations of the inside cables. If the inner shield has a shield transfer impedance per unit length Z'_{T2} and a charge transfer frequency Ω_{T2} , then, V'_s and I'_s can be calculated from (see Ref. 4):

$$V'_s(z) = Z'_{T2} I(z) \quad (16)$$

$$I'_s(z) = \Omega_{T2} Q'(z) \quad (17)$$

With the above expressions one can then define an effective transfer impedance per unit length Z'_{TV} and an effective charge transfer frequency per unit length Ω'_{TV} for the double shield as follows:

$$Z'_{TV}(z) = V'_s(z) / I_{sc} \quad (18)$$

$$\Omega'_{TV}(z) = j\omega I'_s(z) / I_{sc} \quad (19)$$

Here, the subscript "V" is used to indicate that the quantities are for a localized voltage source which is generated by I_{sc} .

The two quantities Z'_{TV} and Ω'_{TV} are z -dependent. When the frequencies are in the stopbands, they become extremely small for $z \gg z_0$ (see the exponentially decaying term in Equation 12). On the other hand, when the frequencies are inside the passbands, they are oscillatory functions of z and are modulated by the periodicity of the bondings. It thus appears that in order to better quantify the coupling to the wires inside the inner shield, one should apply some average schemes to Z'_{TV} and Ω'_{TV} over the period d . A natural scheme is to define

$$\begin{pmatrix} \bar{Z}'_{TV} \\ \bar{\Omega}'_{TV} \end{pmatrix} = \frac{1}{d} \int_{md}^{(m+1)d} \begin{pmatrix} Z'_{TV}(z) \\ \Omega'_{TV}(z) \end{pmatrix} e^{jkz} dz \quad (20)$$

where $n\pi \leq kd < (n+1)\pi$ when $n\pi \leq \sqrt{-Y'_1 Z'_1} d < (n+1)\pi$, $n = 0, 1, 2, \dots$. These two average quantities are calculated to be

$$\begin{aligned} \bar{Z}'_{TV} / \left(\frac{Z_{T1} Z'_{T2}}{n_p \sqrt{Z'_1 Y'_1}} \right) &= \bar{\Omega}'_{TV} / \left(\frac{\Omega_{T2} Z_{T1} Y'_1}{n_p} \right) \cdot \frac{\sqrt{-Y'_1 Z'_1} d}{kd} \\ &= \frac{-(Z'_1 Y'_1 d) (kd) \exp(jkd/2)}{(\sqrt{-Z'_1 Y'_1} d) (k^2 + Y'_1 Z'_1) d^2} \times \\ &\quad \times \left\{ \frac{\cos(kd/2) \cos[(z_0 - d/2) \sqrt{-Z'_1 Y'_1}]}{\cos(d \sqrt{-Z'_1 Y'_1} / 2)} \right. \\ &\quad \left. - j \frac{\sin(kd/2) \sin[(z_0 - d/2) \sqrt{-Z'_1 Y'_1}]}{\sin(d \sqrt{-Z'_1 Y'_1} / 2)} \right\}^{-1} \quad (21) \end{aligned}$$

where $n_p = 1$ for Figure 3b and $n_p = 2$ for Figure 3a.

\bar{Z}'_{TV} and $\bar{\Omega}'_{TV}$ still depend on where $z = z_0$ is. However, no matter what z_0 is, one can easily observe that the normalized $|\bar{Z}'_{TV}|$ and $|\bar{\Omega}'_{TV}|$ (normalized with respect to their values when there is no bonding, which are, respectively, $Z_{T1} Z'_{T2} / (n_p \sqrt{Z'_1/Y'_1})$ and $Z_{T1} \Omega_{T2} Y'_1 / n_p$) are greater than unity for some regions of $\sqrt{-Z'_1/Y'_1} d$ ($\approx \omega d/c$) and smaller than unity for the others. That is, the bondings improve the shielding effectiveness of the double shield at certain frequencies but degrade it at the others. Plots of the normalized $|\bar{Z}'_{TV}|$ and $|\bar{\Omega}'_{TV}|$ for $z_0 = 0$ and $d/2$ as functions of $\sqrt{-Z'_1/Y'_1} d$ and q_s ($= Z'_1 Y'_1 d$) are given in Figures 8 through 11. In the figures, the curves are not given for the stopbands. In the stopbands, the normalized quantities are exponentially decayed away from the penetration point. Since the ranges of the stopbands increase with q_s , one should try to have q_s as large as possible for better shielding effectiveness. This can be achieved by making $Z'_1 Y'_1 d$ ($\approx L'_1/L_d$) large. Note that making d large, although increasing q_s , widens $\omega d/c$ and hence narrows the stopbands. From the figures, one also sees that arranging the bondings with $d \approx cn\pi/\omega$ (where resonances occur) seriously degrades the shielding effectiveness, and thus should be avoided for the important parts of the EMP spectrum.

2. CURRENT SOURCE

Applying the boundary condition that $I = I^s$ at $z = z_0$, one obtains from Equation 12:

$$V_0 = \frac{j I^s (dY'_d Z'_1) Z'_1 d}{d \sqrt{-Y'_1 Z'_1} (k^2 + Y'_1 Z'_1) d^2} e^{jkd/2} \times \left\{ \frac{\sin(kd/2) \cos[(z_0 - d/2) \sqrt{-Y'_1 Z'_1}]}{\sin(d \sqrt{-Y'_1 Z'_1}/2)} - j \frac{\cos(kd/2) \sin[(z_0 - d/2) \sqrt{-Y'_1 Z'_1}]}{\cos(d \sqrt{-Y'_1 Z'_1}/2)} \right\}^{-1} \quad (22)$$

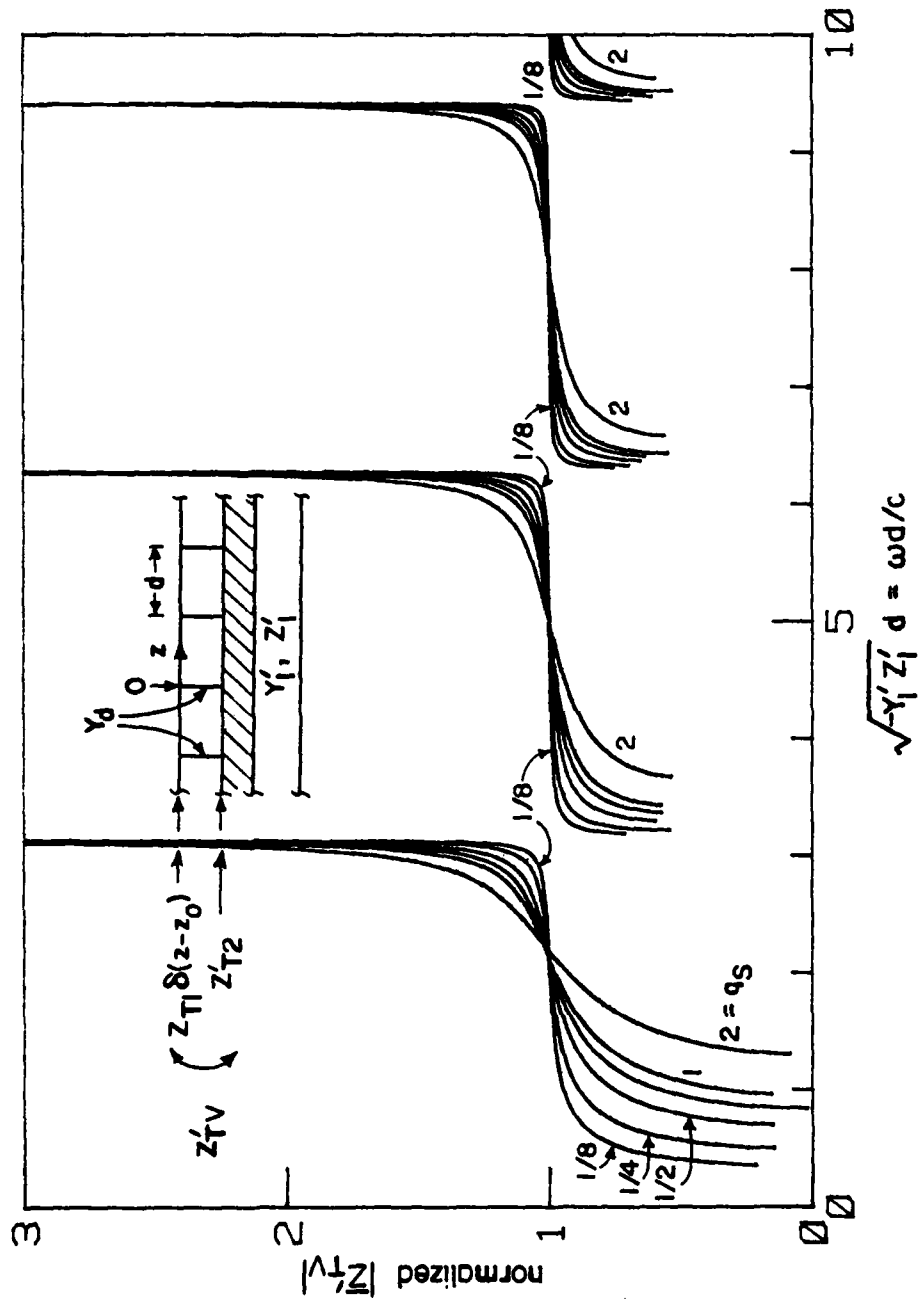


Figure 8. Normalized $|Z'_{TV}|$ (normalized to their values when the cable shields are not bonded) when $z_0 = 0$ versus frequencies for various $q_S = Z'_1 Y_d$.

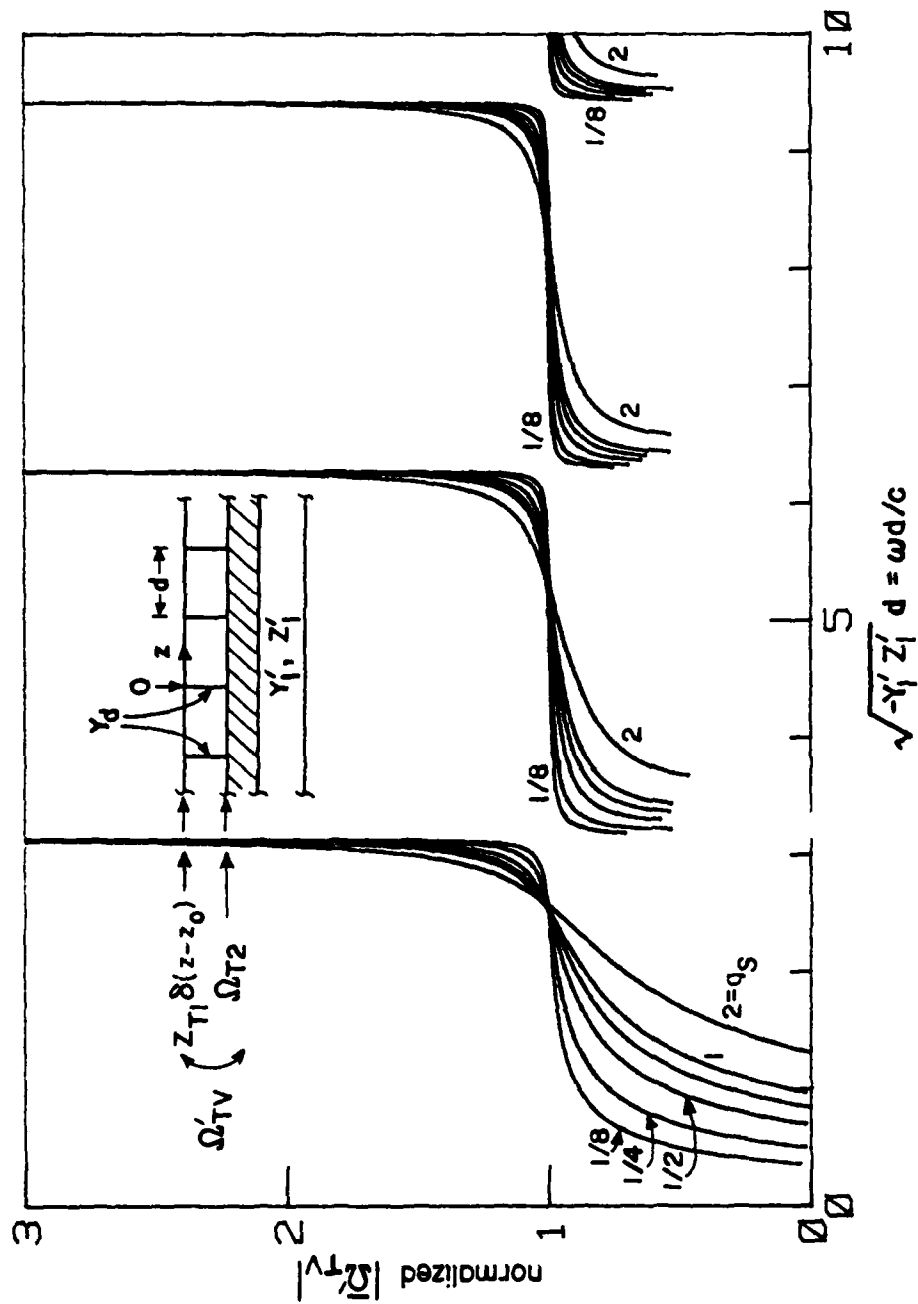


Figure 9. Normalized $|\Omega'_{TV}|$ when $z_0 = 0$ versus frequencies for various $q_S = Z'_1 Y_d d$.

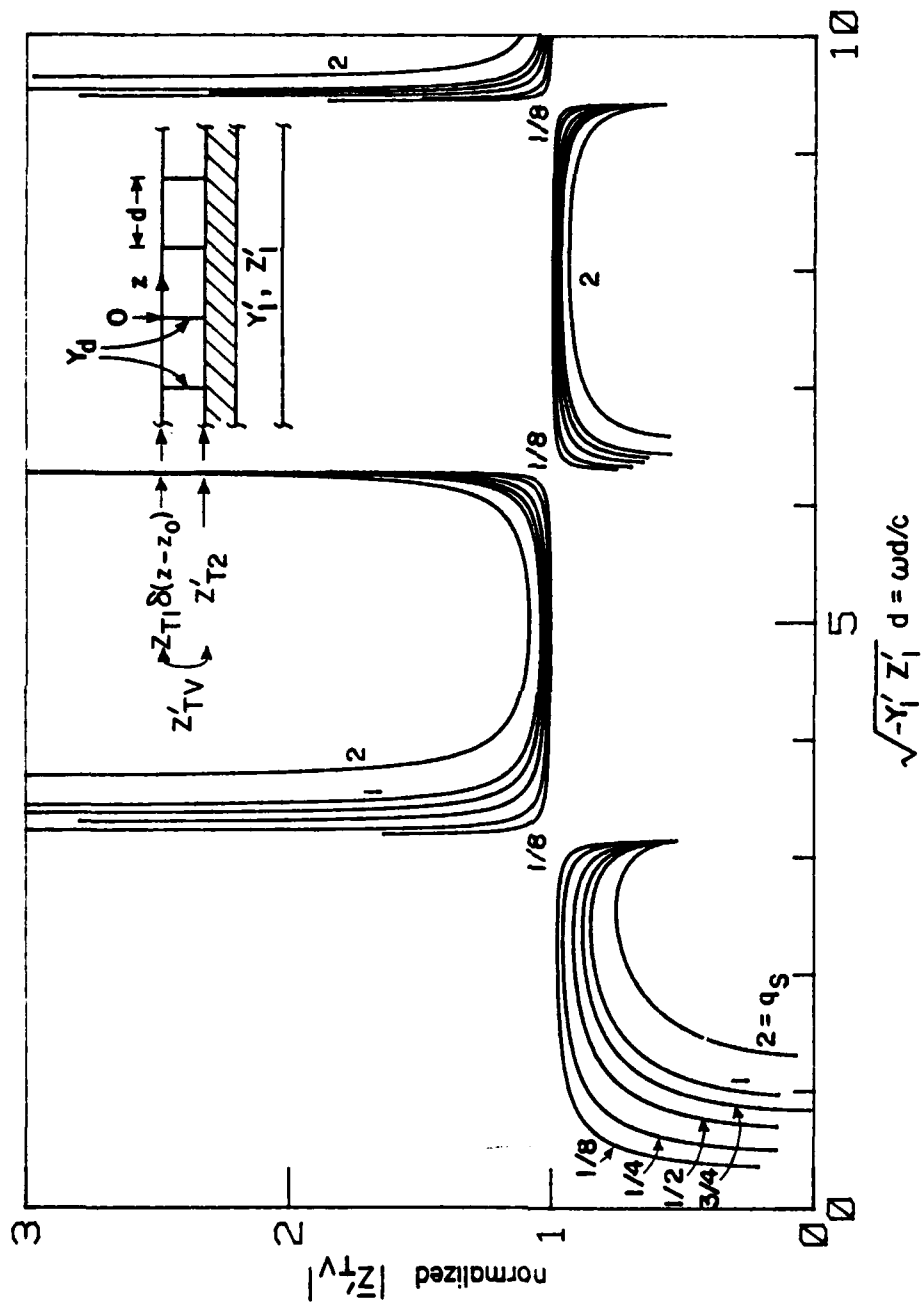


Figure 10. Normalized $|Z'_{TV}|$ when $z_0 = d/2$ versus frequencies for various $q_S = Z'_1 Y_d$.

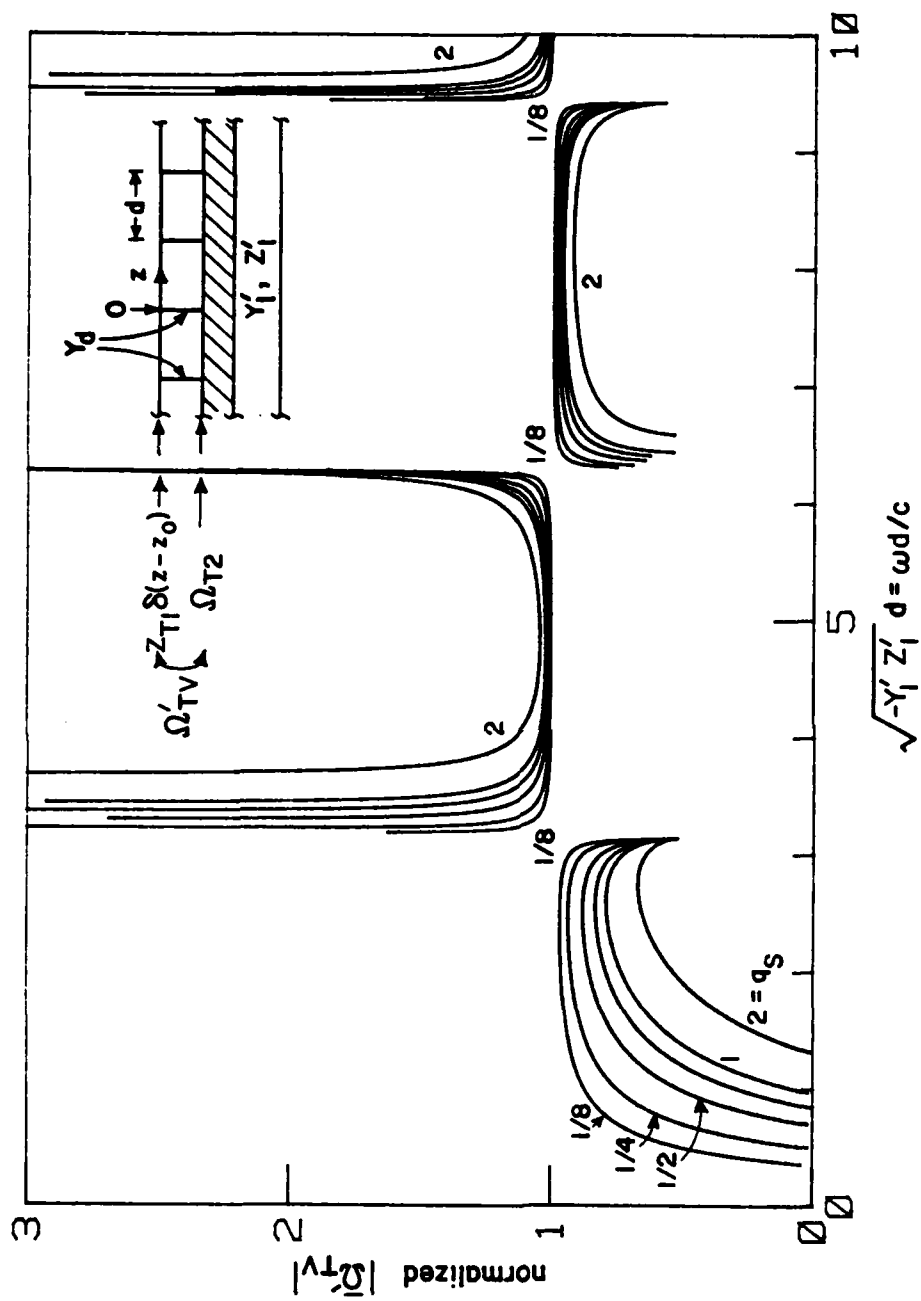


Figure 11. Normalized $|\bar{\Omega}'_{TV}|$ when $z_0 = d/2$ versus frequencies $q_S = Z'_1 Y_d d$.

The voltage, current, and charge distributions of the double shield due to the current source shown in Figure 5 can then be completely described by Equations 8, 11, 12, 13, and 22, provided that I^S is known. Here, similar to the voltage-source case, for the problem of Figure 3b, I^S is I_o^S . To obtain I^S ($I^S = I_1^S$ for $z > z_o$, $I^S = I_2^S$ for $z < z_o$) for the problem of Figure 3a or 4b, one has to solve Equations 11, 12 and the equations given in Figure 4b. For the special cases of $z_o = 0$ and $d/2$, $I^S = I_1^S = I_2^S = I_o^S/2$. From these current and charge distributions, one can calculate the voltage- and current-source terms of the transmission-line equations of the inside cables using Equations 16 and 17.

The current source of the shield I_o^S can generally be estimated from the short-circuit charge density Q'_{sc} on the outermost surface of the double shield and the localized charge transfer frequency Ω_{TI}^L (which has a dimension of frequency \times length, different from that of Ω_{T2}) of the outer shield via (for example, see Equation 38 of Reference 5)

$$I_o^S = Q'_{sc} \Omega_{TI}^L \quad (23)$$

One can also define an effective transfer impedance Z_{TI} and an effective charge transfer frequency for the double shield as follows:

$$Z_{TI}(z) = V'_s(z) / (j\omega Q'_{sc}) \quad (24)$$

$$\Omega_{TI}(z) = I'_s(z) / Q'_{sc} \quad (25)$$

where the subscript "I" is used to indicate that the quantities are for a localized "current" source which is generated by Q'_{sc} .

Similar to Z'_{TV} and Ω'_{TV} of the voltage-source case, Z_{TI} and Ω_{TI} are also z -dependent. They become very small far away from z_o in the stopbands, are oscillatory and modulated by the periodicity of the straps in the passbands. The averaged quantities \bar{Z}_{TI} and $\bar{\Omega}_{TI}$ are given by

$$\begin{aligned}
\bar{Z}_{TI} / \left(\frac{\Omega_{T1}^L Z_{T2}'}{n_p j \omega} \right) &= \frac{\sqrt{-Z_1' Y_1'} d}{kd} \cdot \bar{\Omega}_{TI} / \left(\frac{\Omega_{T1}^L \Omega_{T2} \sqrt{-Z_1' Y_1'} d}{n_p \omega d} \right) \\
&= \frac{-(Z_1' Y_1' d) (kd) \exp(jkd/2)}{\sqrt{-Z_1' Y_1'} d (k^2 + Y_1' Z_1') d^2} \times \\
&\quad \times \left\{ \frac{\sin(kd/2) \cos[(z_o - d/2) \sqrt{-Z_1' Y_1'}]}{\sin(d \sqrt{-Z_1' Y_1'}/2)} \right. \\
&\quad \left. - j \frac{\cos(kd/2) \sin[(z_o - d/2) \sqrt{-Z_1' Y_1'}]}{\cos(d \sqrt{-Z_1' Y_1'}/2)} \right\}^{-1} \quad (26)
\end{aligned}$$

\bar{Z}_{TI} and $\bar{\Omega}_{TI}$ also depend on where $z = z_o$ is. However, no matter where z_o is, one still sees that the normalized $|\bar{Z}_{TI}|$ and $|\bar{\Omega}_{TI}|$ (normalized with respect to their values when there is no bonding, which are, respectively, $\Omega_{T1}^L Z_{T2}' / (j \omega n_p)$ and $\Omega_{T1}^L \Omega_{T2} \sqrt{-Z_1' Y_1'} / (n_p \omega)$) are greater than unity for some $\sqrt{-Z_1' Y_1'} d$ (where the bondings degrade the shielding effectiveness) and smaller than unity for the others. Examples of the normalized $|\bar{Z}_{TI}|$ and $|\bar{\Omega}_{TI}|$ for $z_o = d/2$ as functions of $\sqrt{-Z_1' Y_1'} d$ and q_s are plotted in Figures 12 and 13. Similar to Figures 8 through 11, the values at the stopbands are not given. For better shielding effectiveness, one should try to increase $Z_1' Y_1'$ and avoid $\omega d/c = n\pi$ ($n=1,2,3, \dots$).

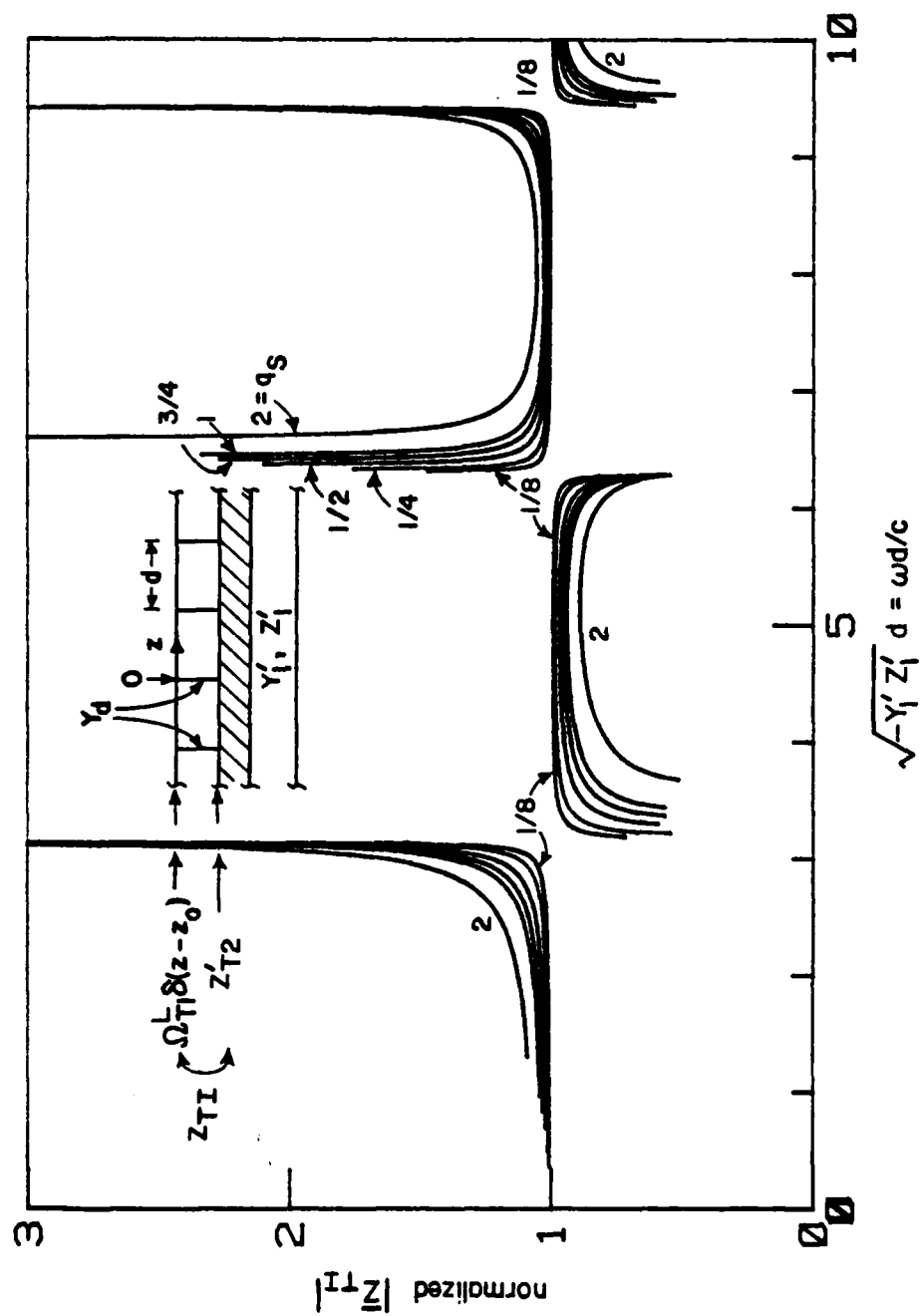


Figure 12. Normalized $|Z_{TI}|$ when $z_0 = d/2$ versus frequencies for various $q_S = Z'_1 Y_d d$.

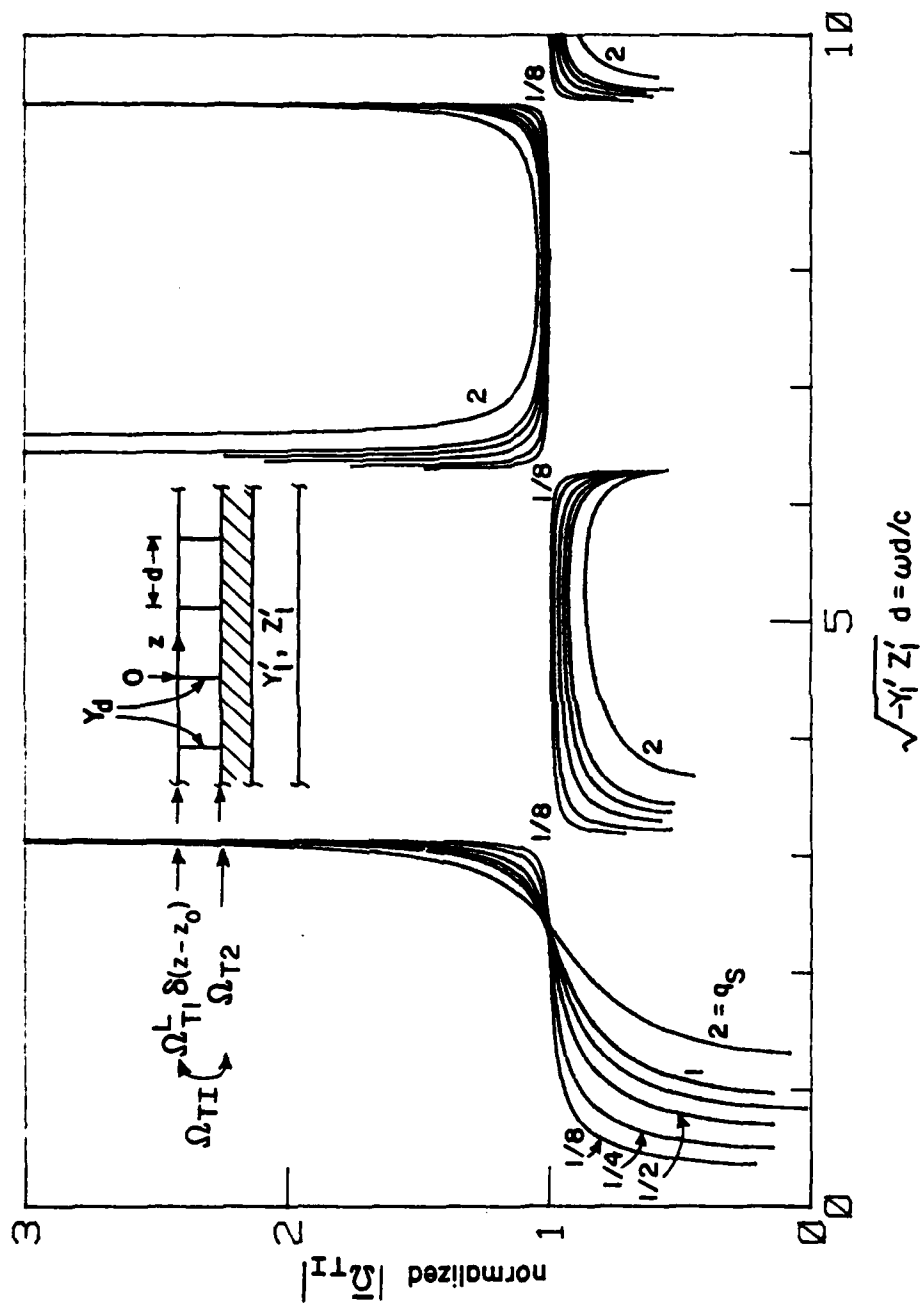


Figure 13. Normalized $|\bar{\Omega}_{TII}|$ when $z_o = d/2$ versus frequencies for various $q_s = Z'_1 Y'_1 d$.

III. DISTRIBUTED EXCITATIONS

In this section both the outer and inner shields are assumed to have uniformly distributed transfer functions: Z'_{T1} (shield transfer impedance per unit length), Ω_{T1} (charge transfer frequency) for the outer shield and Z'_{T2} , Ω_{T2} for the inner shield (Figs. 2 and 14). The outer shield is different from that discussed in Section II which has localized transfer parameters. The total current I_t and total charge per unit length Q'_t of the double-shield cable are assumed known. I_t and Q'_t are also assumed to be dependent upon z as $\exp(-jhz)$ and related to each other via

$$j\omega Q'_t = - \frac{d}{dz} I_t = jh I_t \quad (27)$$

In what follows, results for this distributed double shield without bonding straps are presented first, and then, the more general case with periodic bonding straps is discussed.

1. SCHELKUNOFF'S CIRCUIT (REF. 6)

When the shields are solid tubular conductors, $\Omega_{T1} = \Omega_{T2} = 0$, and the current-source term I'_s of the transmission-line equations of the inside cables vanishes. As for the voltage-source term V'_s , when $hd = 0$ and $\omega\mu_1\sigma_1 \gg h^2$, it can be calculated from the circuit depicted in Figure 15 which is valid regardless whether the bondings are present or not (Ref. 6). The circuit elements in the figure are defined and given as follows:

Z'_{ai} = surface impedance per unit length of the i -th shield
with internal return ($i=1$ for the outer shield,
 $i=2$ for the inner shield)

$$= \frac{\gamma_i}{2\pi a_i \sigma_i D_i} \left[I_0(\gamma_i a_i) K_1(\gamma_i b_i) + K_0(\gamma_i a_i) I_1(\gamma_i b_i) \right]$$

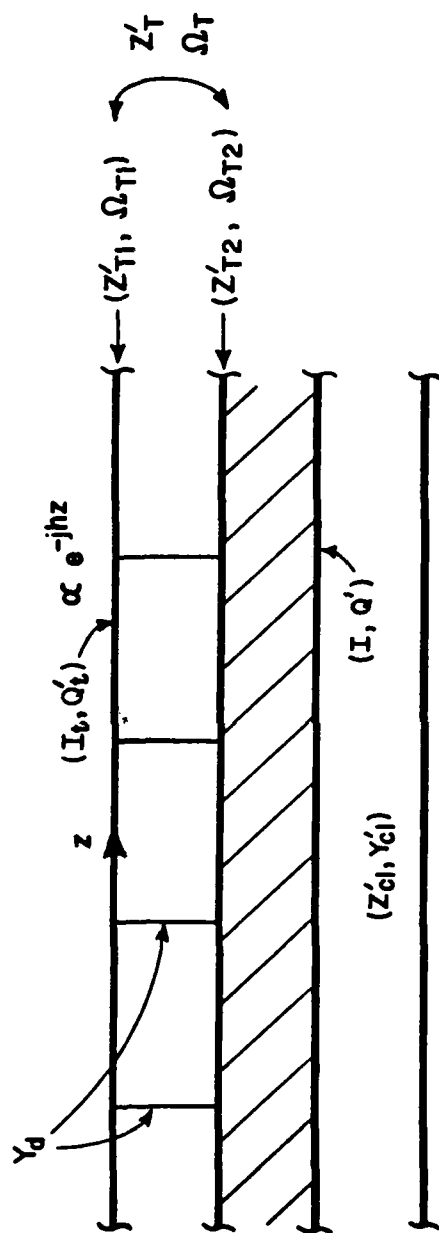
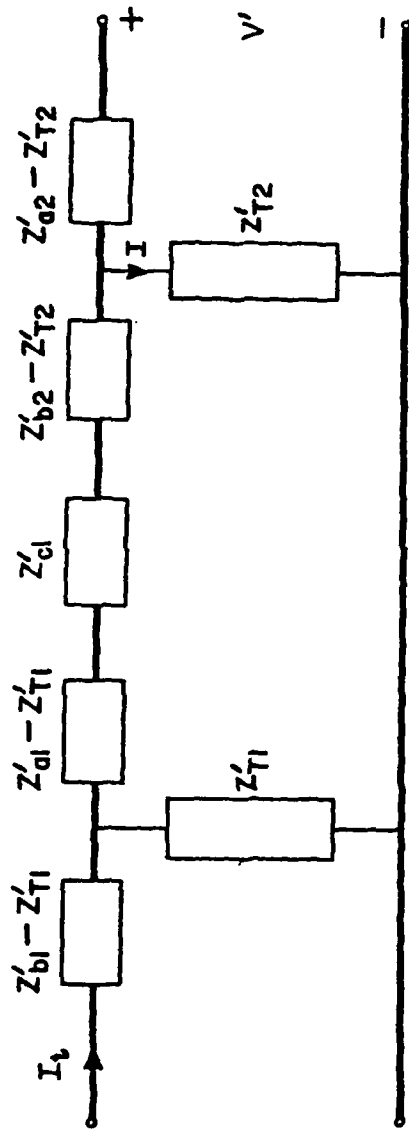


Figure 14. A theoretical model for a distributed excited double shield with periodic bondings.



$$\frac{Z'_{T1}}{Z'_{T2}} = \frac{I}{I_t}$$

Figure 15. Schelkunoff's circuit for the calculation of Z'_T of a solid tubular double shield with or without periodic bondings.

Z'_{bi} = surface impedance per unit length of the i -th shield
with external return

$$= \frac{\gamma_i}{2\pi b_i \sigma_i D_i} \left[I_0(\gamma_i b_i) K_1(\gamma_i a_i) + K_0(\gamma_i b_i) I_1(\gamma_i a_i) \right] \quad (28)$$

$$Z'_{Ti} = \frac{1}{2\pi \sigma_i a_i b_i D_i}$$

Z'_{cl} = series impedance per unit length of the double
shield when assumed perfect

$$= j\omega \mu_0 \ln(a_1/b_2)/(2\pi)$$

where

$$D_i = I_1(\gamma_i b_i) K_1(\gamma_i a_i) - I_1(\gamma_i a_i) K_1(\gamma_i b_i)$$

$$\gamma_i^2 = j\omega \mu_i \sigma_i = 2j/\delta_i^2 \quad (29)$$

$\mu_i, \sigma_i, a_i, b_i, \delta_i$ = permeability, conductivity, inner
radius, outer radius, skin depth
of the i -th shield

and I_0, I_1, K_0, K_1 are the modified Bessel functions. From the circuit,
one immediately finds that the effective transfer impedance per unit length
 $Z'_T (= V'_s/I_t)$ of the double shield is given by

$$Z'_T = \frac{Z'_{T1} Z'_{T2}}{Z'_{a1} + Z'_{b2} + Z'_{cl}} = \frac{Z'_{T1} Z'_{T2}}{Z'_1} \quad (30)$$

where

$$Z'_1 = Z'_{a1} + Z'_{b2} + Z'_{cl} \quad (31)$$

Evidently, Equation 30 and the circuit in Figure 15 can be extended easily
to describe the effective transfer impedance per unit length of a N -surface
solid tubular shield with $N > 2$.

Although Equation 30 looks simple, the circuit elements in the expression are complicated functions of frequency and shield parameters (see Eqs. 28 and 29). When Δ_i ($= b_i - a_i$, the thickness of the i -th shield) $\ll a_i, b_i$ and $\gamma_i a_i, \gamma_i b_i \gg 1$, the circuit elements $Z'_{bi}, Z'_{ai}, Z'_{Ti}$ can be approximated by

$$Z'_{ai} = Z'_{bi} = Z'_{Ti} = \frac{\gamma_i \Delta_i}{2\pi \sqrt{a_i b_i} \sigma_i \Delta_i} \coth(\gamma_i \Delta_i) \quad (32)$$

$$Z'_{Ti} = \frac{\gamma_i \Delta_i}{2\pi \sqrt{a_i b_i} \sigma_i \Delta_i} \operatorname{csch}(\gamma_i \Delta_i) \quad (33)$$

where Z'_{Ti} is referred to as the internal impedance per unit length of the i -th shield. Equations 32 and 33 can be further approximated by

$$Z'_{ai} = Z'_{bi} = Z'_{Ti} = R'_{dc,i} = \frac{1}{2\pi \sqrt{a_i b_i} \sigma_i \Delta_i} \quad (34)$$

when $\gamma_i \Delta_i \ll 1$ (i.e., $\delta_i \gg \Delta_i$), and

$$Z'_{ai} = Z'_{bi} = Z'_{Ti} = \gamma_i \Delta_i R'_{dc,i} \quad (35)$$

$$Z'_{Ti} = 2\gamma_i \Delta_i R'_{dc,i} e^{-\gamma_i \Delta_i} \quad (36)$$

when $\gamma_i \Delta_i \gg 1$ (i.e., $\Delta_i \gg \delta_i$). Here, $R'_{dc,i}$ is the dc-shield resistance per unit length of the i -th shield and the real part of γ_i is taken to be positive.

2. CASEY'S CIRCUIT (REF. 7)

When $\delta_i \gg \Delta_i$ (which guarantees $Z'_{ai} = Z'_{bi} = Z'_{Ti} = Z'_{Li}$, see Eq. 34), $h_{b1}^2 \approx -Z'_{l1} Y'_{b1} b_1^2 \approx -Z'_{cl} Y'_{cl} b_1^2 \ll 1$ (Y'_{cl} is the shunt admittance per unit length of the double shield when assumed perfect and no bonding straps), and there is no bonding strap, the circuit diagram shown in Figure 16 can be used to calculate the current I flowing on the inner shield (Ref. 7). In the

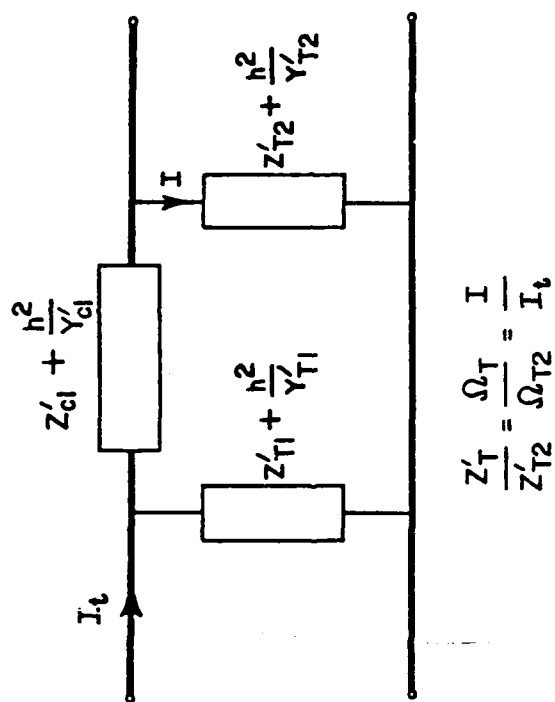


Figure 16. Casey's circuit for the calculations of Z'_T and Ω_T of a double shield without periodic bonding.

circuit Y'_{Ti} ($i=1,2$) are the capacitive transfer admittances per unit length of the shields, which are related to Ω_{Ti} via,

$$\Omega_{Ti} = -sY'_i/Y'_{Ti} \quad (37)$$

where

$$\frac{1}{Y'_1} = \frac{1}{Y'_{c1}} + \frac{1}{Y'_{T1}} + \frac{1}{Y'_{T2}} \quad (38)$$

$$\frac{1}{Y'_2} = \frac{1}{Y'_{c2}} + \frac{1}{Y'_{T2}} \quad (39)$$

and Y'_{c2} is the shunt admittance per unit length of transmission line formed by the inner shield and the wires within when $Y'_{T2} = \infty$.

From the circuit, one has

$$\begin{aligned} \frac{I}{I_t} &= \frac{Z'_{T1} + h^2/Y'_{T1}}{(Z'_{T1} + h^2/Y'_{T1}) + (Z'_{T2} + h^2/Y'_{T2}) + (Z'_{c1} + h^2/Y'_{c1})} \\ &= \frac{Z'_{T1} + h^2/Y'_{T1}}{Z'_1 + h^2/Y'_1} \end{aligned} \quad (40)$$

where

$$Z'_1 = Z'_{T1} + Z'_{T2} + Z'_{c1} \quad (41)$$

from which one immediately has

$$\frac{Z'_T}{Z'_{T2}} = \frac{\Omega_T}{\Omega_{T2}} = \frac{Z'_{T1} + h^2/Y'_{T1}}{Z'_1 + h^2/Y'_1} \quad (42)$$

When $h \rightarrow 0$ and $Y'_{T1} = Y'_{T2} = \infty$, Equation 42, indeed, reduces to Equation 30 with $\delta_1 \gg \Delta_1$. It is believed that the above thin shield ($\delta_1 \gg \Delta_1$)

approximation, Equation 42, can also be used for thick shields provided that Z'_1 defined in Equation 41 is replaced by Equation 31, i.e.,

$$Z'_1 = Z'_{a1} + Z'_{b2} + Z'_{c1}$$

and a more general circuit can be constructed (Fig. 17). Here, the circuit elements Z'_{a1} and Z'_{b2} should be defined in a broader sense than Equation 28 to include all kinds of penetrations. This circuit can also be easily extended to describe a N-surface shield with $N > 2$.

Up to this point the discussion in Part 2 has been restricted to the situation that there is no bonding connecting the shields. When there are periodic bondings with period $d \ll h^{-1}$, $(\sqrt{-Y'_1 Z'_1})^{-1}$, it is postulated that the circuits and equations can still be used provided that Y'_1 is replaced by $Y'_1 + Y_d/d$, i.e., Equation 42 becomes

$$\frac{Z'_T}{Z'_{T2}} = \frac{\Omega_T}{\Omega_{T2}} = \frac{Z'_{T1} + h^2/Y'_{T1}}{Z'_1 + h^2/(Y'_1 + Y_d/d)} \quad (43)$$

In the following, a general analysis of a double shield with periodic bondings will be given. The results of the analysis will show whether the simple Equation 43 is accurate enough under the imposed conditions.

3. GENERAL FORMULATION

To obtain the current I flowing on the inner shield one has to solve the following transmission-line equations (Fig. 14):

$$\frac{dV}{dz} + Z'_1 I = Z'_{T1} I_t \quad (44)$$

$$\frac{dI}{dz} + \left[Y'_1 + Y_d \sum_{n=-\infty}^{\infty} \delta(z - nd) \right] V = -j\omega \frac{Y'_1}{Y'_{T1}} Q'_t \quad (45)$$

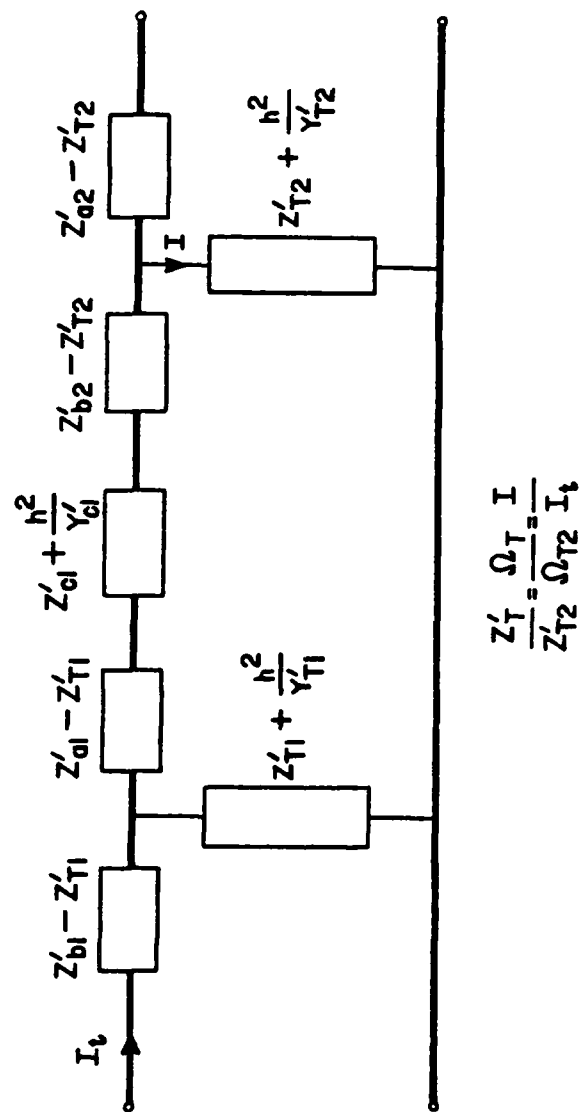


Figure 17. Generalized Casey's circuit (constraints $\delta_i \gg \Delta_i$ in Casey's circuit are lifted) for the calculations of Z'_T and Ω_T of a double shield without periodic bonding.

The shields are assumed to be infinitely extended in both $+z$ and $-z$ directions so that only the particular solution of the equations need be considered. This particular solution can be written as follows (from Floquet's theorem)

$$I(z) = e^{-jhz} \sum_{n=-\infty}^{\infty} I_n^p e^{-j2n\pi z/d} \quad (46)$$

$$V(z) = e^{-jhz} \sum_{n=-\infty}^{\infty} V_n^p e^{-j2n\pi z/d} \quad (47)$$

After substituting Equations 46 and 47 into Equations 44 and 45, and going through some complicated algebraic manipulations and series summations, one eventually has, for $md \leq z < (m+1)d$,

$$I(z) = I_t \frac{Y_1'}{Y_{T1}'} \frac{h^2 + Z_{T1}' Y_{T1}'}{h^2 + Z_1' Y_1'} \left\{ 1 + \frac{hY_d}{2Y_1'} \frac{Z_{T1}' Y_{T1}' - Z_1' Y_1'}{Z_{T1}' Y_{T1}' + h^2} \times \right. \\ \left. \times \sum_{n=1}^{\infty} \frac{\sin[(h+(-1)^n \sqrt{-Y_1' Z_1'})d/2] \exp[-j(h-(-1)^n \sqrt{-Y_1' Z_1'})(md - z + d/2)]}{\cos(d\sqrt{-Y_1' Z_1'}) - \cos(hd) + Y_d Z_1' \sin(d\sqrt{-Y_1' Z_1'}) / (2\sqrt{-Y_1' Z_1'})} \right\} \quad (48)$$

from which $Q'(z)$, Z_T' and Ω_T can be calculated via

$$Q'(z) = -\frac{1}{j\omega} \frac{d}{dz} I(z) \quad (49)$$

$$Z_T' = Z_{T2}' I(z) / I_t \quad (50)$$

$$\Omega_T = \frac{j\Omega_{T2}}{h} \frac{d}{dz} \frac{I(z)}{I_t} \quad (51)$$

Both Z_T' and Ω_T are z -dependent. In order to better quantify the transfer functions, one takes the average values of Z_T' and Ω_T over the period d of the bonding straps. These average values, designated as \bar{Z}_T' and $\bar{\Omega}_T$, are independent of z and are given as

$$\begin{aligned}
\frac{\bar{Z}'_T}{Z'_{T2}} &= \frac{\bar{\Omega}_T}{\Omega_{T2}} = \frac{I_o^P e^{-jhz}}{I_t} \\
&= \frac{Y'_1}{Y'_{T1}} \frac{h^2 + Z'_{T1} Y'_{T1}}{h^2 + Z'_1 Y'_1} \left\{ 1 + \frac{h^2}{h^2 + Z'_1 Y'_1} \frac{Z'_{T1} Y'_{T1} - Z'_1 Y'_1}{Z'_{T1} Y'_{T1} + h^2} \times \right. \\
&\quad \left. \times \frac{Y_d}{d Y'_1} \frac{\cos(d\sqrt{-Y'_1 Z'_1}) - \cos(hd)}{\cos(d\sqrt{-Y'_1 Z'_1}) - \cos(hd) + Y_d Z'_1 \sin(d\sqrt{-Y'_1 Z'_1}) / (2\sqrt{-Y'_1 Z'_1})} \right\} \quad (52)
\end{aligned}$$

It can be shown that Equation 52 reduces to Equation 43 when

$$|hd - \sqrt{-Y'_1 Z'_1} d| = |\alpha| \ll 1, \quad hd \gg q_S (= Z'_{c1} Y_d d) \quad (53)$$

$$|\tan hd| \gg |\alpha|, \quad (\text{i.e., } |hd - n\pi| \gg |\alpha|, n=0,1,2, \dots) \quad (54)$$

The conditions 53 and 54, obviously, are different and less restrictive than those imposed on Equation 43 during the discussion in Part 2. In most practical situations, Conditions 53 and 54 can be satisfied, and Equation 43 can be used. In the case that the constraints 53 and 54 are not met, one has to resort to Equation 52 which is a complicated function of the frequency and the shield parameters. The shield parameters Z'_{T1} , Y'_{T1} , Y'_1 , Z'_1 , etc., are generally complex values. However, when the diffusion penetration is not important (which is true for most highly conducting shields at frequencies larger than 10 kHz), the shield parameters Z'_{T1} , Y'_{T1} , etc., become purely imaginary (i.e., the penetration is through the apertures such as in the case of braided cable shields), and Equation 52 becomes a real function. This real function is plotted in Figures 18 through 25 as a function of $hd = \sqrt{-Y'_{c1} Z'_{c1}} d = \omega d/c$ (from 0 to 10) by using $q_Z = Z'_{T1}/Z'_{c1}$, $q_Y = Y'_{c1}/Y'_{T1}$ and $q_S = Z'_{c1} Y_d d$ ($= 0.1, 0.5, 1, 2$) as parameters (also assume $Z'_{T2}/Z'_{c1} = 0$, $Y'_{c1}/Y'_{T2} = 0$). The values for the parameters $(q_Y, q_Z) = (0.004, 0.01)$ and $(0.001, 0.002)$ are for some typical braided cable shields (see

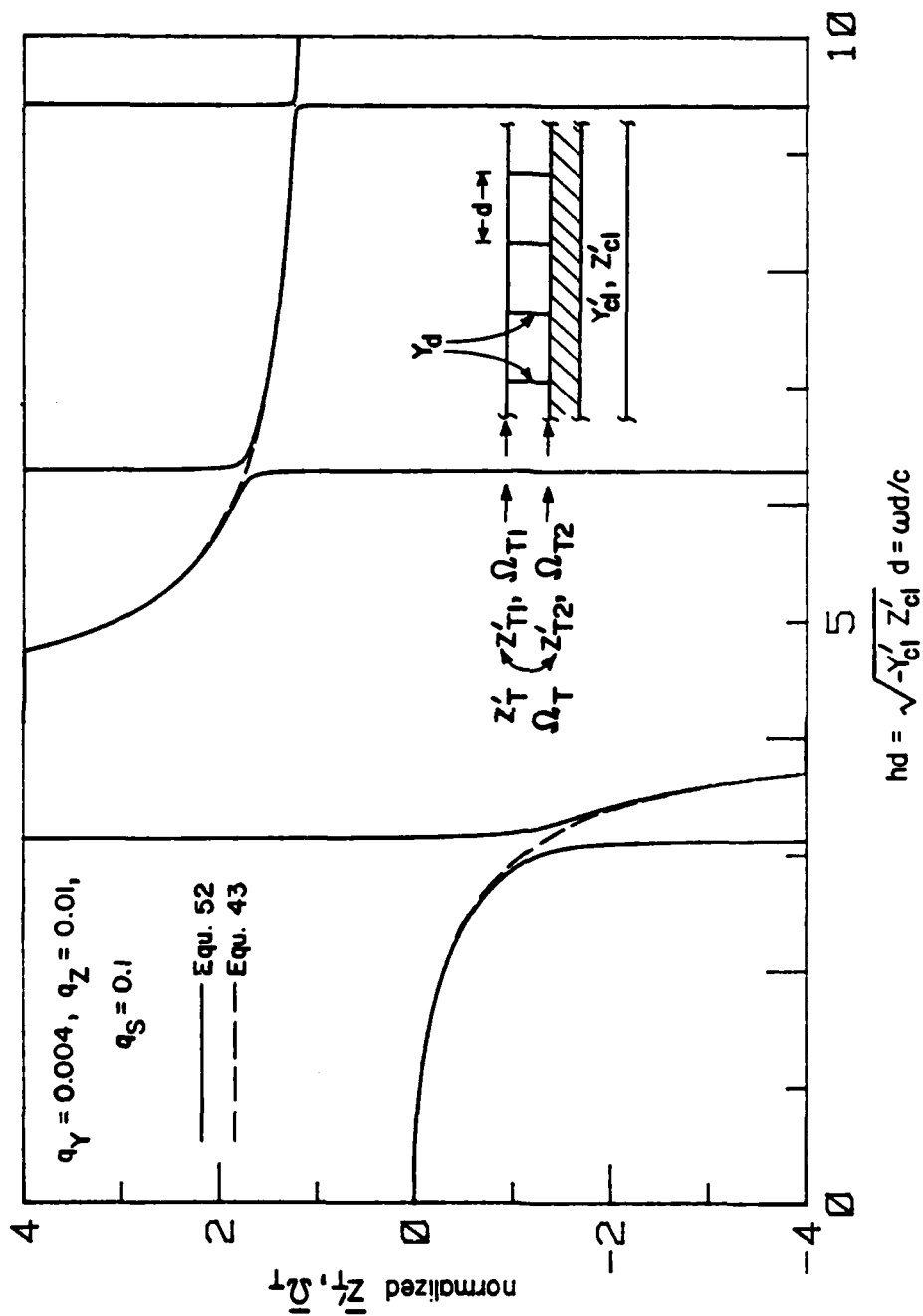


Figure 18. Normalized \bar{Z}_T' and $\bar{\Omega}_T'$ (normalized to their values when the cable shields are not bonded), based on the general Equation 52 and the approximated Equation 43, versus frequencies for $q_S = Z'_{c1} Y'_d d = 0.1$, $q_Y = Y'_{c1} / Y'_{T1} = 0.004$ and $q_Z = Z'_{T1} / Z'_{c1} = 0.01$.

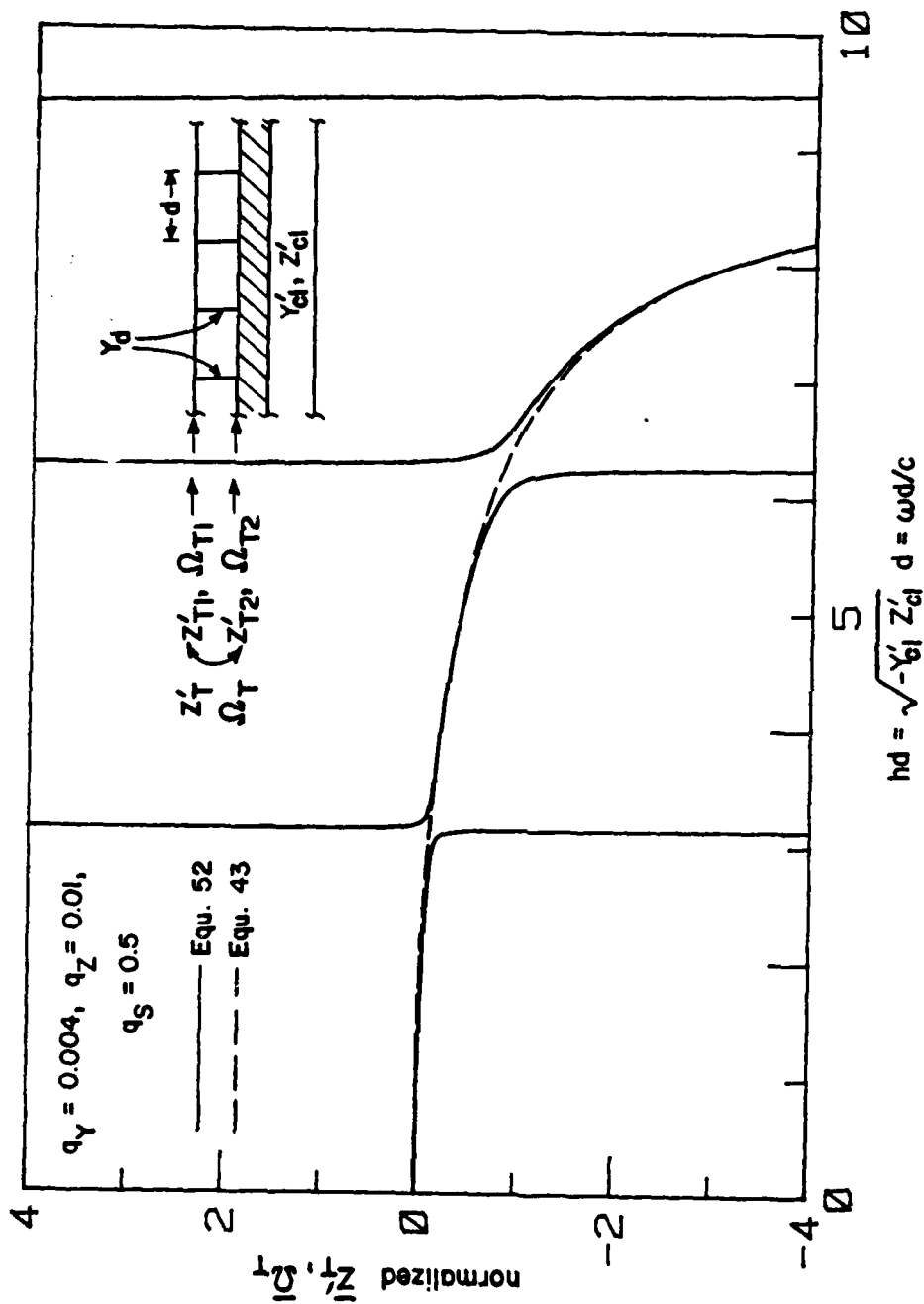


Figure 19. Normalized \bar{Z}_T' and $\bar{\Omega}_T$ (normalized to their values when the cable shields are not bonded), based on the general Equation 52 and the approximated Equation 43, versus frequencies for $q_S = Z_{cl}' Y_d d \approx 0.5$, $q_Y = Y_{cl}' / Y_{T1}' = 0.004$ and $q_Z = Z_{T1}' / Z_{cl}' = 0.01$.

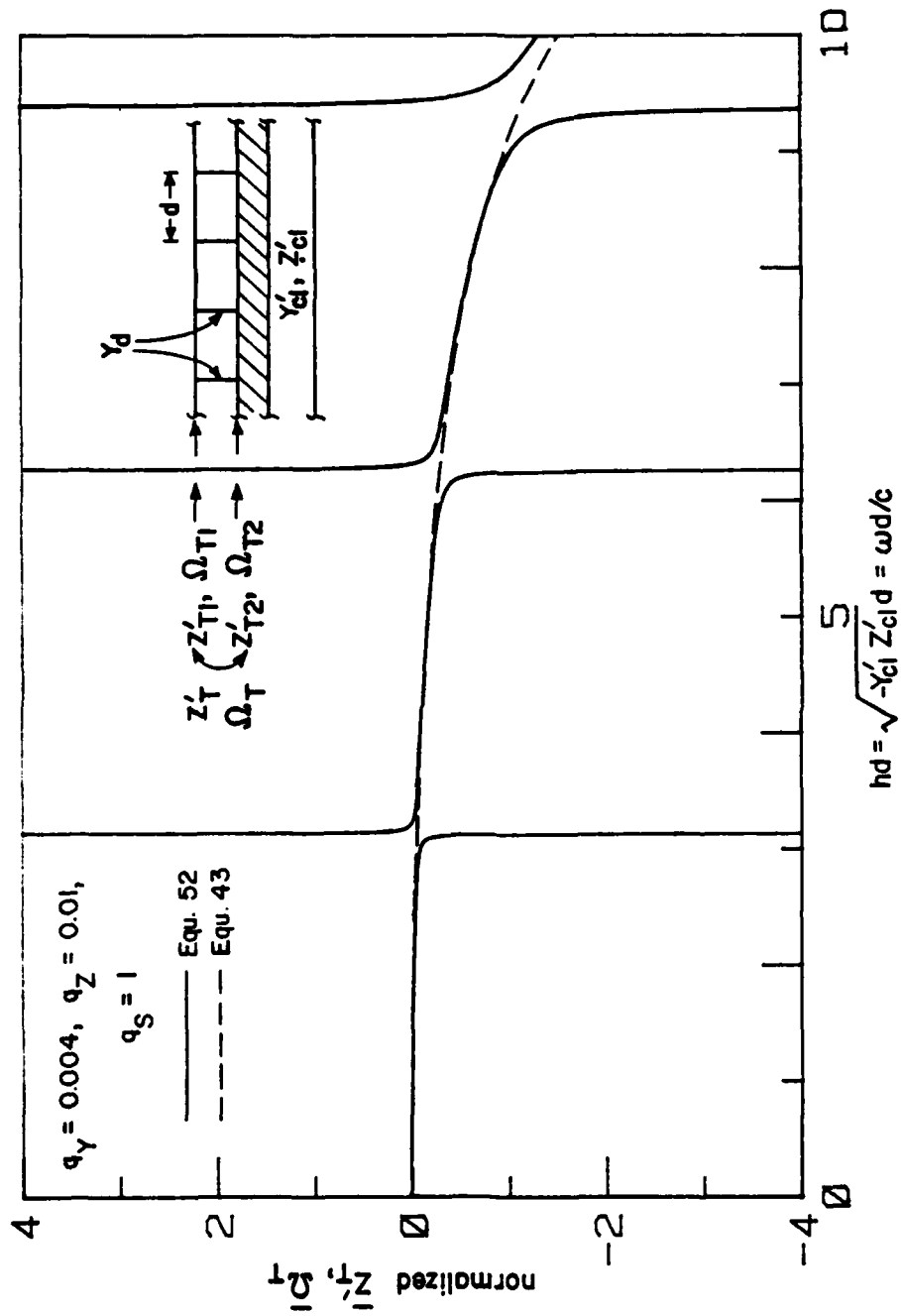


Figure 20. Normalized Z'_T and $\bar{\Omega}_T$ (normalized to their values when the cable shields are not bonded), based on the general Equation 52 and the approximated Equation 43, versus frequencies for $q_S = Z'_{cl} Y_d d = 1$, $q_Y = Y'_{cl} / Y'_T = 0.004$ and $q_Z = Z'_{T1} / Z'_{cl} = 0.01$.

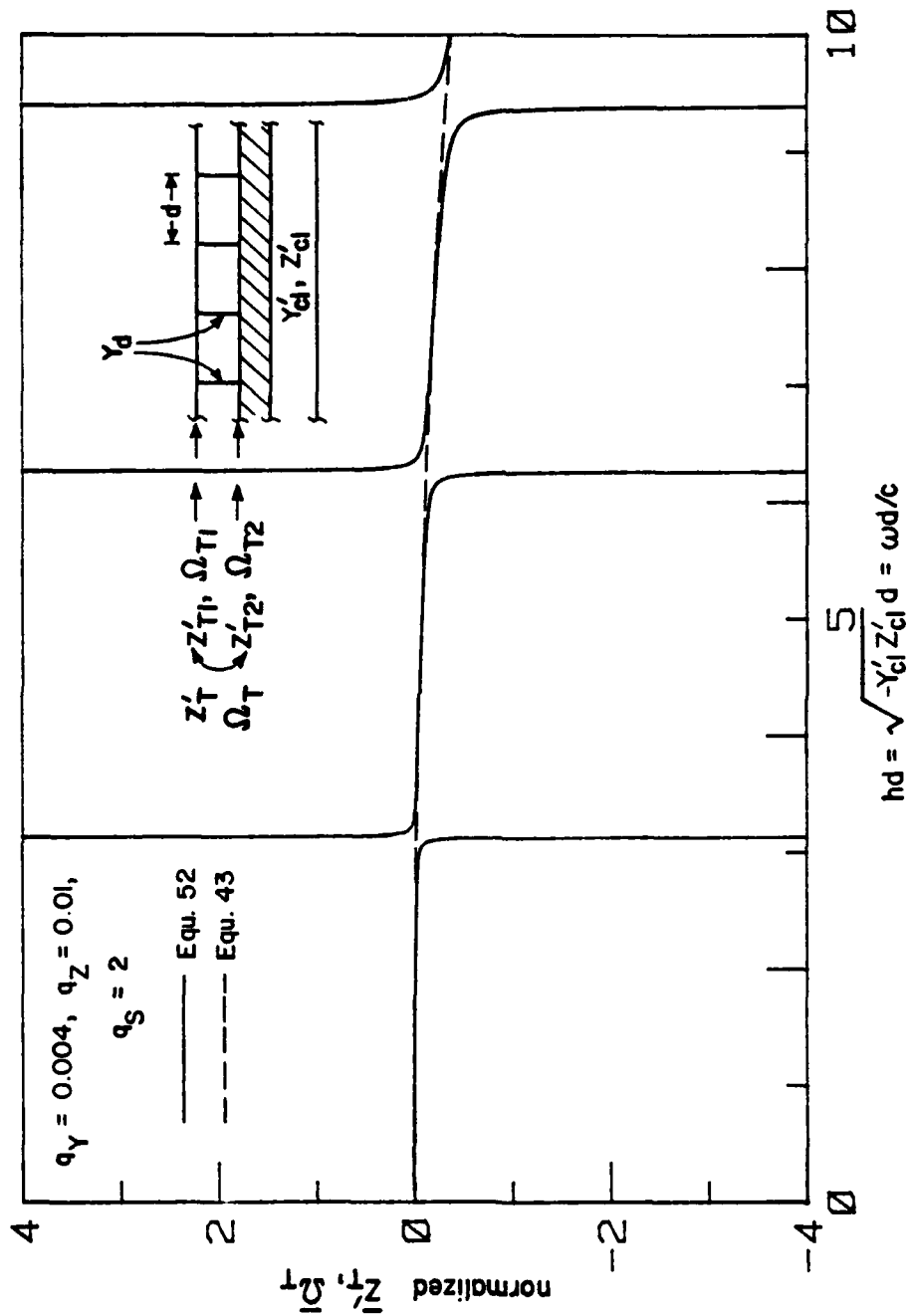


Figure 21. Normalized \bar{Z}'_T and $\bar{\Omega}_T$ (normalized to their values when the cable shields are not bonded), based on the general Equation 52 and the approximated Equation 43, versus frequencies for $q_S = Z'_{c1} Y_d = 2$, $q_Y = Y'_{c1} / Y'_{T1} = 0.004$ and $q_Z = Z'_{T1} / Z'_{c1} = 0.01$.

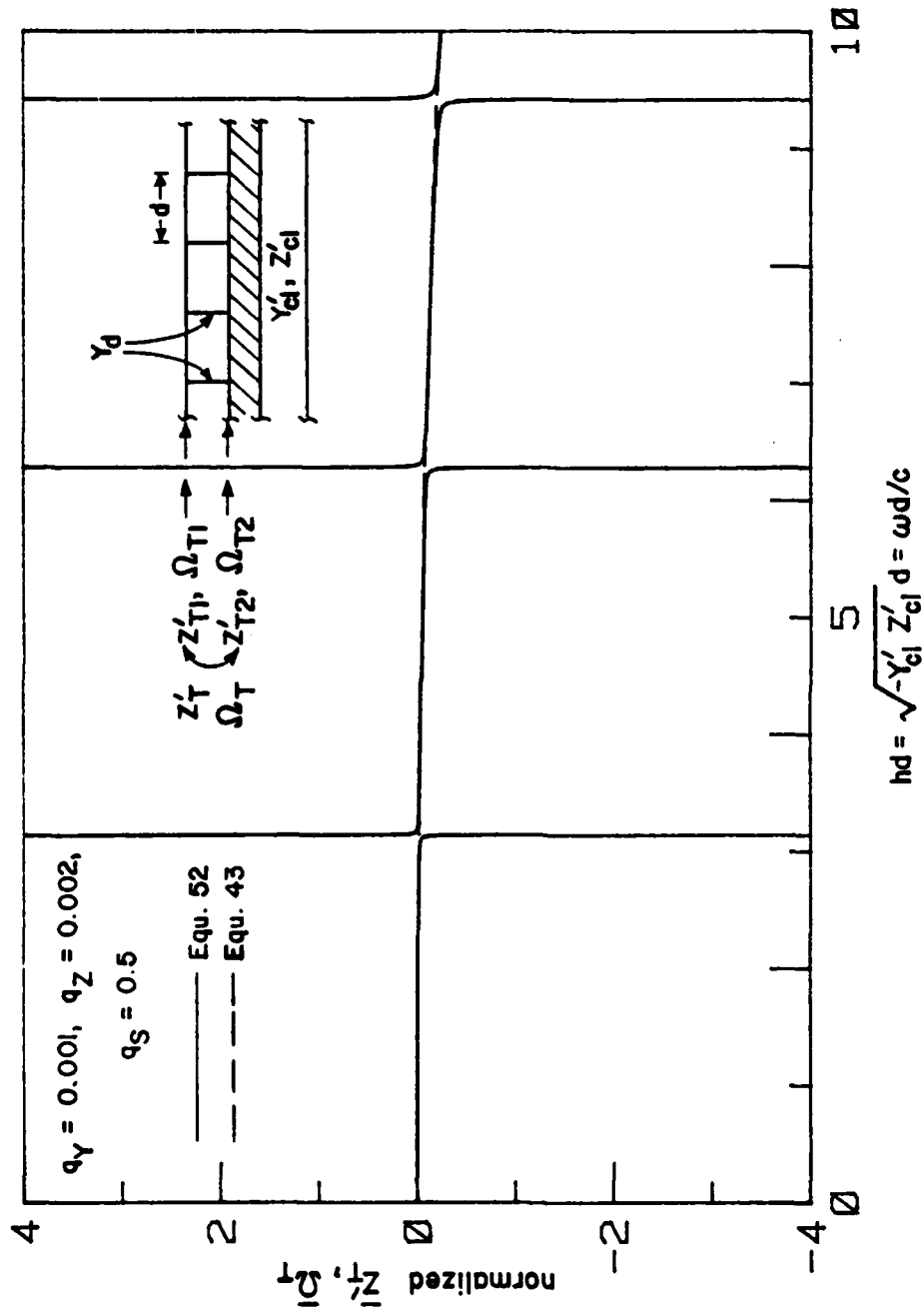


Figure 23. Normalized \bar{Z}_T' and $\bar{\Omega}_T'$ (normalized to their values when the cable shields are not bonded), based on the general Equation 52 and the approximated Equation 43, versus frequencies for $q_S = Z'_{c1} Y_d = 0.5$, $q_Y = Y'_{c1} / Y_{T1}' = 0.001$ and $q_Z = Z'_{T1} / Z'_{c1} = 0.002$.

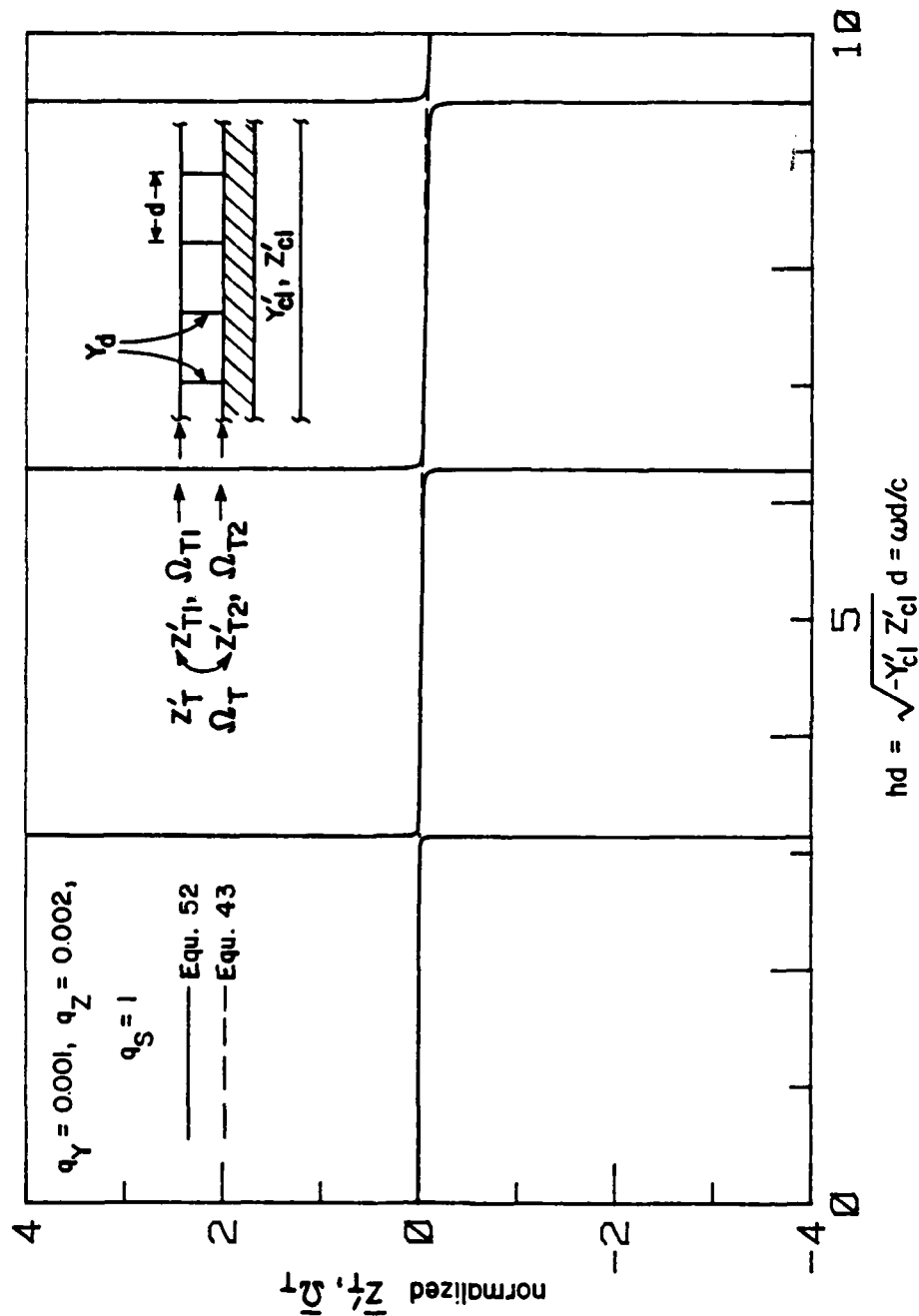


Figure 24. Normalized \bar{Z}_T' and $\bar{\Omega}_T'$ (normalized to their values when the cable shields are not bonded), based on the general Equation 52 and the approximated Equation 43, versus frequencies for $q_S = Z_{cl}' / Y_d = 1$, $q_Y = Y_{cl}' / Y_{T1}' = 0.001$ and $q_Z = Z_{T1}' / Z_{cl}' = 0.002$.

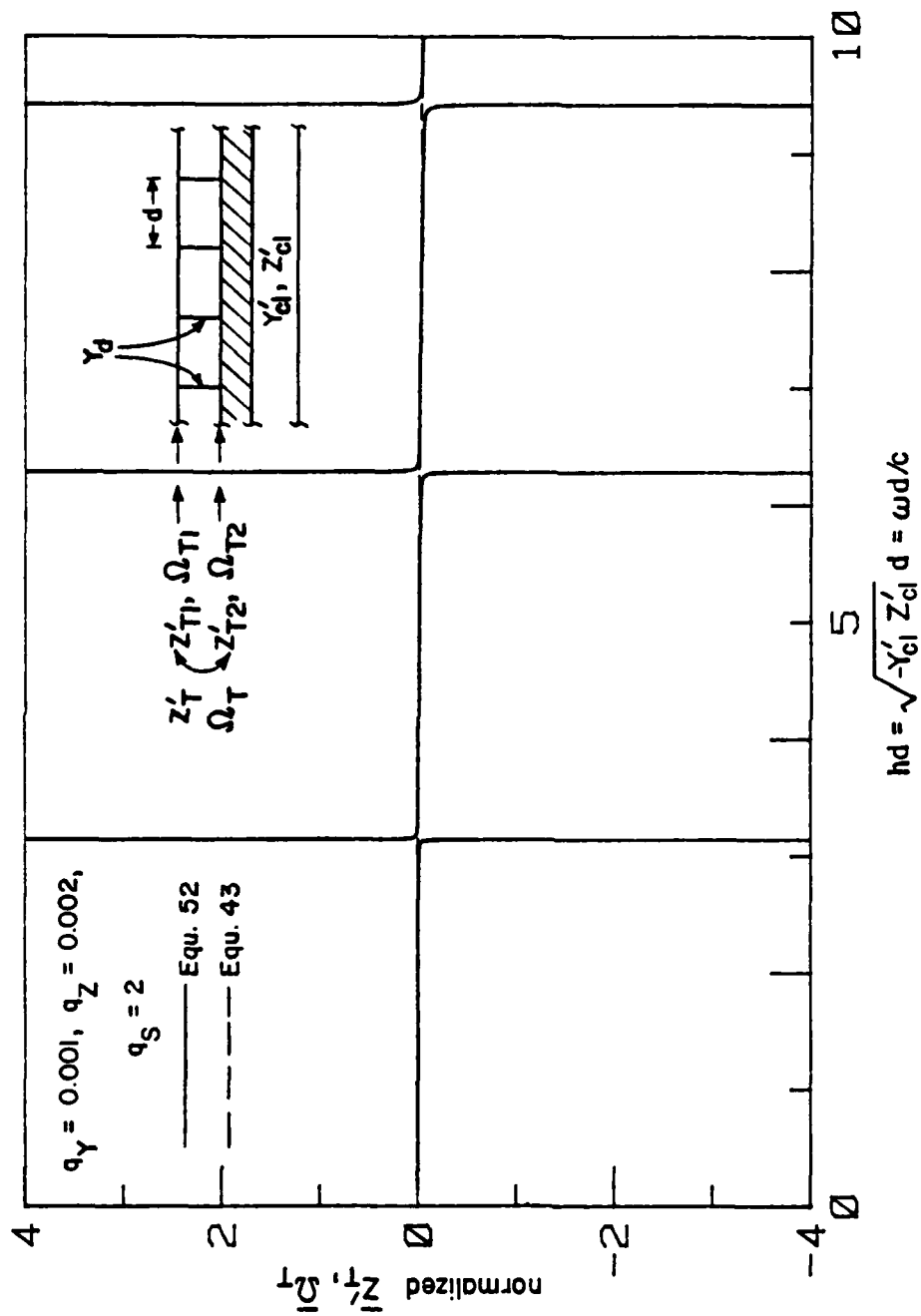


Figure 25. Normalized Z'_T and $\bar{\Omega}_T$ (normalized to their values when the cable shields are not bonded), based on the general Equation 52 and the approximated Equation 43, versus frequencies for $q_S = Z'_{c1} Y_d d = 2$, $q_Y = Y'_{c1} / Y'_{T1} = 0.001$ and $q_Z = Z'_{T1} / Z'_{c1} = 0.002$.

Pages 581 and 584 of Ref. 4). In the figures, the curves of the approximate Equation 43 are also given. The agreement between Equations 43 and 52 in the region where $\omega d/c$ is not close to $n\pi$ ($n=1,2,\dots$) is clearly shown even when hd is smaller or in the order of q_s . The reason they agree when $hd \leq q_s$ is simply because both Equations 43 and 52 have values in the order of q_Y or q_Z ($\ll 1$). Because of this, probably one can lift the condition $hd \gg q_s$ in Equation 53. From the figures one can draw the same conclusions as those of the discrete excitation case that the bondings improve the shielding effectiveness at certain frequency ranges while degrade it at others. In order to widen the frequency ranges for better shielding effectiveness, one may try to increase $Z'_1 Y_d$. Also one should not use a d -value which causes resonances (where $\omega d/c \approx n\pi$, $n=1,2,\dots$) and thus seriously degrades the shielding effectiveness.

Equation 52 can also be rewritten in the following form:

$$\frac{\bar{Z}'_T}{Z'_{T2}} = \frac{\bar{\Omega}_T}{\Omega_{T2}} = \frac{Z'_{T1} + h^2/Y'_{T1}}{Z'_1 + h^2/(Y'_1 + qY_d/d)} \quad (55)$$

where

$$q = \frac{q_1}{1 + dY_d Z'_1 (q_2 - q_1) / [(h^2 + Y'_1 Z'_1) d^2]} \quad (56)$$

$$q_1 = (Z'_{T1} Y'_{T1} - Z'_1 Y'_1) / (Z'_{T1} Y'_{T1} + h^2) \quad (57)$$

$$q_2 = \frac{\sin(d\sqrt{-Y'_1 Z'_1}) / (d\sqrt{-Y'_1 Z'_1})}{[\cos(d\sqrt{-Y'_1 Z'_1}) - \cos(hd)] / [(h^2 + Y'_1 Z'_1) d^2 / 2]} \quad (58)$$

Equation 55 can be easily represented by a circuit (Fig. 26). Under the assumption that the diffusion penetration is not important, the q -values are plotted in Figures 27 and 28 as functions of $hd = \sqrt{-Y'_1 Z'_1} d = \omega d/c$, with q_Z , q_Y and q_s as parameters. The values of the parameters in Figures 27

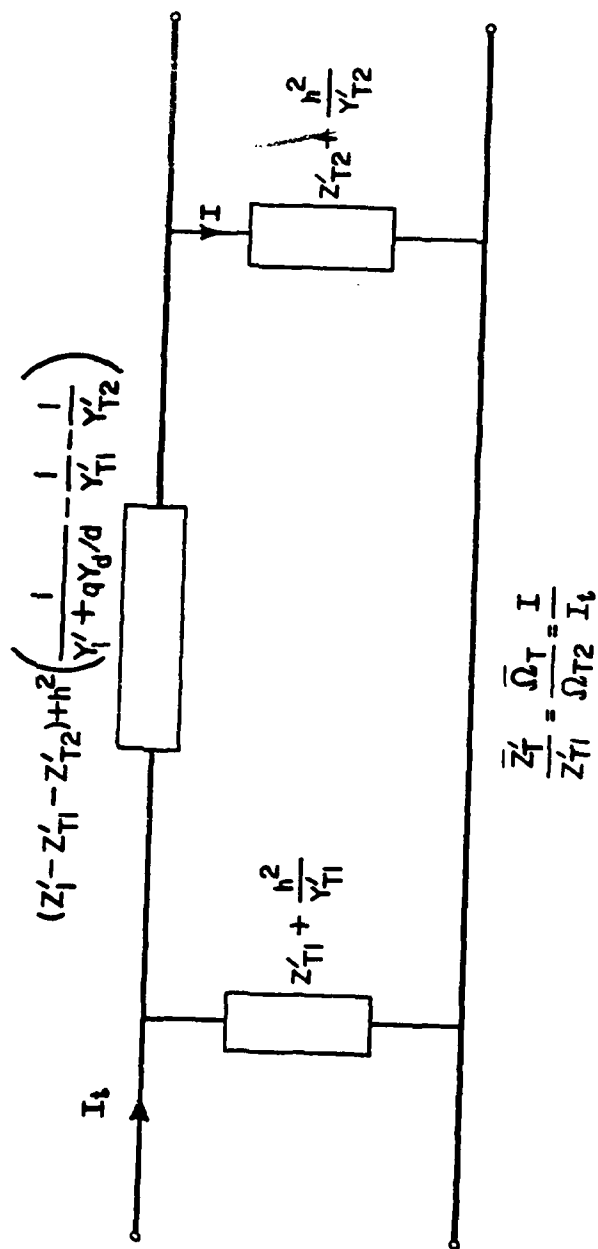


Figure 26. The general circuit for the calculations of \bar{Z}'_T and $\bar{\Omega}_T$ of a double shield with periodic bondings.

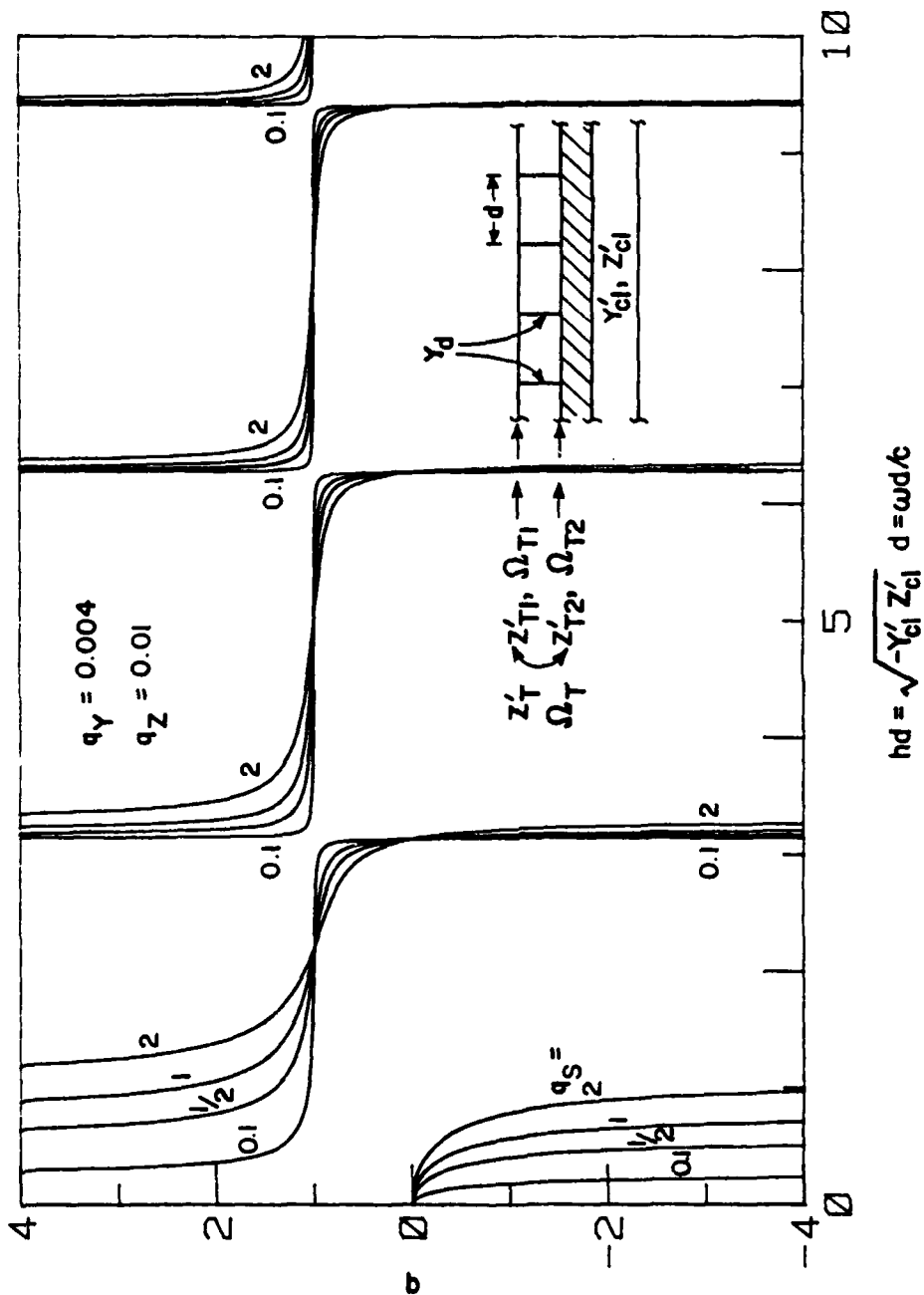


Figure 27. The values of "q", to be used in the circuit of Figure 26, versus frequencies for $q_Y = Y'_{cl}/Y'_{T1} = 0.004$, $q_Z = Z'_{T1}/Z'_{cl} = 0.01$ and various $q_S = Z'_cl Y'_d$.

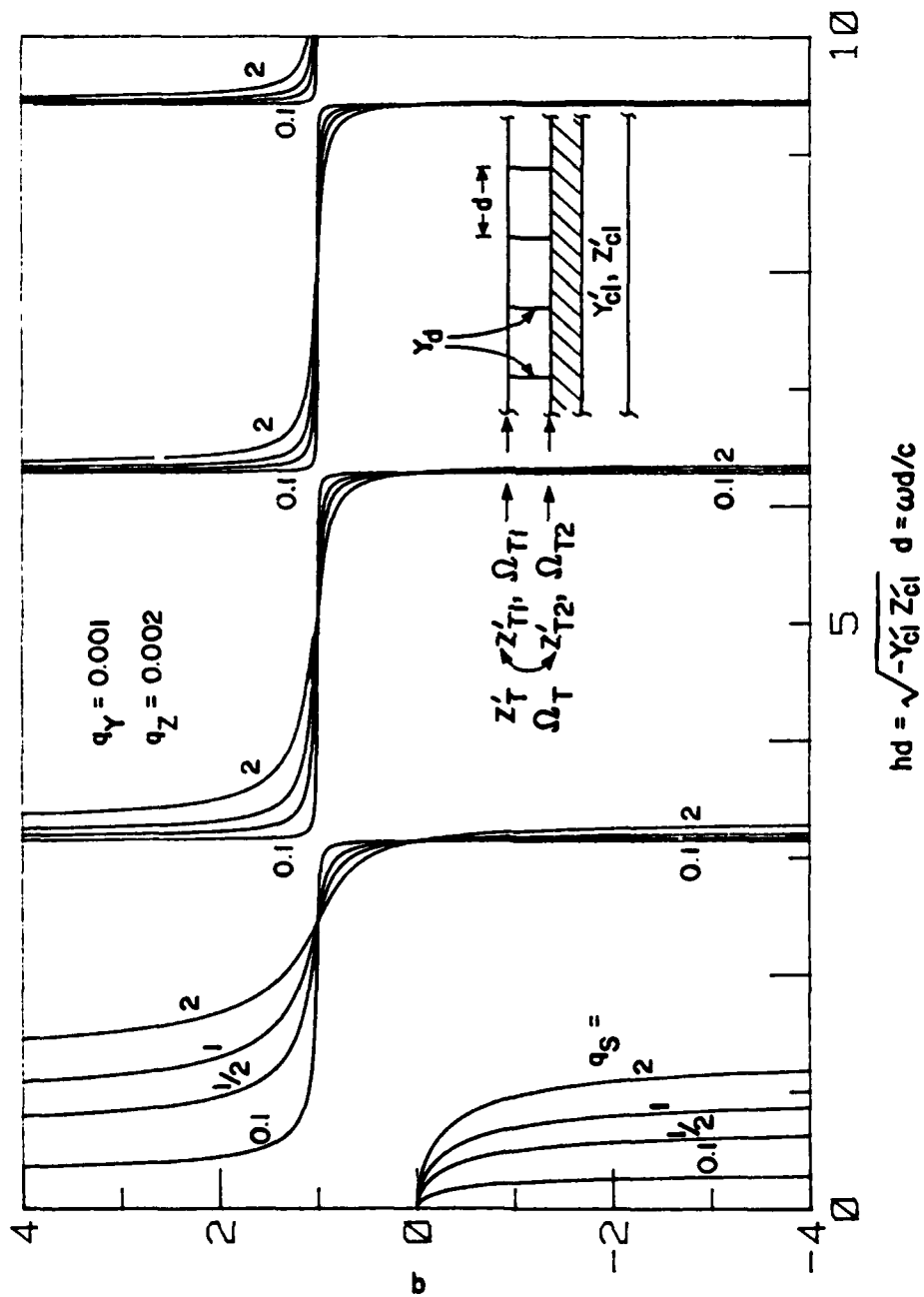


Figure 28. The values of "q", to be used in the circuit of Figure 26, versus frequencies for $q_Y = Y'_{cl} / Y'_{T1} = 0.001$, $q_Z = Z'_{T1} / Z'_{cl} = 0.002$ and various $q_S = Z'_{cl} Y'_d$.

and 28 are the same as those of Figures 18 through 25. From the figures, one can easily see that $q \approx 1$ when Conditions 53 and 54 are satisfied; that is, Equation 55 reduces to Equation 43. This is another proof that the simplified Equation 43 can be used for Equation 52 or 55 when the Conditions 53 and 54 are satisfied.

IV. SUMMARY

In this section, the results of Sections II and III are summarized and some examples are worked out to show how the results can be used.

1. DISCRETE EXCITATIONS

When the outer shield of a double-shield configuration is coupled to a localized voltage and/or current source (Figs. 1 and 3), one may employ the Floquet theorem to the periodic transmission-line equations to determine the disturbances propagating down the bonded double shield. A passband-stopband structure in the dispersion relation between ω and k is observed (Eq. 8 and Fig. 6). In the stopbands the disturbances decay exponentially away from the penetration point, whereas in the passbands the disturbances oscillate persistently. In the stopband the decaying constant can be easily determined from the dispersion relation. Curves of the decaying constant are plotted in Figure 7. At low frequencies the decaying constants can be calculated from the simple approximate Equations 9 and 10.

a. Voltage source (V_o^S , see Figs. 3b and 4a)

The voltage source can be calculated from

$$V_o^S = I_{sc} Z_{T1} \quad (59)$$

where I_{sc} is the short-circuit current on the outermost surface of the double shield, and Z_{T1} is the localized transfer impedance of the outer shield. This voltage source gives rise to V_s' and I_s' which are the voltage- and current-sources exciting the wires inside the inner shield. By defining a combined effective transfer impedance per unit length Z_{TV}' and a combined effective charge transfer frequency per unit length Ω_{TV}' as

$$Z_{TV}' = V_s' / I_{sc}$$

$$\Omega_{TV}' = j\omega I_s' / I_{sc}$$

one can fully describe the coupling through the bonded double shield due to a voltage source V_o^s (or I_{sc} , see Eq. 59). Z'_{TV} and Ω'_{TV} are averaged over the period d via Equation 20. The averaged quantities \bar{Z}'_{TV} and $\bar{\Omega}'_{TV}$ are given in Equation 21 and plotted in Figures 8 through 11 after normalized to their values for no bonding strap $(Z_{T1}Z'_{T2}(Z'_1/Y'_1)^{-1/2}/n_p$ and $Z_{T1}\Omega'_{T2}Y'_1/n_p$, respectively, where $n_p = 1$ for Figure 3b and $n_p = 2$ for Figure 4, Z'_{T2} and Ω'_{T2} are the coupling coefficients of the inner shield).

b. Current source (I_o^s , see Figs. 3b and 4b)

The current source can be calculated from

$$I_o^s = Q'_{sc} \Omega_{T1}^L \quad (60)$$

where Q'_{sc} is the short-circuit charge density on the outermost surface of the double shield and Ω_{T1}^L is the localized charge transfer frequency of the outer shield. This current source gives rise to different V'_s and I'_s (different from those due to V_o^s). By defining a combined effective transfer impedance Z_{TI} and a combined effective charge transfer frequency Ω_{TI} via

$$Z_{TI} = V'_s / (j\omega Q'_{sc})$$

$$\Omega_{TI} = I'_s / Q'_{sc}$$

one can describe the coupling through the bonded double shield due to a current source I_o^s (or Q'_{sc} , see Eq. 60). Z_{TI} and Ω_{TI} are also averaged via Equation 20. The averaged quantities \bar{Z}_{TI} and $\bar{\Omega}_{TI}$ are given in Equation 26 and plotted in Figures 12 and 13 after normalized to their values for no bonding strap $(\Omega_{T1}^L Z'_{T2} / (n_p j\omega), \Omega_{T1}^L \Omega'_{T2} / (cn_p)$ respectively).

Figures 8 through 13 (or, more generally, Eqs. 21 and 26) show that the absolute values of the normalized transfer quantities are less than one (where the bonding straps improve the shielding effectiveness) at some frequency ranges and greater than one at the others. The figures also show that the transfer quantities become infinite at $\omega d/c = n\pi$ ($n = 1, 2, 3, \dots$). The transfer quantities, however, are not given in the stopbands (also see Figs. 6 and 7) where they are extremely small far away from the penetration point.

From the above observations, one concludes that in order to have a better shielding effectiveness, the periodic bonding should be employed such that the important part of the EMP spectrum lies inside the first stopband. This can generally be realized by choosing an appropriate d when Y_d and Z'_1 are specified. Also, in order to have a broader first stopband and a greater decaying constant, one should try to make $Z'_1 Y_d$ larger.

c. Examples

For a coaxial double shield with outer radius $(b) = 5$ cm and inner radius $(a) = 3$ cm, one has

$$Z'_1 \approx j\omega L'_1 \approx \frac{j\omega\mu_0}{2\pi} \ln\left(\frac{b}{a}\right) \approx 10^{-7} j\omega \text{ } (\Omega/\text{m}) \quad (61)$$

i.e.,

$$L'_1 \approx 10^{-7} \text{ H/m}$$

Also, suppose that highly conducting wires of radius $t = 1$ mm are to be used for bonding, then,

$$Y_d \approx (j\omega L_d)^{-1} \approx (j\omega)^{-1} \frac{2\pi}{\mu_0(b-a)} \frac{1}{\ln(2(b-a)/t)} \quad (62)$$

$$\approx 6.7 \times 10^7 (j\omega)^{-1} \text{ } (\Omega)^{-1}$$

i.e.,

$$L_d \approx 1.5 \times 10^{-8} \text{ H}$$

Thus,

$$Z'_1 Y_d \approx 6.8 \text{ } (\text{m}^{-1})$$

The question now arises as to the spacing d to be used. Take $d = 0.6$ m and 0.3 m as given in Table 1. Both cases give rather wide first stopbands which cover the important EMP spectrum. However, the case of $d = 0.3$ m gives a wider first stopband and a larger decaying constant (note that a decaying constant of $1(\text{m}^{-1})$ corresponds to an attenuation of 8.7 dB/m).

Another important quantity is $Z_1'Y_d$, which should be made as large as possible for better shielding effectiveness. If the double shield is coaxial, one can use a smaller $(b-a)$ to obtain a larger $Z_1'Y_d$ (Eqs. 61 and 62). The case of $b=4$ cm and $d=0.6$ m is also given in Table 1. From the table, it is observed that the first stopband is wider and the decaying constant is larger for $b=4$ cm, $d=0.6$ m than the case for $b=5$ cm, $d=0.6$ m.

TABLE 1. EXAMPLES OF BONDED COAXIAL-CABLE SHIELDS

	b = 5 cm a = 3 cm t = 1 mm ($L_1' = 0.1 \mu\text{h/m}$, $L_d = 15 \text{ nh}$)		b = 4 cm a = 3 cm t = 1 mm ($L_1' = 57 \text{ nh/m}$, $L_d = 6 \text{ nh}$)
Period of Bondings	d = 0.3 m	d = 0.6 m	d = 0.6 m
$Z_1'Y_d (= L_1'/L_d)$	6.7 m^{-1}		9.6 m^{-1}
1st Stopband	0 \leftrightarrow 205 MHz	0 \leftrightarrow 137 MHz	0 \leftrightarrow 160 MHz
$ \text{Im}(k) $, Below 10 MHz	4.4 m^{-1}	2.9 m^{-1}	3.4 m^{-1}

2. DISTRIBUTED EXCITATIONS

Given the distributed transfer parameters of both the inner and outer shields (Figs. 2 and 14), the effective overall transfer parameters of the double shield can be represented by simple circuit diagrams. These circuit diagrams are summarized below.

a. Schelkunoff's circuit (Ref. 6)

When the shields are solid tubular conductors whose skin depths, linear cross-sectional dimensions and the period of the bonding straps are much smaller than the wavelength of the EMP disturbance, the effective transfer impedance of the double shield Z_T' (the effective charge transfer frequency Ω_T is, of course, zero) is independent of the bonding straps and can be calculated from the circuit depicted in Figure 15 or from Equation 30. The circuit elements in Figure 15 and Equation 30 are given in Equations 28 and 29, and also Equations 32 through 36 for some special cases. The circuit can be easily extended for a N-surface solid tubular shield with $N > 2$.

b. Casey's circuit (Ref. 7)

When (a) the skin depths of the shields are much greater than their thickness ($\delta \gg \Delta$, thin shields), (b) the linear cross-sectional dimensions of the double shield are much less than the wavelength of the EMP disturbance ($hb \approx \sqrt{-Y'_1 Z'_1} b \ll 1$), and (c) there is no bonding strap, then, Z'_T and Ω_T can be calculated from the circuit of Figure 16 or from Equation 42. The circuit elements in the figure and the equation are given in Equations 37, 38, 39, and 41.

When the shields are not thin, the circuit of Figure 17 (called the generalized Casey's circuit) can be used to replace that of Figure 16 for calculating Z'_T and Ω_T . Equation 42 is still applicable, except that the circuit element Z'_1 , originally given by Equation 41, becomes

$$Z'_1 = Z'_{a1} + Z'_{b2} + Z'_{c1}$$

Here, Z'_{a1} and Z'_{b2} are defined in a broader sense than Equation 28 to include all kinds of penetrations. Both circuits in Figures 16 and 17 can also be easily extended to describe a N-surface shield with $N > 2$.

c. General circuit

When there are periodic bondings connecting the shields, \bar{Z}'_T and $\bar{\Omega}_T$ (the average values of Z'_T and Ω_T over the period of the bondings) can be calculated from the circuit in Figure 26 or from Equation 55 (or equivalently, Equation 52). The constant q (qY_d/d may be named the effective shunt admittance per unit length of the bondings) in Equation 55 and Figure 26 is a complicated function of the shield and bonding parameters (Eqs. 56 through 58). However, when the conditions given in Equations 53 and 54 are met, q is approximately equal to 1, i.e., Equation 55 reduces to Equation 43. The truth of this statement is further supported by the curves in Figures 27 and 28 for q and the curves in Figures 18 through 25 for the normalized \bar{Z}'_T and $\bar{\Omega}_T$ (normalized to their corresponding values for no bonding strap, i.e., Equation 55 with $q = 0$). Actually, in Figures 18 through 25, the curves of Equation 43

agree with those based on the exact Equation 55 even in the region where $hd \lesssim q_S$ (i.e., the condition $hd \gg q_S$ in Equation 53 is violated, and q is quite different from one as shown in Figures 27 and 28), provided hd is not close to $n\pi$. One thus concludes that when $q_S \gtrsim 0.1$, $|hd - \sqrt{-Y'_1 Z'_1} d| \ll 1$ and hd is not close to $n\pi$ ($n=1,2,\dots$) Equation 43 or the circuit in Figure 26 with $q=1$ is a good approximation for calculating \bar{Z}'_T and $\bar{\Omega}'_T$.

From the results presented, one concludes that in order to shield against the distributed excitations more effectively, the periodic bondings should be implemented in such a way that $Z'_{cl} Y_d$ is large and $\omega d/c < \pi$ for the important parts of the EMP spectrum.

d. Examples

Consider a coaxial double shield (Fig. 2) with outer radius $b = 5$ cm, inner radius $a = 3$ cm and with highly conducting bonding straps of radius $t = 1$ mm. Also, take the practical values $q_Y = Y'_{cl}/Y'_{T1} = 0.004$ and $q_Z = Z'_{T1}/Z'_{cl} = 0.01$. Then,

$$Z'_{cl} Y_d \approx 6.7 \text{ (m}^{-1}\text{)}$$

from which

$$q_S = Z'_{cl} Y_d \approx \begin{cases} 2 & \text{for } d = 0.3 \text{ m} \\ 1 & \text{for } d = 0.15 \text{ m} \end{cases}$$

From Figures 20 and 21, one immediately sees that the normalized transfer functions are less than 0.1 (i.e., the bonding straps reduce the EMP penetration by more than 20 dB) for

$$\text{frequencies} < \begin{cases} 470 \text{ MHz} & \text{when } d = 0.3 \text{ m} \\ 940 \text{ MHz} & \text{when } d = 0.15 \text{ m} \end{cases}$$

Both 470 MHz and 940 MHz are extremely high to be important.

However, if the bonding straps between the coaxial double shield give a much smaller $Z'_{cl}Y_d$ value, say,

$$Z'_{cl}Y_d \approx 0.67 \text{ m}^{-1}$$

then, when $d = 0.15 \text{ m}$ is used the same quality in the shielding effectiveness as that of $Z'_{cl}Y_d \approx 6.7 \text{ m}^{-1}$ and $d = 0.15 \text{ m}$ can be obtained only for frequencies up to at most 300 MHz (see Fig. 18). Thus, bonding straps with greater $Z'_{cl}Y_d$ are preferred.

REFERENCES

1. Hart, W. C., et al., Team B Study Effort, Vol. II, AFWL-TR-80-36, Air Force Weapons Laboratory, Kirtland AFB, NM, August 1981.
2. Lam, J., "Propagation Characteristics of a Periodically Loaded Transmission Line," Interaction Notes, Note 302, Air Force Weapons Laboratory, Kirtland AFB, NM, November 1976.
3. Gradshteyn, I. S., and I. W. Ryzhik, Table of Integrals, Series and Products, Academic Press, New York and London, 1965.
4. Lee, K. S. H., Editor, EMP Interaction: Principles, Techniques and Reference Data, EMP Interaction Notes, Note 2-1, Air Force Weapons Laboratory, Kirtland AFB, NM, 1979.
5. Lee, K. S. H., and C. E. Baum, "Application of Modal Analysis to Braided-Shield Cables," IEEE Trans. on EMC, Vol. EMC-17, No. 3, August 1975, also Interaction Notes, Note 132, Air Force Weapons Laboratory, Kirtland AFB, NM, January 1973.
6. Schelkunoff, S. A., "The Electromagnetic Theory of Coaxial Transmission Lines and Cylindrical Shields," Bell Syst. Tech. J., Vol. 13, October 1934.
7. Casey, K. F., "On the Effective Transfer Impedance of Thin Coaxial Cable Shields," IEEE Trans. on EMC, Vol. EMC-18, No. 3, August 1976, also, Interaction Notes, Note 267, Air Force Weapons Laboratory, Kirtland AFB, NM, March 1976.

PART II

MULTISURFACE SHIELDED ENCLOSURES WITH
PARTICULAR REFERENCE TO BONDING BETWEEN SHIELDS

PREFACE

I would like to thank W.S. Kehrer, C.E. Baum, J.P. Castillo and K.C. Chen of the Air Force Weapons Laboratory for their interest and suggestions in this report. Sections V and VI were worked out in collaboration with F.C. Yang of Dikewood.

CONTENTS

<u>Section</u>		<u>Page</u>
I	INTRODUCTION	71
II	SPHERICAL SHIELDS	73
	1. Two Spherical Shields	73
	2. N Spherical Shields	79
III	CYLINDRICAL SHIELDS	83
IV	EQUIVALENT CIRCUIT REPRESENTATION - GENERALIZATION TO SHIELDS OF ARBITRARY SHAPE	87
V	TWO SPHERICAL SHIELDS OF ARBITRARY ELECTRICAL THICKNESS	93
VI	EFFECT OF BONDING	96
VII	CONCLUSIONS	105
	REFERENCES	106
	APPENDIX A - THE CONSTANTS	107
	APPENDIX B - CALCULATION OF ψ_{OAB}	109

ILLUSTRATIONS

<u>Figure</u>		<u>Page</u>
1	Problems for discussion	72
2	Two-surface spherical enclosure: (a) Two spherical shields in a slowly varying magnetic field; (b) Equivalent of (a) with appropriate boundary conditions.	74
3	Frequency spectrum of the ratio $ \tilde{H}_1/\tilde{H}_0 $.	76
4	Time behavior of the penetrant field for an impulse external field.	78
5	Multisurface spherical shields.	80
6	Frequency spectrum asymptotes and break points where $\bar{\omega}_1$, $\bar{\omega}_2$, $\bar{\omega}_3$ are given in Table 1 ($\bar{\omega}_1 = \bar{s}_1 $, $\bar{\omega}_2 = \bar{s}_2 $, etc.).	81
7	Multisurface cylindrical shields.	84
8	Frequency spectrum asymptotes and break points given in Table 2.	86
9	Equivalent circuits of a spherical shield.	88
10	Equivalent circuit of a two-surface enclosure.	91
11	Frequency spectrum of the transfer function $ \tilde{H}_1/\tilde{H}_0 $ for two electrically thick spherical shields ($\Delta_1 = \Delta_2$, $\Delta_2/a_2 = \pi \times 10^{-3}$).	95
12	Different arrangements of conducting straps bonding two spherical shields.	97
13	A two-spherical shield enclosure with two bonding straps lying in the equatorial plane perpendicular to the external magnetic field H_0 .	98
14	Frequency spectrum of the bonding strap current. The normalizing factor is \tilde{V}_0/R_s , where $\tilde{V}_0 = F\tilde{H}_0/\tau_2$. $F\tilde{H}_0$ is equal to the flux linking the two triangles by the external field.	101

ILLUSTRATIONS (Continued)

<u>Figure</u>		<u>Page</u>
15	Time behavior of the bonding strap current due to an impulsive external magnetic field $H_0 \delta(t)$. The normalizing factor is V_0/R_s with $V_0 = FH_0/\tau_2^2$. Note that H_0 has the dimension of ampere-second.	102
16	Time behavior of the time rate of change of the bonding strap current due to an impulsive external field $H_0 \delta(t)$. The normalizing factor is $V_0/R_s \tau_2$. The numbers in parenthesis indicate the values the curves intercept the ordinate axis.	103
B1	Geometry for calculating the flux ψ_{OAB} .	110

TABLES

<u>Table</u>		<u>Page</u>
1	s-plane poles for two-surface and three-surface spherical enclosures. The values are for $\bar{s} = \tau_1 s$ with $\alpha = a_2/a_1 = a_3/a_2$ and $\tau_2/\tau_1 = \tau_3/\tau_2 = \alpha$.	81
2	s-plane poles for two-surface and three-surface cylindrical shields. The values are for $\bar{s} = st_1$ with $\beta = b_2/b_1 = b_3/b_2$ and $t_2/t_1 = t_3/t_2 = \beta$.	86
3	Peak values for I_b and \dot{I}_b .	104

I. INTRODUCTION

One of the most effective methods of protecting a system from undesirable EMP effects is by use of shielding. Although the basic principles of shielding for a single-surface enclosure are well understood (Ref. 1), the extension of these principles to multisurface enclosures is by no means straightforward. Unique to multisurface shielding is the mutual interaction among the shields, which may degrade the intended shielding performance of the enclosure. Another unique feature is the bonding that is often employed between the shields in order to reduce electrostatic hazards. This bonding practice may have an adverse effect on the protection of a shielded enclosure against magnetic-field penetration. The effects of shield-shield interaction and bonding will be treated in this report.

Figure 1 shows various topics that will be addressed in this report. In Section II, the problem of two concentric spherical shields will be solved using the theory of inductive shielding (Ref.1), and the results will be generalized to N-surface spherical shields. The corresponding results for cylindrical shields will be presented in Section III. Equivalent circuits will be constructed in Section IV to interpret the analytical results for a two-surface spherical enclosure; the results will be generalized to two-surface enclosures of arbitrary shape. In Section VI the effect of bonding on magnetic-field penetration into a two-surface enclosure will be discussed. Finally, the most important results are summarized in Section VII.

The underlying assumptions of inductive shielding are (1) the electric field is neglected everywhere except in the enclosure's wall where it is related to the induced current by Ohm's law, and (2) the wall thickness is much smaller than the typical linear dimension of the enclosure. In addition, this report assumes the wall thickness to be smaller than the wall's skin depth, except in Section V where this assumption is removed.

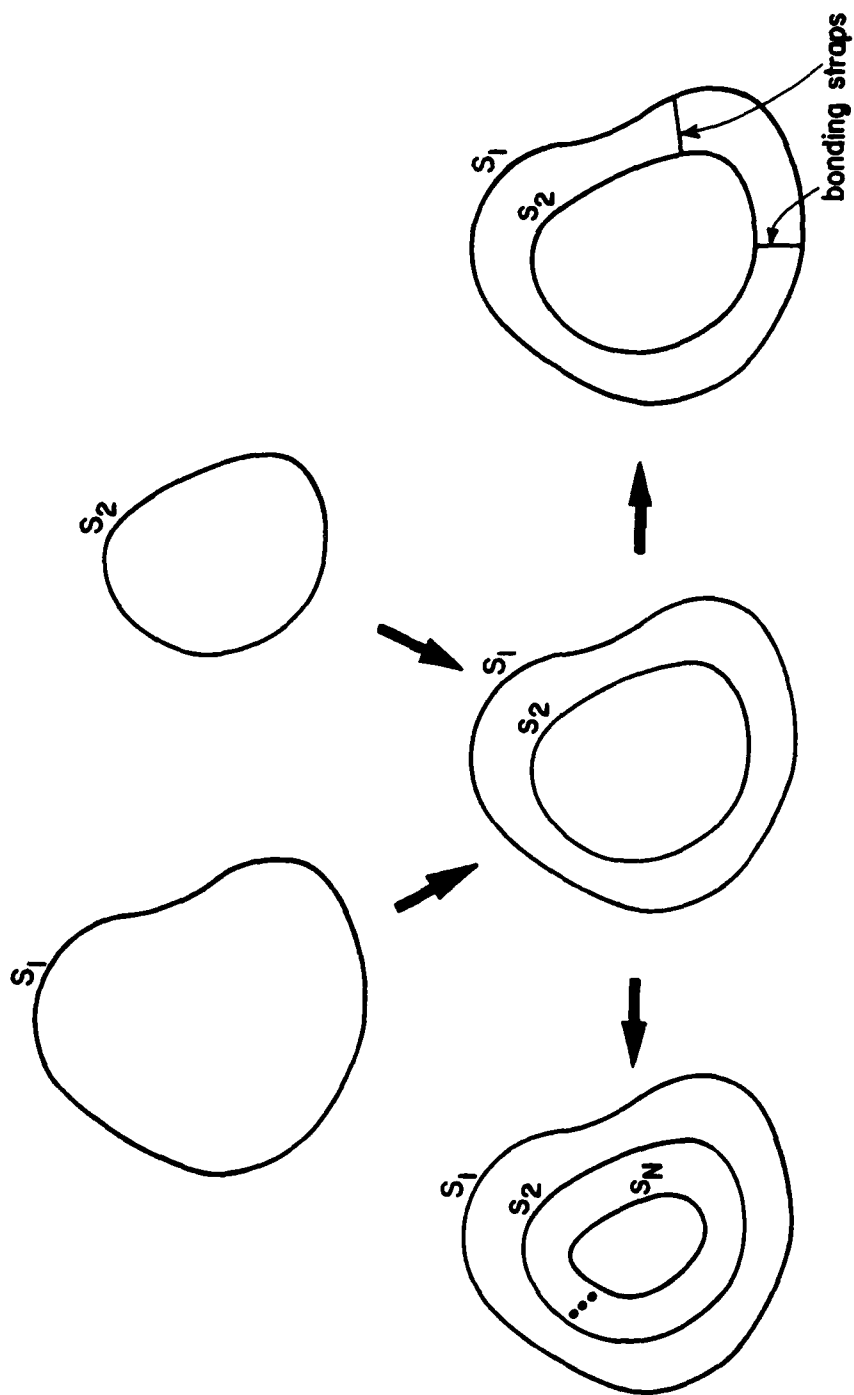


Figure 1. Problems for discussion.

II. SPHERICAL SHIELDS

In this section, the problem of two concentric spherical shells will first be treated with explicit simple engineering results given in frequency and time domains. The results for two shells will then be generalized to N concentric spherical shells. Discussions of equivalent circuits, generalization to shields of arbitrary shape, and effects of electrical bonding between the shells will be relegated to later sections.

1. TWO SPHERICAL SHIELDS

Figures 2a and 2b show an enclosure with two concentric spherical shields immersed in a slowly varying magnetic field $H_0(t)$. Insofar as the penetrant field $H_1(t)$ is concerned, one may replace Figure 2a with Figure 2b with appropriate boundary conditions that duplicate the shielding properties of the walls (Ref. 1). The magnetic scalar potential ϕ for the three regions shown in Figure 2b takes the form

$$\begin{aligned}\phi_1 &= -\tilde{H}_0 r \cos\theta + A \frac{a_1^3}{r^2} \cos\theta & r \geq a_1 \\ \phi_2 &= B r \cos\theta + C \frac{a_1^3}{r^2} \cos\theta & a_1 \geq r \geq a_2 \\ \phi_3 &= D r \cos\theta & r \leq a_2\end{aligned}\tag{1}$$

where \tilde{H}_0 is the Laplace transform of $H_0(t)$. The constants A , B , C and D are determined by the following boundary conditions (Ref. 1 and Appendix A):

$$\begin{aligned}\frac{\partial}{\partial r} \phi_1 &= \frac{\partial}{\partial r} \phi_2, & \text{at } r = a_1 \\ \frac{\partial}{\partial r} \phi_2 &= \frac{\partial}{\partial r} \phi_3, & \text{at } r = a_2\end{aligned}\tag{2}$$

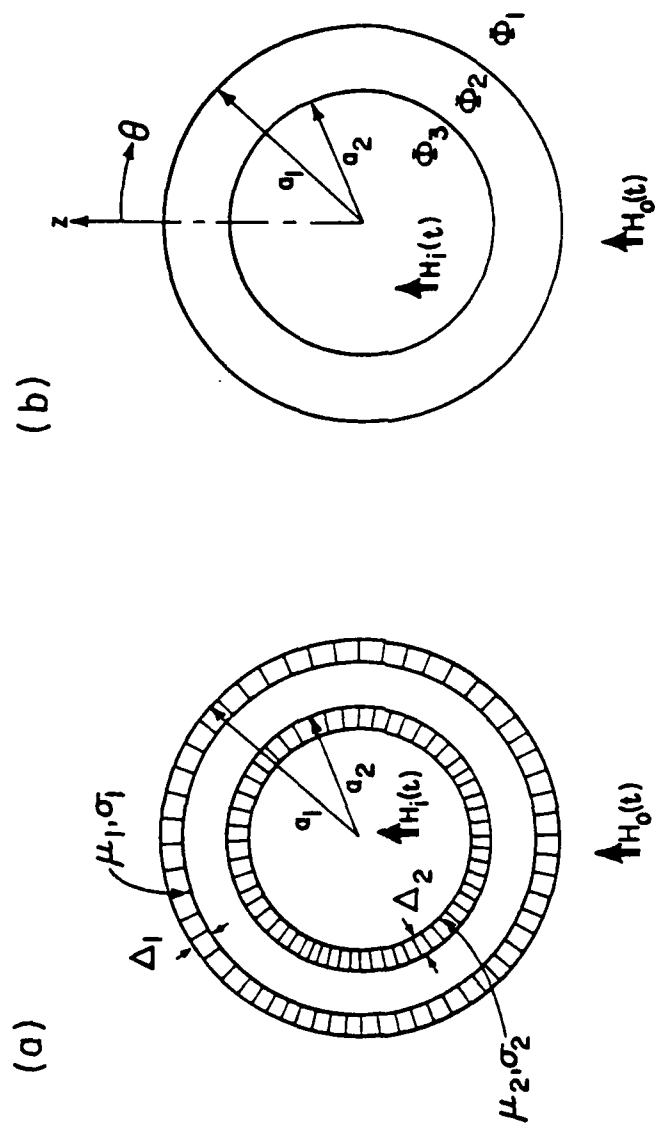


Figure 2. Two-surface spherical enclosure: (a) Two spherical shields in a slowly varying magnetic field; (b) Equivalent of (a) with appropriate boundary conditions.

$$\begin{aligned}\nabla_s^2 (\phi_2 - \phi_1) &= s\mu_o \Delta_1 \sigma_1 \frac{\partial}{\partial r} \phi_1, & \text{at } r=a_1 \\ \nabla_s^2 (\phi_3 - \phi_2) &= s\mu_o \Delta_2 \sigma_2 \frac{\partial}{\partial r} \phi_2, & \text{at } r=a_2\end{aligned}\quad (3)$$

Equations 2 mean that the normal component of the magnetic field is continuous across the shield, while Equations 3 state that its tangential component is discontinuous by the amount of the current induced in the shield. From Equations 1 through 3 one finds that

$$\frac{\tilde{H}_1}{\tilde{H}_o} = \frac{1}{(1+\tau_1 s)(1+\tau_2 s) - (a_2/a_1)^3 \tau_1 \tau_2 s^2} \quad (4)$$

with

$$\begin{aligned}\tau_1 &= \frac{1}{3} \mu_o a_1 \sigma_1 \Delta_1 \\ \tau_2 &= \frac{1}{3} \mu_o a_2 \sigma_2 \Delta_2\end{aligned}\quad (5)$$

If no interaction between the shields is assumed, Equation 4 becomes

$$\left. \frac{\tilde{H}_1}{\tilde{H}_o} \right|_{\text{no int}} = \frac{1}{(1+\tau_1 s)(1+\tau_2 s)} \quad (6)$$

as one would expect, since Equation 6 is the product of the transfer function of each individual shield. Equations 4 and 6 are plotted in Figure 3.

The time-domain solution of Equation 4 is

$$\frac{H_1(t)}{H_o} = \frac{1}{\sqrt{(\tau_1 - \tau_2)^2 + 4\tau_1 \tau_2 a^3}} \left(e^{-t/T_1} - e^{-t/T_2} \right) \quad (7)$$

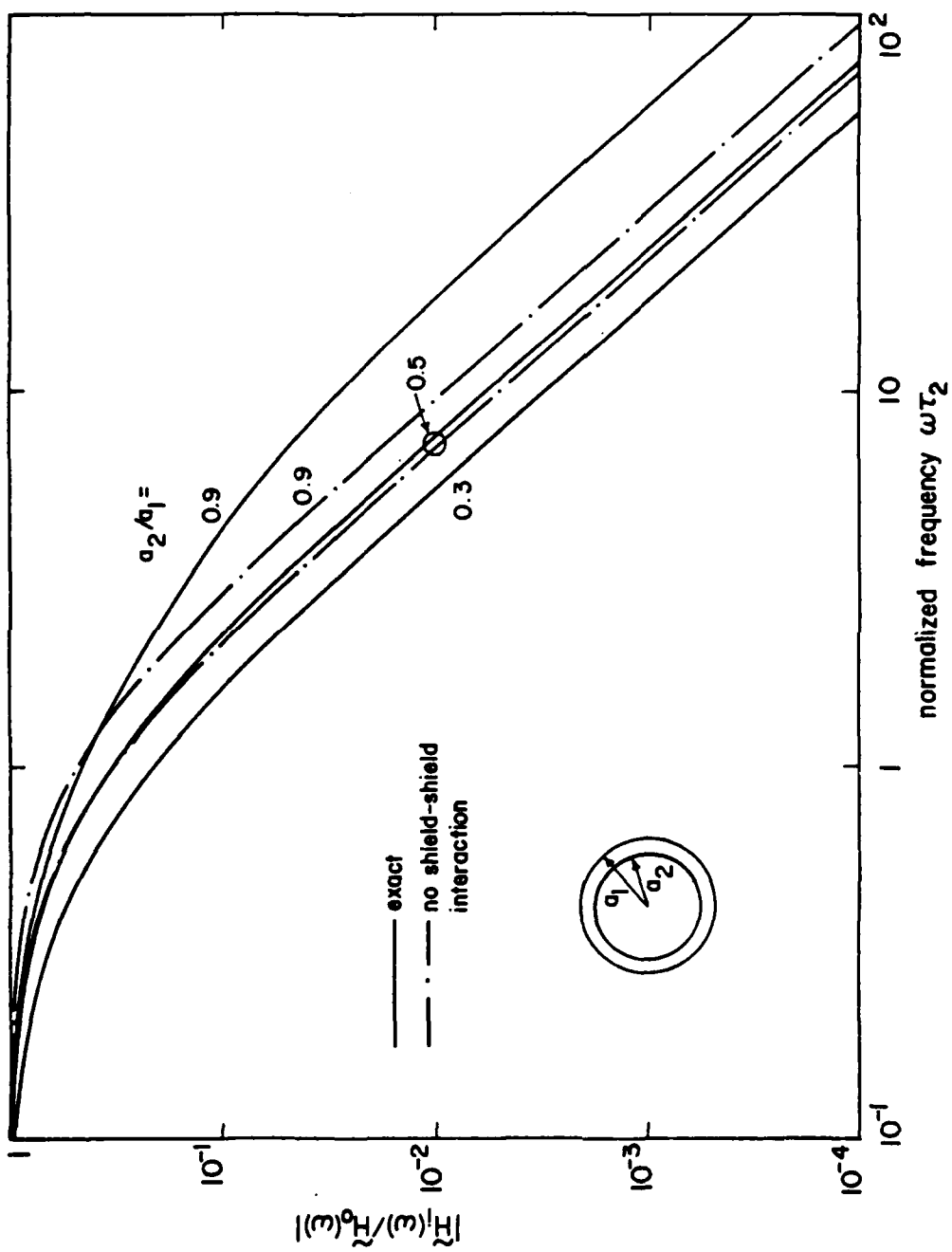


Figure 3. Frequency spectrum of the ratio $|\tilde{H}_1/\tilde{H}_0|$.

where

$$T_{1,2} = \frac{2\tau_1\tau_2(1-\alpha^3)}{\tau_1 + \tau_2 \mp \sqrt{(\tau_1 - \tau_2)^2 + 4\tau_1\tau_2\alpha^3}} \quad (8)$$

and $\alpha = a_2/a_1$, while the time-domain solution of Equation 6 is

$$\left. \frac{H_1(t)}{H_0} \right|_{\text{no int}} = \frac{1}{\tau_1 - \tau_2} \left(e^{-t/\tau_1} - e^{-t/\tau_2} \right) \quad (9)$$

Here, H_0 is the impulse strength of the external fields, and for most applications can be taken to be the time-integral of the magnetic field of a typical high-altitude EMP (Ref. 1).

Equations 7 and 9 are plotted in Figure 4 where one may see that for the case $a_2/a_1 = 0.9$, the neglect of shield-shield interaction amounts to 20% underestimate of the penetrant field.

From the viewpoint of the EMP hardness designer the currents induced in each enclosure's shield are important, since they are the only means to prevent the external field from penetrating into the interior of the enclosure. Let $\tilde{K}_{1\phi}$ and $\tilde{K}_{2\phi}$ denote the induced sheet currents in first and second shields of Figure 2. Then, from Equations 1 through 3 one obtains

$$\begin{aligned} \tilde{K}_{1\phi} &= \frac{1}{a_1} \frac{\partial \phi_2}{\partial \theta} - \frac{1}{a_1} \frac{\partial \phi_1}{\partial \theta} \quad (\text{at } r = a_1) \\ &= -\frac{3}{2} \tilde{H}_0 \frac{\tau_1 s(1 + \tau_2 s) - \alpha^3 \tau_1 \tau_2 s^2}{(1 + \tau_1 s)(1 + \tau_2 s) - \alpha^3 \tau_1 \tau_2 s^2} \sin \theta \end{aligned} \quad (10)$$

$$\begin{aligned} \tilde{K}_{2\phi} &= \frac{1}{a_2} \frac{\partial \phi_3}{\partial \theta} - \frac{1}{a_2} \frac{\partial \phi_2}{\partial \theta} \quad (\text{at } r = a_2) \\ &= -\frac{3}{2} \tilde{H}_0 \frac{\tau_2 s}{(1 + \tau_1 s)(1 + \tau_2 s) - \alpha^3 \tau_1 \tau_2 s^2} \sin \theta \end{aligned} \quad (11)$$

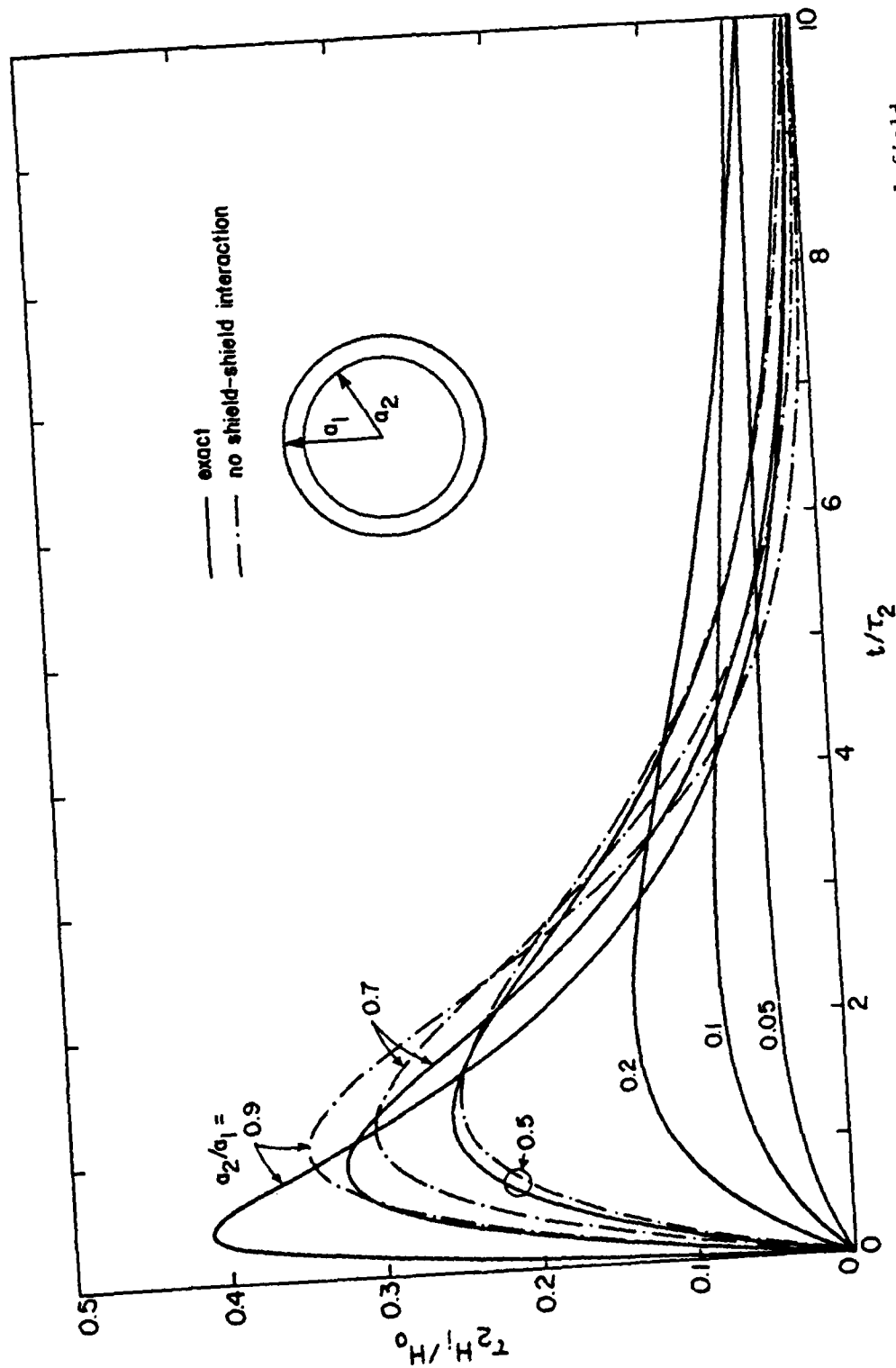


Figure 4. Time behavior of the penetrant field for an impulse external field.

These expressions for the currents will give a clue to construct equivalent circuits in Section IV.

2. N SPHERICAL SHIELDS

Let $\tilde{H}_i^{(2)}$, $\tilde{H}_i^{(3)}$, ... $\tilde{H}_i^{(N)}$ denote, respectively, the field that penetrates into a two-surface, three-surface, ... N-surface spherical enclosure.

For a two-surface enclosure Equation 4 gives

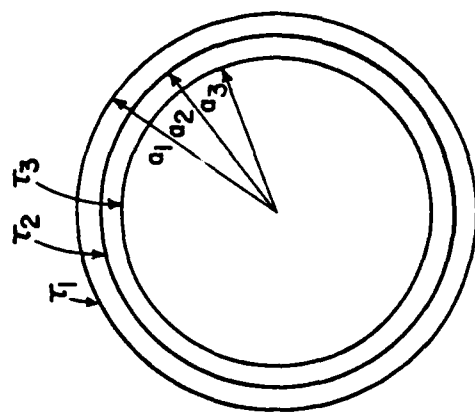
$$\begin{aligned}\tilde{H}_0/\tilde{H}_i^{(2)} &= (1 + \tau_1 s)(1 + \tau_2 s) - \left(\frac{a_2}{a_1}\right)^3 \tau_1 \tau_2 s^2 \\ &= 1 + (\tau_1 + \tau_2)s + \left[1 - (a_2/a_1)^3\right] \tau_1 \tau_2 s^2\end{aligned}\quad (12)$$

For a three-surface shielded enclosure (Fig. 5a) one uses the same, although more complicated, procedure for the two-surface enclosure and finds

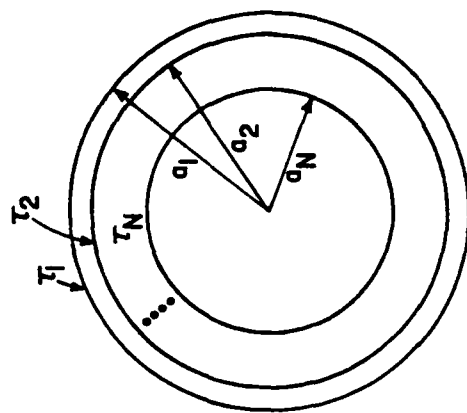
$$\begin{aligned}\tilde{H}_0/\tilde{H}_i^{(3)} &= 1 + (\tau_1 + \tau_2 + \tau_3)s + \left[1 - (a_2/a_1)^3\right] \tau_1 \tau_2 s^2 + \left[1 - (a_3/a_2)^3\right] \tau_2 \tau_3 s^2 \\ &\quad + \left[1 - (a_3/a_1)^3\right] \tau_3 \tau_1 s^2 + \left[1 - (a_2/a_1)^3\right] \left[1 - (a_3/a_2)^3\right] \tau_1 \tau_2 \tau_3 s^3\end{aligned}\quad (13)$$

The poles of $\tilde{H}_i(s)$ in the complex s -plane for two and three spherical shields are given in Table 1. These poles will immediately enable one to plot the frequency spectrum of the penetrant field, since they are the "break points" in the log-log scale plot (Fig. 6). From the table it is clear that as the second and/or the third shield get closer to the outer shield, the pole corresponding to the outermost shield moves toward the $j\omega$ -axis away from its unperturbed value -1 , while the pole corresponding to the second (third) shield (the second (third) column of Table 1) moves away from its unperturbed value $-1/\alpha$ ($-1/\alpha^2$) further away from the $j\omega$ -axis.

For an N-surface spherical enclosure (Fig. 5b) one can write down, on a close examination of Equations 12 and 13,



(a) Three-surface spherical enclosure



(b) N-surface spherical enclosure

Figure 5. Multisurface spherical shields.

TABLE 1. s -PLANE POLES FOR TWO-SURFACE AND THREE-SURFACE SPHERICAL ENCLOSURES. THE VALUES ARE FOR $\bar{s} = \tau_1 s$ WITH $\alpha = a_2/a_1 = a_3/a_2$ AND $\tau_2/\tau_1 = \tau_3/\tau_2 = \alpha$

α	Two Shields		Three Shields		
	\bar{s}_1	\bar{s}_2	\bar{s}_1	\bar{s}_2	\bar{s}_3
0.1	- 1.00	-10.01	- 1.00	-10.01	-100.11
0.2	- 1.00	- 5.05	- 1.00	- 5.04	- 25.25
0.3	- 0.99	- 3.46	- 0.99	- 3.43	- 11.55
0.4	- 0.96	- 2.77	- 0.96	- 2.67	- 6.96
0.5	- 0.91	- 2.52	- 0.90	- 2.29	- 5.10
0.6	- 0.83	- 2.57	- 0.79	- 2.13	- 4.49
0.7	- 0.73	- 2.96	- 0.66	- 2.17	- 4.72
0.8	- 0.65	- 3.96	- 0.53	- 2.56	- 6.03
0.9	- 0.57	- 7.22	- 0.42	- 4.10	- 10.81

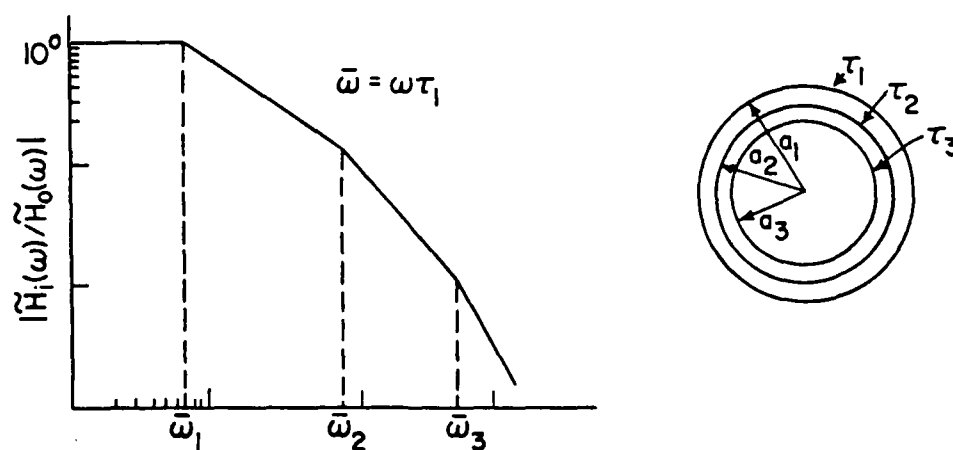


Figure 6. Frequency spectrum asymptotes and break points where $\bar{\omega}_1$, $\bar{\omega}_2$, $\bar{\omega}_3$ are given in Table 1 ($\bar{\omega}_1 = |\bar{s}_1|$, $\bar{\omega}_2 = |\bar{s}_2|$, etc.).

$$\begin{aligned}
\tilde{H}_0/\tilde{H}_i^{(N)} &= 1 + s \sum_{i=1}^N \tau_i + s^2 \sum_{i>j}^N \left[1 - (a_i/a_j)^3 \right] \tau_i \tau_j + \dots \\
&\dots + s^N \prod_{i=1}^N \left[1 - (a_i/a_{i-1})^3 \right] \tau_i
\end{aligned} \tag{14}$$

where $a_0 = \infty$. As expected, $\tilde{H}_i^{(N)}$ has N poles lying on the negative real axis of the s -plane.

III. CYLINDRICAL SHIELDS

The procedure of solving the problem of a multisurface cylindrical shield where the external magnetic field is perpendicular to the axis of the shield follows exactly that of the spherical shield described in Section II. The other polarization where the external magnetic field is parallel to the axis of the shield is treated in Reference 2. From the geometry depicted in Figures 7a,d one can immediately write down

$$\begin{aligned}\phi_1 &= -\tilde{H}_0 \rho \cos\phi + \frac{A}{\rho} \cos\phi & \rho &\geq b_1 \\ \phi_2 &= B\rho \cos\phi + \frac{C}{\rho} \cos\phi & b_1 &\geq \rho \geq b_2 \\ \phi_3 &= D\rho \cos\phi & \rho &\leq b_2\end{aligned}\quad (15)$$

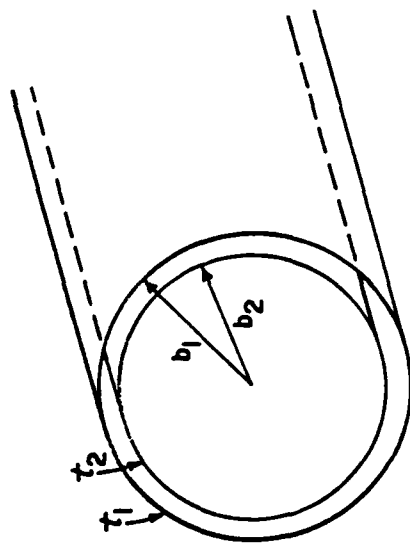
Applying at $\rho = b_1$ and $\rho = b_2$ the boundary conditions (Ref.1)

$$\begin{aligned}\frac{\partial}{\partial \rho} \phi_1 &= \frac{\partial}{\partial \rho} \phi_2 & \rho &= b_1 \\ \frac{\partial}{\partial \rho} \phi_2 &= \frac{\partial}{\partial \rho} \phi_3 & \rho &= b_2 \\ \nabla_s^2(\phi_2 - \phi_1) &= st_1 \frac{\partial}{\partial \rho} \phi_1 & \rho &= b_1 \\ \nabla_s^2(\phi_3 - \phi_2) &= st_2 \frac{\partial}{\partial \rho} \phi_2 & \rho &= b_2\end{aligned}\quad (16)$$

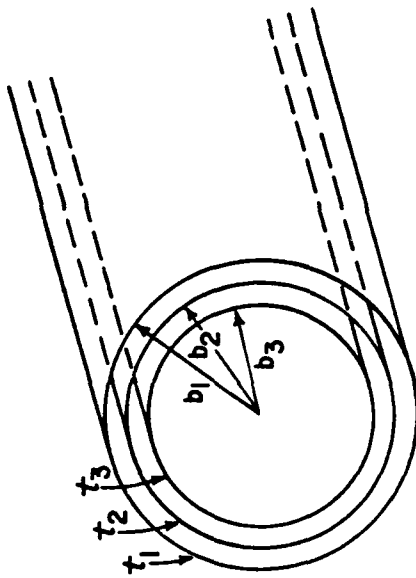
to Equations 15 one gets

$$\frac{\tilde{H}_1(s)}{\tilde{H}_0(s)} = \frac{1}{(1+st_1)(1+st_2) - (b_2/b_1)^2 t_1 t_2 s^2}\quad (17)$$

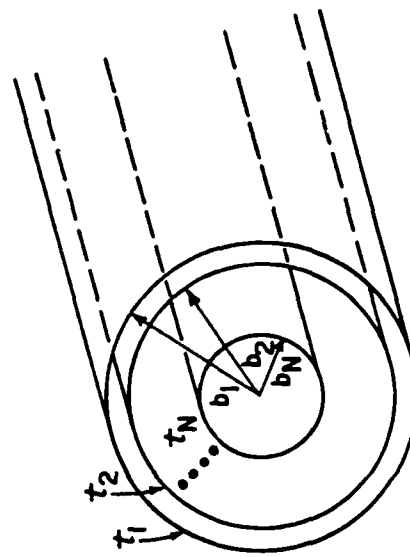
where



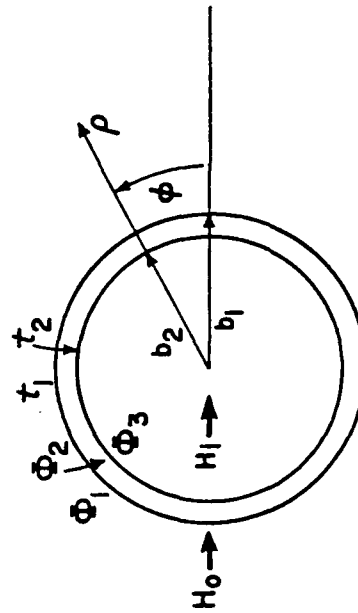
(a) Two-surface cylindrical shield



(b) Three-surface cylindrical shield



(c) N-surface cylindrical shield



(d) Cross section of (a)

Figure 7. Multisurface cylindrical shields.

$$t_1 = \frac{1}{2} \mu_o b_1 \sigma_1 \Delta_1 \quad (18)$$

$$t_2 = \frac{1}{2} \mu_o b_2 \sigma_2 \Delta_2$$

Similarly, for a three-surface cylindrical shield (Fig. 7b) one has

$$\begin{aligned} \tilde{H}_o(s)/\tilde{H}_1^{(3)}(s) = & 1 + (t_1 + t_2 + t_3)s + \left[1 - (b_2/b_1)^2\right]t_1 t_2 s^2 + \left[1 - (b_3/b_2)^2\right]t_2 t_3 s^2 \\ & + \left[1 - (b_3/b_1)^2\right]t_3 t_1 s^2 + \left[1 - (b_2/b_1)^2\right]\left[1 - (b_3/b_2)^2\right]t_1 t_2 t_3 s^3 \end{aligned} \quad (19)$$

and for an N-surface cylindrical shield (Fig. 7c) one has

$$\begin{aligned} \tilde{H}_o(s)/\tilde{H}_1^{(N)}(s) = & 1 + s \sum_{i=1}^N t_i + s^2 \sum_{i>j}^{N,N} \left[1 - (b_i/b_j)^2\right] t_i t_j + \dots \\ & \dots + s^N \prod_{i=1}^N \left[1 - (b_i/b_{i-1})^2\right] t_i \end{aligned} \quad (20)$$

where $b_o = \infty$. A comparison of Equations 17 through 20 with Equations 4, 5, 13, and 14 reveals that the results for spherical shields obtained in the last section can be directly used for cylindrical shields if one replaces

<u>spherical shields</u>		<u>cylindrical shields</u>
$(a_i/a_j)^3$	by	$(b_i/b_j)^2$
τ_i	by	t_i

Therefore, in the following two sections on equivalent-circuit representation and effects of bonding, discussions will be restricted only to the case of spherical shields.

Table 2 gives the s-plane poles for \tilde{H}_1 for two and three cylindrical shields, while Figure 8 shows the frequency spectrum asymptotes and break points for $|\tilde{H}_1/\tilde{H}_o|$.

TABLE 2. s-PLANE POLES FOR TWO-SURFACE AND THREE-SURFACE CYLINDRICAL SHIELDS. THE VALUES ARE FOR $\bar{s} = st_1$ WITH $\beta = b_2/b_1 = b_3/b_2$ AND $t_2/t_1 = t_3/t_2 = \beta$

β	Two Shields		Three Shields		
	\bar{s}_1	\bar{s}_2	\bar{s}_1	\bar{s}_2	\bar{s}_3
0.1	- 1.00	-10.11	- 1.00	-10.10	-101.12
0.2	- 0.99	- 5.26	- 0.99	- 5.21	- 26.30
0.3	- 0.96	- 3.80	- 0.96	- 3.66	- 12.68
0.4	- 0.92	- 3.25	- 0.91	- 2.98	- 8.20
0.5	- 0.85	- 3.15	- 0.82	- 2.67	- 6.51
0.6	- 0.77	- 3.40	- 0.71	- 2.60	- 6.13
0.7	- 0.69	- 4.07	- 0.59	- 2.80	- 6.74
0.8	- 0.62	- 5.63	- 0.49	- 3.47	- 8.85
0.9	- 0.55	-10.56	- 0.40	- 5.85	- 16.09

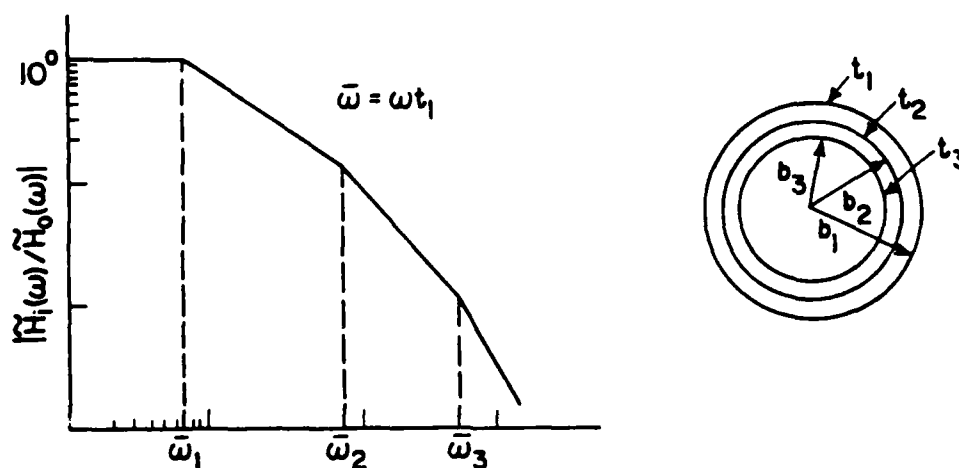


Figure 8. Frequency spectrum asymptotes and break points given in Table 2.

IV. EQUIVALENT CIRCUIT REPRESENTATION - GENERALIZATION TO SHIELDS OF ARBITRARY SHAPE

The results obtained in the last two sections will be interpreted in terms of equivalent circuits in this section. The advantages of equivalent circuit representation of mathematical results are two-fold: (1) it is useful for interpreting results and understanding physical mechanism involved, and (2) it is a quick way to generalize the results for specific shapes of enclosure to arbitrary shapes of enclosure.

To gain more familiarity with what follows one starts with one-surface spherical shielded enclosure (Fig. 9a) whose low-frequency transfer function is (Ref. 1)

$$\frac{\tilde{H}_1(s)}{\tilde{H}_0(s)} = \frac{1}{1+\tau s} \quad (21)$$

with

$$\tau = \frac{1}{3} \mu_0 a \sigma \Delta \quad (22)$$

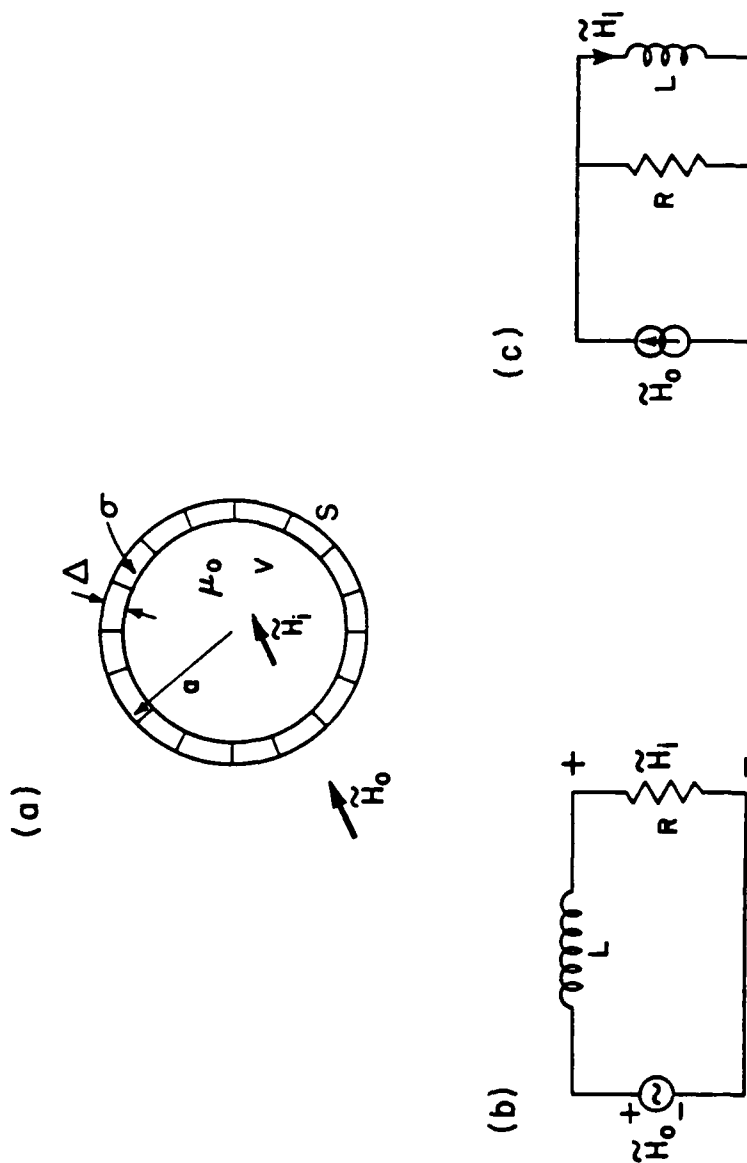
where μ_0 , σ , a and Δ are defined in Figure 9a. Equation 21 can be represented by either the equivalent circuit of Figure 9b or Figure 9c where

$$L = \frac{1}{3} \mu_0 a, \quad R = \frac{1}{\sigma \Delta} \quad (23)$$

The inductance L can be expressed in terms of the volume V and the surface S of the enclosure as

$$L = \mu_0 V/S \quad (24)$$

which also applies directly to cylindrical as well as two-parallel-plate enclosures (Ref.1). Equation 21 can thus be used as the transfer function of a single-surface shielded enclosure of arbitrary shape if τ is interpreted as



$$\frac{\vec{H}_1}{\vec{H}_0} = \frac{R}{R + sL}$$

Figure 9. Equivalent circuits of a spherical shield.

$$\tau = \frac{L}{R} \quad (25)$$

with L given by Equation 24 and R by $(\sigma\Delta)^{-1}$.

The extension of the equivalent circuit given in either Figure 9b or 9c for a single-surface enclosure to a two-surface enclosure turns out to be a nontrivial matter. In principle, one may start with the transfer function given in Equation 4 and constructs an equivalent circuit for it using the techniques known in circuit synthesis (Ref. 3). This approach, however, does not easily lead to a circuit which represents the actual physical phenomenon of the problem. To derive the desirable circuit one returns to the induced currents in the shields given by Equations 10 and 11. The total induced current in each shield is obtained by integrating Equations 10 and 11. Thus,

$$\tilde{I}_1 = \int_0^\pi \tilde{K}_{1\phi} a_1 d\theta = -3\tilde{H}_0 a_1 \frac{\tau_1 s(1+\tau_2 s) - \alpha^3 \tau_1 \tau_2 s^2}{(1+\tau_1 s)(1+\tau_2 s) - (a_2/a_1)^3 \tau_1 \tau_2 s^2} \quad (26)$$

$$\tilde{I}_2 = \int_0^\pi \tilde{K}_{2\phi} a_2 d\theta = -3\tilde{H}_0 a_2 \frac{\tau_2 s}{(1+\tau_1 s)(1+\tau_2 s) - \alpha^3 \tau_1 \tau_2 s^2} \quad (27)$$

To generalize Equations 26 and 27 to two-surface enclosures of arbitrary shape one simply sets

$$\tau_1 = \frac{L_1}{R_1}, \quad \tau_2 = \frac{L_2}{R_2}, \quad \alpha^3 \tau_1 \tau_2 = M^2/(R_1 R_2) \quad (28)$$

where the self-inductances L_1, L_2 , the mutual inductance M , and the resistances R_1, R_2 are given by

$$L_1 = \frac{\mu_0 V_1}{S_1}, \quad L_2 = \frac{\mu_0 V_2}{S_2}, \quad M^2 = \frac{V_2}{V_1} L_1 L_2 \quad (29)$$

$$R_1 = \frac{1}{\sigma_1 \Delta_1}, \quad R_2 = \frac{1}{\sigma_2 \Delta_2}$$

Here, V_1 and V_2 are the volumes enclosed respectively by the surfaces S_1 and S_2 of the first and second shield. Equations 26 and 27 can be written in the general form

$$\tilde{I}_1 = \frac{sL_1(sL_2 + R_2) - s^2M^2}{(sL_1 + R_1)(sL_2 + R_2) - s^2M^2} \tilde{I}_0 \quad (30)$$

$$\tilde{I}_2 = \frac{sMR_1}{(sL_1 + R_1)(sL_2 + R_2) - s^2M^2} \tilde{I}_0 \quad (31)$$

with

$$\tilde{I}_0 = -3\tilde{H}_0 a_1 \quad (32)$$

It can be easily verified that the equivalent circuit shown in Figure 10 leads to Equations 30 and 31.

It remains to show how \tilde{I}_1 and \tilde{I}_2 are related to the penetrant field \tilde{H}_i given by Equation 4, which can be expressed in the generalized form

$$\frac{\tilde{H}_i}{\tilde{H}_0} = \frac{R_1 R_2}{(sL_1 + R_1)(sL_2 + R_2) - s^2M^2} \quad (33)$$

From Equations 30 and 31 one gets

$$1 - \frac{1}{\tilde{I}_0} \left(\tilde{I}_1 + \frac{L_2}{M} \tilde{I}_2 \right) = \frac{R_1 R_2}{(sL_1 + R_1)(sL_2 + R_2) - s^2M^2} \quad (34)$$

The scaling factor L_2/M can be expressed in terms of the geometric parameters of the two shields with Equations 29 and is given by

$$\frac{L_2}{M} = \sqrt{\frac{S_1}{S_2}} \quad (35)$$

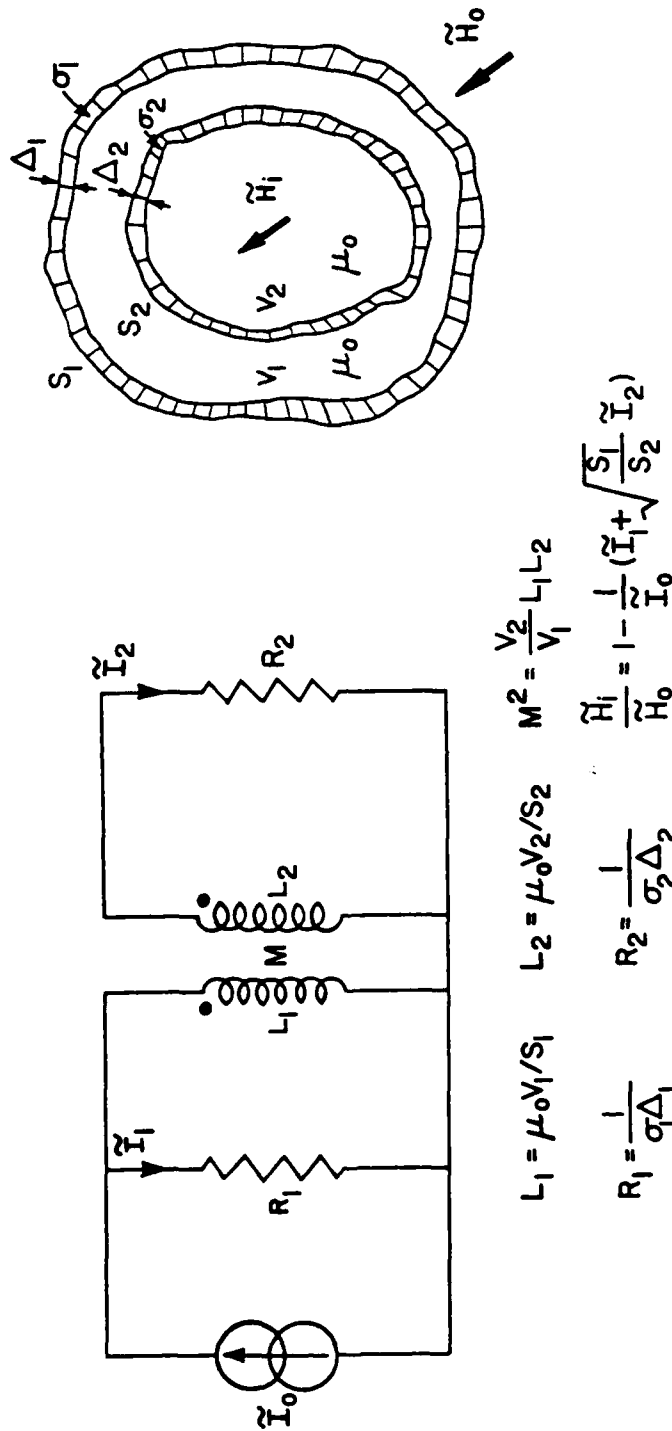


Figure 10. Equivalent circuit of two-surface enclosure.

Hence, one has on comparing Equations 33 and 34

$$\frac{\tilde{H}_1}{\tilde{H}_0} = 1 - \frac{1}{\tilde{I}_0} \left(\tilde{I}_1 + \sqrt{\frac{S_1}{S_2}} \tilde{I}_2 \right) \quad (36)$$

which is to say, one can first calculate \tilde{I}_1 and \tilde{I}_2 from the equivalent circuit of Figure 10 from which the penetrant field \tilde{H}_1 is directly deduced from Equation 36.

A final point should be made about the scaling factor $\sqrt{S_1/S_2}$ in Equation 36. This factor comes about because the magnetic field \tilde{H} is proportional to current density \tilde{K} rather than the total current \tilde{I} .

V. TWO SPHERICAL SHIELDS OF ARBITRARY ELECTRICAL THICKNESS

In the previous sections the thickness of the shield's wall was assumed to be electrically thin. This assumption holds true for low frequencies and/or poorly conducting shields. In this section this assumption will be removed and the shield's wall can be of arbitrary electrical thickness.

As in Equation 1 let the scalar potential ϕ for the three regions shown in Figure 2b take the form

$$\begin{aligned}\phi_1 &= -\tilde{H}_0 r \cos\theta + A' \frac{a_1^3}{r^2} \cos\theta & r \geq a_1 \\ \phi_2 &= B' r \cos\theta + C' \frac{a_1^3}{r^2} \cos\theta & a_1 \geq r \geq a_2 \\ \phi_3 &= D' r \cos\theta & r \leq a_2\end{aligned}\quad (37)$$

Instead of the boundary conditions given by Equations 2 and 3, the boundary conditions are now given by (Ref. 1)

$$\begin{aligned}\frac{\partial}{\partial r} (\phi_2 + \phi_1) &= \alpha_1 \nabla_s^2 (\phi_2 - \phi_1) & \text{at } r = a_1 \\ \frac{\partial}{\partial r} (\phi_2 - \phi_1) &= \beta_1 \nabla_s^2 (\phi_2 + \phi_1) & \text{at } r = a_1\end{aligned}\quad (38)$$

$$\begin{aligned}\frac{\partial}{\partial r} (\phi_3 + \phi_2) &= \alpha_2 \nabla_s^2 (\phi_3 - \phi_2) & \text{at } r = a_2 \\ \frac{\partial}{\partial r} (\phi_3 - \phi_2) &= \beta_2 \nabla_s^2 (\phi_3 + \phi_2) & \text{at } r = a_2\end{aligned}\quad (39)$$

where

$$\begin{aligned}\alpha_i &= \frac{\mu_i \Delta_i}{\mu_0 p_i} \frac{1}{\tanh(p_i/2)} \\ \beta_i &= \frac{\mu_i \Delta_i}{\mu_0 p_i} \tanh(p_i/2) \\ p_i^2 &= s \mu_i \sigma_i \Delta_i^2\end{aligned}\quad (40)$$

and $i=1,2$. The constants A' , B' , C' and D' can be found by substituting Equation 37 into Equations 38, 39 and 40, and are given in Appendix A. The penetrant field \tilde{H}_i is obtained from $-\nabla\phi_3$ and given by

$$\frac{\tilde{H}_i}{\tilde{H}_0} = \frac{1}{(\cosh p_1 + K_1 p_1 \sinh p_1)(\cosh p_2 + K_2 p_2 \sinh p_2) - (a_2/a_1)^3 K_1 p_1 K_2 p_2 \sinh p_1 \sinh p_2} \quad (41)$$

with

$$K_1 = \frac{\mu_0 a_1}{3\mu_1 \Delta_1}, \quad K_2 = \frac{\mu_0 a_2}{3\mu_2 \Delta_2} \quad (42)$$

Just like Equation 4 the combined transfer function of two shields is the reciprocal of the product of the transfer functions of individual shields minus an interaction term.

For electrically thin shield walls (i.e., $p_1, p_2 \ll 1$), Equation 41 reduces to Equation 4, as it should. On the other hand, if the shield's walls are electrically thick (i.e., $p_1, p_2 \gg 1$), then Equation 41 gives

$$\frac{\tilde{H}_i}{\tilde{H}_0} \sim \frac{e^{-(p_1+p_2)}}{(1+K_1 p_1)(1+K_2 p_2) - (a_2/a_1)^3 K_1 p_1 K_2 p_2} \quad (43)$$

in which one may drop the ones in comparison with $K_1 p_1$ and $K_2 p_2$. However, Equation 43 is preferable since it is similar in form to Equation 4 for the case of an electrically thin shield.

Equation 43 is plotted in Figure 11 with and without the interaction term $(a_2/a_1)^3 K_1 p_1 K_2 p_2$. It can be concluded that for $a_2/a_1 = 0.9$ and $\omega\tau_2 > 100$ (which corresponds to $f > 16$ kHz for $\tau_2 \approx 1$ ms), the shield-shield interaction reduces the shielding effectiveness by at least a factor of 3 or 10 dB.

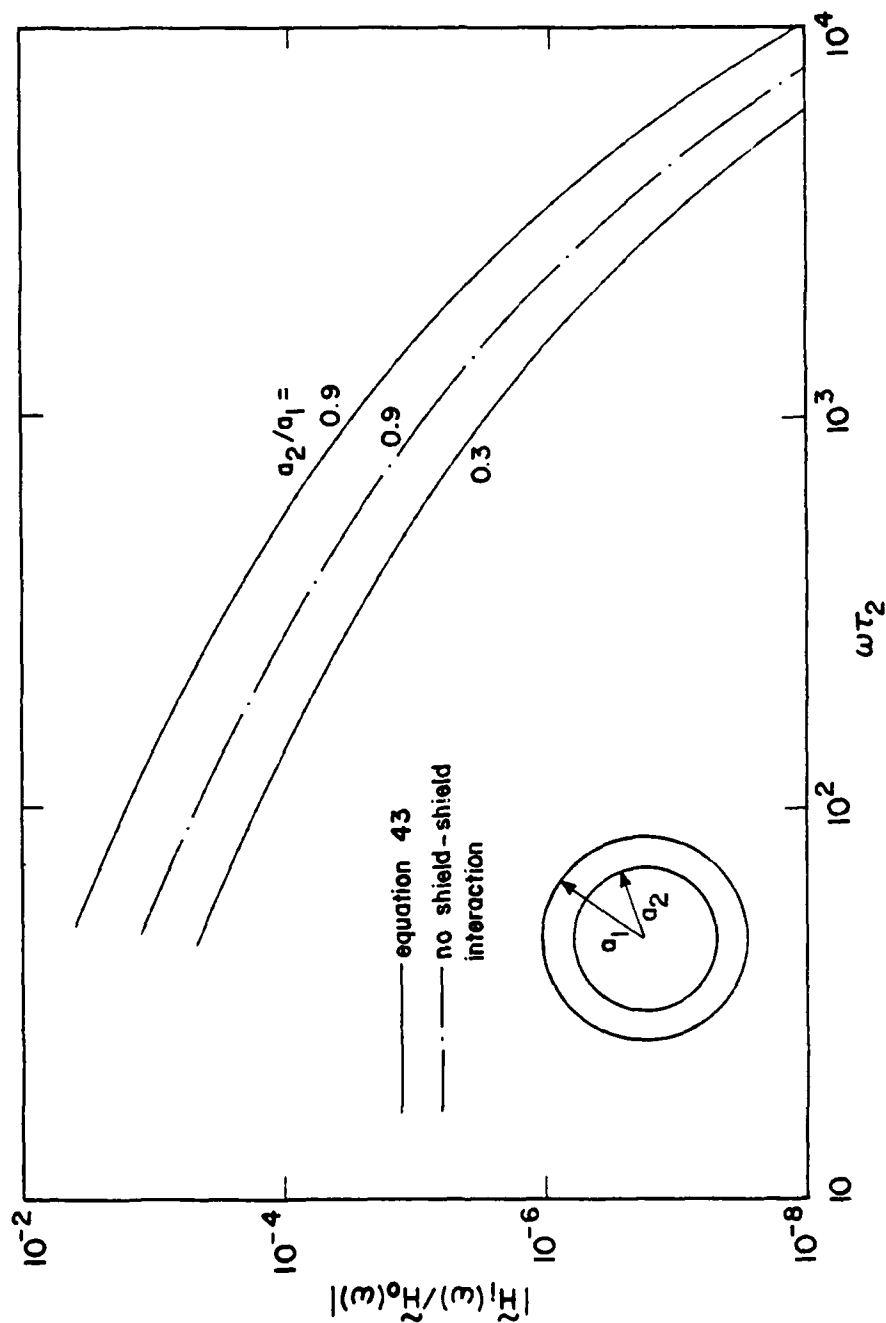


Figure 11. Frequency spectrum of the transfer function $|\tilde{H}_1/\tilde{H}_0|$ for two electrically thick spherical shields ($\Delta_1 = \Delta_2$, $\Delta_2/a_2 = \pi \times 10^{-3}$).

AD-A115 187

MISSION RESEARCH CORP ALBUQUERQUE NM

F/G 20/3

OPTIMAL APPLICATION OF MULTILAYER SHIELDING FOR MAXIMAL EM FIEL--ETC(U)

APR 82 F C YANG, K S LEE

F29601-70-C-0082

NL

UNCLASSIFIED

APML-TR-61-127

2 of 2

2 of 2

2 of 2

2 of 2

2 of 2

2 of 2

2 of 2

2 of 2

2 of 2

2 of 2

2 of 2

2 of 2

2 of 2

2 of 2

2 of 2

2 of 2

2 of 2

2 of 2

2 of 2

2 of 2

2 of 2

2 of 2

2 of 2

2 of 2

2 of 2

2 of 2

2 of 2

2 of 2

2 of 2

2 of 2

2 of 2

2 of 2

2 of 2

2 of 2

2 of 2

2 of 2

2 of 2

2 of 2

2 of 2

2 of 2

2 of 2

2 of 2

2 of 2

2 of 2

2 of 2

2 of 2

2 of 2

2 of 2

2 of 2

2 of 2

2 of 2

2 of 2

2 of 2

2 of 2

2 of 2

2 of 2

2 of 2

2 of 2

2 of 2

2 of 2

2 of 2

2 of 2

2 of 2

2 of 2

2 of 2

2 of 2

2 of 2

2 of 2

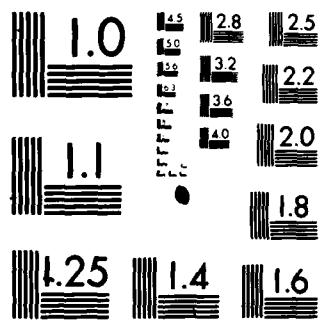
END

DATE

FILED

7-82

DTIC



MICROCOPY RESOLUTION TEST CHART
NATIONAL BUREAU OF STANDARDS 1963-A

VI. EFFECT OF BONDING

Although bonding is often employed between shields in engineering practice to reduce electrostatic hazards, there is no quantitative information on its possible effect on the shielding performance of a shielded enclosure against the low-frequency magnetic-field penetration. This section is devoted to calculating this effect for two electrically-thin spherical shields.

Figure 12 shows various types of connection arrangements of bonding straps between the two surfaces of a spherical enclosure. Later in this section it will become clear that the bonding strap arrangements (a) through (d) have no effect on the magnetic-field shielding performance of the enclosure, while the arrangement (e) has a significant adverse effect. Before proceeding it is appropriate to remark that the low-frequency electric field within a conducting enclosure comes mainly from the eddy currents in the enclosure's wall induced by the time rate of change of the external magnetic field. It is this electric field that is affected by the bonding straps in the inductive shielding approximation.

Return now to Figure 12e (which is redrawn in Figure 13) and calculate the current induced in the bonding straps. Let the unprimed quantities be the quantities in the absence of the bonding straps, and the primed quantities the quantities due to the presence of the bonding straps. Then, integrating the equation

$$\nabla \times \vec{E} = -s\mu_0 \vec{H} \quad (44)$$

over the area enclosed and traced out counter clockwise by the loop BCDAB of Figure 13, one gets

$$V_{BC} + V'_{BC} - V_{AD} - V'_{AD} = s\psi_{ABCD} + s\psi'_{ABCD} \quad (45)$$

where V is the voltage drop and ψ is the magnetic flux. In deriving Equation 45 the bonding straps have been assumed to be good conductors; otherwise, a term for the voltage drop along AB and CD has to be added to the left hand side of the equation.

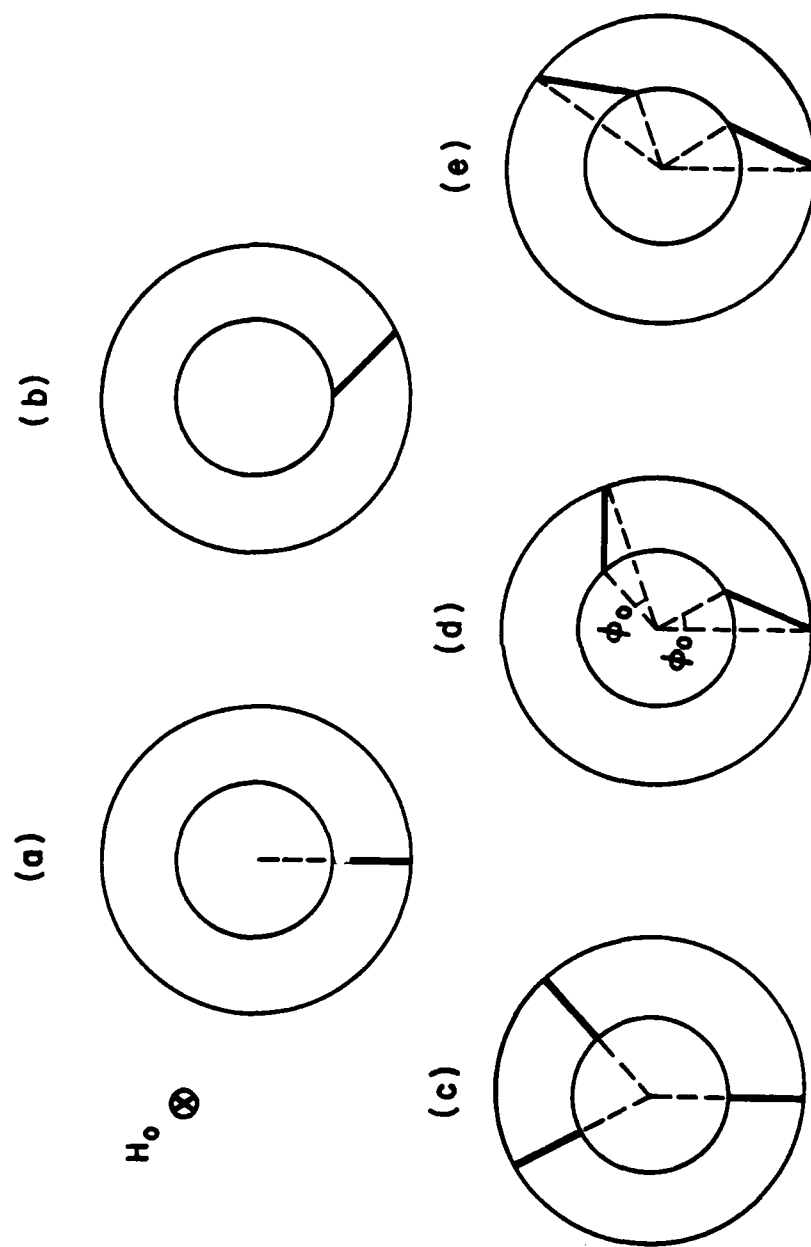


Figure 12. Different arrangements of conducting straps bonding two spherical shields.

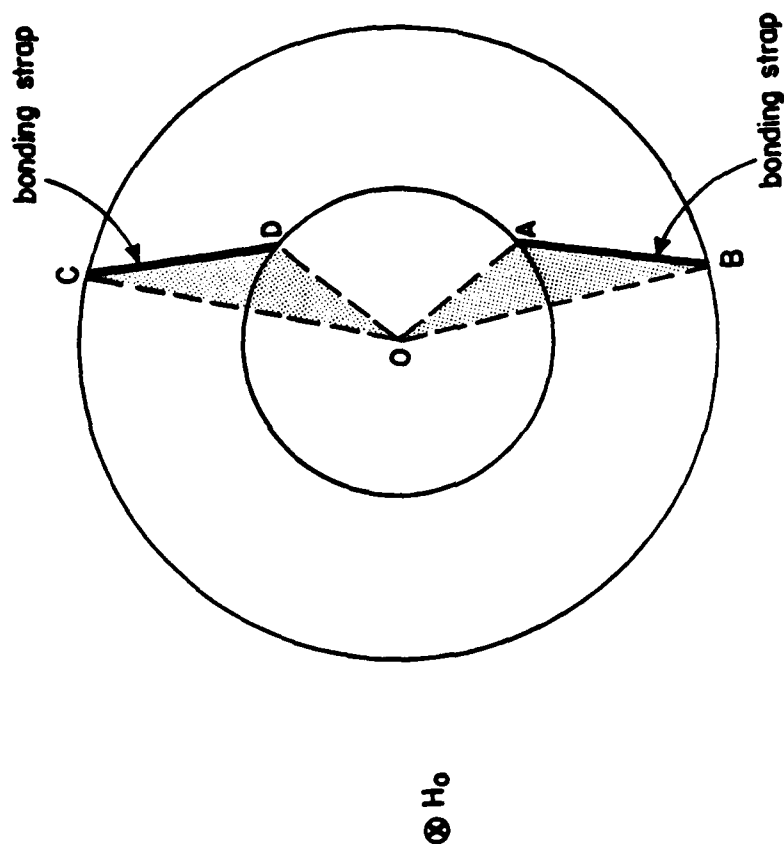


Figure 13. A two-spherical shield enclosure with two bonding straps lying in the equatorial plane perpendicular to the external magnetic field H_0 .

Let \tilde{I}_b = current in bonding strap, L_b = inductance of one bonding strap, R_{BC} or R_{DA} = resistance between B,C of the outer shield, or D,A of the inner shield. It is obvious from Equation 44 that

$$\begin{aligned}
 \tilde{I}_b (R_{BC} + R_{DA} + 2sL_b) &= s\psi_{ABCD} - V_{BC} + V_{AD} \\
 &= s\psi_{ABCD} - s\psi_{OBCO} + s\psi_{OADO} \\
 &= -s(\psi_{OAB} + \psi_{OCD}) \\
 &= -2s\psi_{OAB}
 \end{aligned} \tag{46}$$

The second step of the right hand side follows from repeated applications of Equation 44. It has been assumed for simplicity that the two bonding straps are identical. Hence, the triangle OAB is equivalent to the triangle OCD.

Similarly, an application of Equation 44 to the area enclosed by the loop BADCB going counter clockwise in Figure 13 gives Equation 46, as it should.

Solving Equation 46 for \tilde{I}_b and using the expression in Appendix B for ψ_{OAB} one obtains

$$\begin{aligned}
 \tilde{I}_b &= \frac{-2s\psi_{OAB}}{R_{BC} + R_{DA} + 2sL_b} \\
 &= -\frac{F\tilde{H}_0}{R_s} \frac{s(1+sT_0)}{(1+sT_b)(1+sT_1)(1+sT_2)}
 \end{aligned} \tag{47}$$

where $R_s = R_{BC} + R_{DA}$, $T_b = 2L_b/R_s$, T_1 and T_2 are given in Equation 8, F and T_0 are given in Appendix B. It can be shown that for practical cases T_0 is small compared to the decay time constant τ_2 of the inner shield. Hence for low frequencies one may use the approximation

$$\frac{\tilde{I}_b}{\tilde{V}_0/R_s} = -\frac{s\tau_2}{(1+sT_b)(1+sT_1)(1+sT_2)} \tag{48}$$

with $\tilde{V}_0 = F\tilde{H}_0/\tau_2$, where $F\tilde{H}_0$ is identically equal to the external magnetic flux linking the two triangles shown in Figure 13.

The magnitude of Equation 48 is plotted in Figure 14 against $\omega\tau_2$ with T_b/τ_2 as a parameter. The time histories of I_b and \dot{I}_b are shown in Figures 15 and 16 for an impulsive external magnetic field $H_0\delta(t)$, which is a valid representation of any pulsed external field whose pulse width is less than the diffusion time through the shield's wall. The diffusion time of a typical metallic enclosure is on the order of tens of microseconds. The parameter T_b/τ_2 is roughly equal to the ratio of the inductance of the two bonding straps to the inductance of the inner enclosure, the latter being given by $\mu_0 a_2/3$; that is to say

$$\frac{T_b}{\tau_2} = \frac{2L_b}{L_2} = \frac{6L_b}{\mu_0 a_2} \quad (49)$$

where L_b can be estimated from the approximate formula

$$L_b = \frac{\mu_0 \ell}{2\pi} \ln(\ell/r) \quad (50)$$

with ℓ = length of one bonding strap, r = effective cross-sectional radius of the strap. It can be seen from Equations 49 and 50 that T_b/τ_2 is usually less than unity. The smaller is this parameter the more current will be induced in the bonding straps, as can be observed in Figures 14 through 16. Of course, the more current there is in the bonding straps the more penetration there is into the enclosure. Table 3 summarizes the peak values for $I_b(t)$ and $\dot{I}_b(t)$ for various values of T_b/τ_2 . In the table it is assumed that $a_2/a_1 = 0.9$, $R_s = (\sigma\Delta)^{-1}$, and the two shields have the same thickness, conductivity and permeability.

To get some rough estimate on the field due to the bonding strap current I_b one may divide I_b by $2\pi a_2$. From Table 3 and for the case $T_b/\tau_2 = 0.01$ the peak penetrant fields due to I_b are

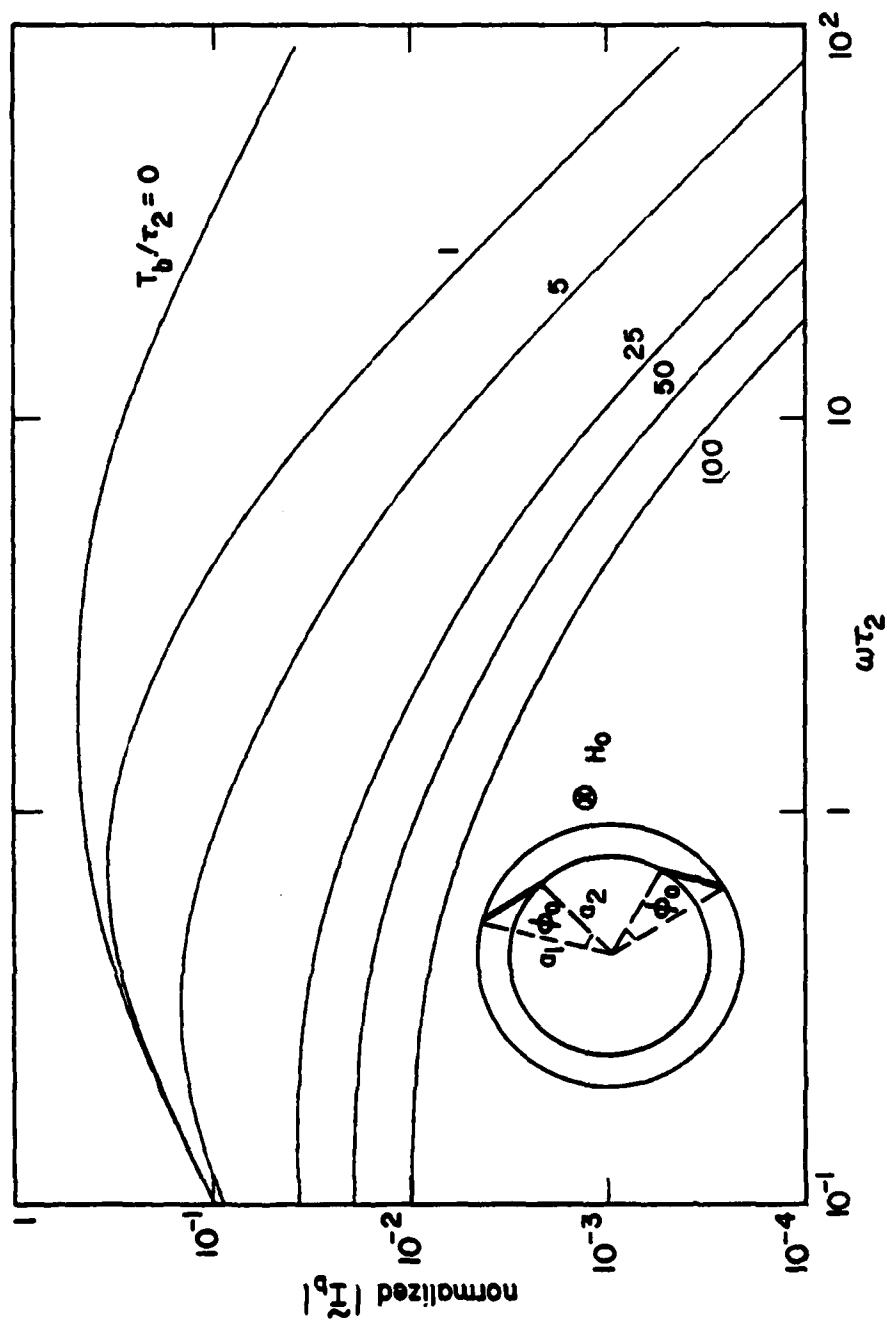


Figure 14. Frequency spectrum of the bonding strap current. The normalizing factor is \tilde{V}_0/R_s , where $\tilde{V}_0 = \tilde{FH}_0/\tau_2$. \tilde{FH}_0 is equal to the flux linking the two triangles by the external field.

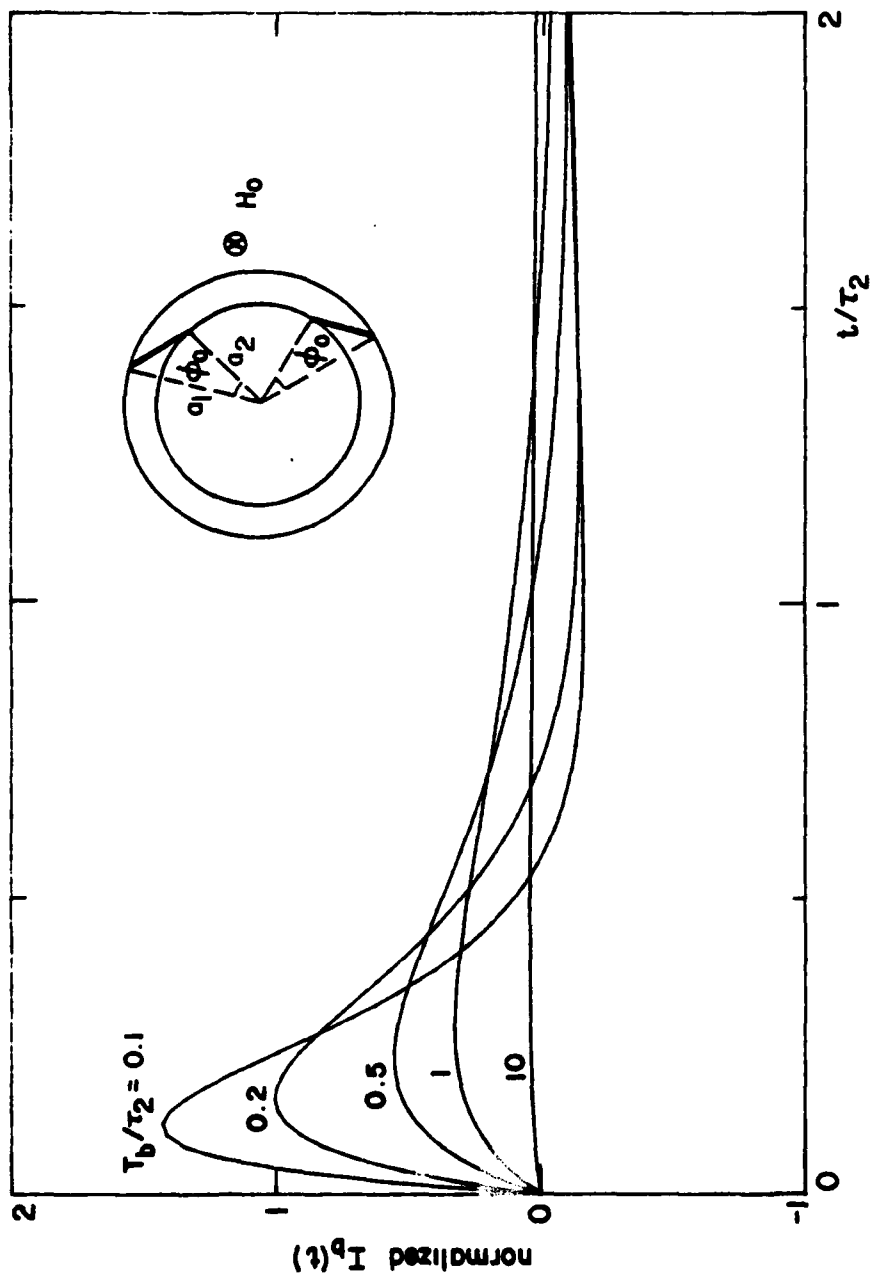


Figure 15. Time behavior of the bonding strap current due to an impulsive external magnetic field $H_0 \delta(t)$. The normalizing factor is V_0/R_s with $V_0 = FH_0^2/\tau_2^2$. Note that H_0 has the dimension of ampere-second.

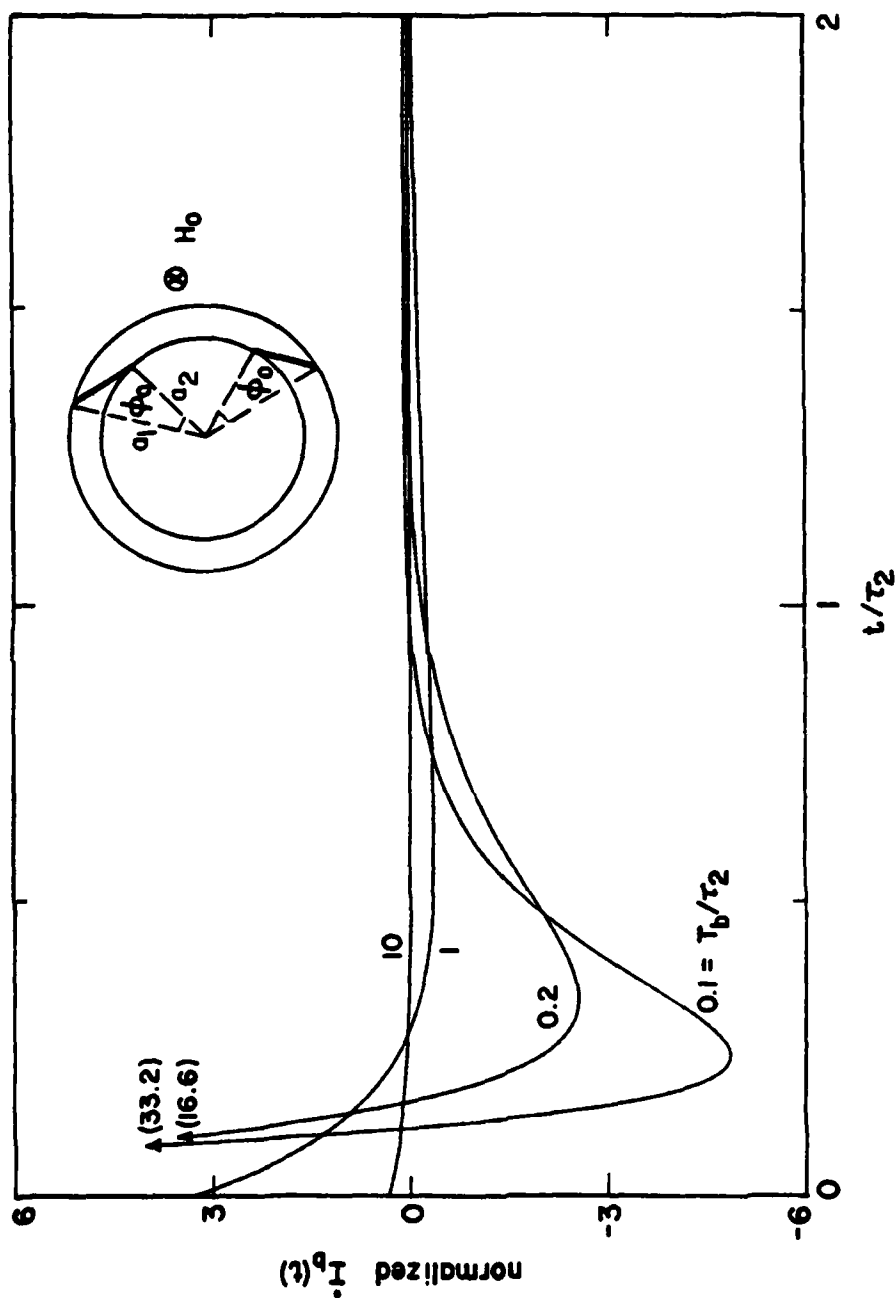


Figure 16. Time behavior of the time rate of change of the bonding strap current due to an impulsive external field $H_0 \delta(t)$. The normalizing factor is $V_0/R_s \tau_2$. The numbers in parenthesis indicate the values the curves intercept the ordinate axis.

TABLE 3. PEAK VALUES FOR I_b AND \dot{I}_b

T_b/τ_2	0.01	0.1	0.2	0.5	1	≥ 5
$\frac{\tau_2 I_b(\text{peak})}{H_o a_2 \sin \phi_o}$	3.1	1.57	1.11	0.61	0.36	$\frac{0.43 \tau_2}{T_b}$
$\frac{\tau_2^2 \dot{I}_b(\text{peak})}{H_o a_2 \sin \phi_o}$	370	37.0	19.0	7.4	3.7	$\frac{3.7 \tau_2}{T_b}$

$$H_i^{(1)}(\text{peak}) \approx \frac{1}{2\tau_2} H_o \sin \phi_o$$

$$\dot{H}_i^{(1)}(\text{peak}) \approx \frac{60}{\tau_2^2} H_o \sin \phi_o \quad (51)$$

That part due to direct field penetration can be read off from Figure 4 for $a_2/a_1 = 0.9$ and is given by

$$H_i^{(0)}(\text{peak}) \approx \frac{0.4}{\tau_2} H_o$$

$$\dot{H}_i^{(0)}(\text{peak}) \approx \frac{3.5}{\tau_2^2} H_o \quad (52)$$

The total peak penetrant fields, $H_i(\text{peak})$ and $\dot{H}_i(\text{peak})$, with bonding straps are the sum of Equations 51 and 52. It can be seen that the bonding straps will increase $H_i(\text{peak})$ by a factor of two and $\dot{H}_i(\text{peak})$ by as much as an order of magnitude.

VII. CONCLUSIONS

It is found that the inductive interactions among the shields and the presence of conducting straps bonding the shields reduce the effectiveness of a multisurface shielded enclosure against the penetration of external magnetic fields.

For a two-surface spherical shielded enclosure the important findings can be summarized as follows. Let

$H_{i,p}$ = peak interior (penetrant) field

$\dot{H}_{i,p}$ = peak time rate of change of $H_i(t)$ = peak electromotance force (emf) density

$|\tilde{H}_i|$ = frequency spectrum of $H_i(t)$

and let the ratio of radii of inner to outer shield = 0.9.

1. Neglect of interaction of electrically thin shields underestimates
 - $H_{i,p}$ by 20%
 - $\dot{H}_{i,p}$ by a factor of 4
 - $|\tilde{H}_i|$ by one order of magnitude for $f > 100$ kHz and enclosures with L/R time constant ≈ 100 μ s.
2. Neglect of interaction of electrically thick shields under-estimates
 - $|\tilde{H}_i|$ by a factor of 3 for $f > 160$ kHz and enclosures with L/R time constant ≈ 100 μ s.
3. Two bonding straps, each subtending a 22.5° angle at the center and with inductance $2L_b = 0.01 L_2$ ($L_2 \approx 0.2$ μ H for an enclosure of one-meter diameter), increase
 - $H_{i,p}$ by a factor of 2
 - $\dot{H}_{i,p}$ by one order of magnitude

REFERENCES

- [1] Lee, K.S.H., ed., EMP Interaction: Principles, Techniques and Reference Data, AFWL TR-79-403, Air Force Weapons Laboratory, Kirtland AFB, NM, 1979.
- [2] Baum, C.E., "Conducting Shields for Electrically Small Cylindrical Loops," Sensor and Simulation Notes, Note 40, Air Force Weapons Laboratory, Kirtland AFB, NM, May 1967.
- [3] Guillemin, E.A., Synthesis of Passive Networks, John Wiley & Sons, Inc., New York, 1957.

APPENDIX A
THE CONSTANTS

The constants A, B, C, and D that appear in Equation 1 are given by

$$A = -\frac{\tilde{H}_0}{2} \frac{s(\tau_1 + \alpha^3 \tau_2) + s^2 \tau_1 \tau_2 (1 - \alpha^3)}{(1 + s\tau_1)(1 + s\tau_2) - s^2 \tau_1 \tau_2 \alpha^3}$$

$$B = -\tilde{H}_0 \frac{1 + s\tau_2}{(1 + s\tau_1)(1 + s\tau_2) - s^2 \tau_1 \tau_2 \alpha^3}$$

$$C = -\frac{\tilde{H}_0}{2} \frac{s\tau_2 \alpha^3}{(1 + s\tau_1)(1 + s\tau_2) - s^2 \tau_1 \tau_2 \alpha^3}$$

$$D = -\tilde{H}_0 \frac{1}{(1 + s\tau_1)(1 + s\tau_2) - s^2 \tau_1 \tau_2 \alpha^3}$$

where $\alpha = a_2/a_1$, $\tau_1 = \mu_0 a_1 \sigma_1 \Delta_1/3$, $\tau_2 = \mu_0 a_2 \sigma_2 \Delta_2/3$.

The constants A', B', C', and D' that appear in Equation 37 are given by

$$A' = -\frac{\tilde{H}_0}{2F} \left\{ \left(K_1 p_1 - \frac{4}{9K_1 p_1} \right) \sinh p_1 \left[\cosh p_2 + \left(K_2 p_2 + \frac{2}{9K_2 p_2} \right) \sinh p_2 \right] + \right. \\ \left. + \left(\frac{a_2}{a_1} \right)^3 \left(K_2 p_2 - \frac{4}{9K_2 p_2} \right) \sinh p_2 \left[\cosh p_1 - \left(K_1 p_1 + \frac{2}{9K_1 p_1} \right) \sinh p_1 \right] \right\}$$

$$B' = -\frac{\tilde{H}_0}{F} \left[\cosh p_2 + \left(K_2 p_2 + \frac{2}{9K_2 p_2} \right) \sinh p_2 \right]$$

$$C' = -\frac{\tilde{H}_0}{2F} \left(\frac{a_2}{a_1} \right)^3 \left(K_2 p_2 - \frac{4}{9K_2 p_2} \right) \sinh p_2$$

$$D' = -\tilde{H}_0/F$$

where

$$p_1 = s\mu_1\sigma_1\Delta_1^2, \quad p_2 = s\mu_2\sigma_2\Delta_2^2$$

$$K_1 = \frac{\mu_o a_1}{3\mu_1\Delta_1}, \quad K_2 = \frac{\mu_o a_2}{3\mu_2\Delta_2}$$

$$F = \left[\cosh p_1 + \left(K_1 p_1 + \frac{2}{9K_1 p_1} \right) \sinh p_1 \right] \left[\cosh p_2 + \left(K_2 p_2 + \frac{2}{9K_2 p_2} \right) \sinh p_2 \right] -$$

$$- \left(\frac{a_2}{a_1} \right)^3 \left(\frac{1}{9K_1 p_1} - K_1 p_1 \right) \left(\frac{4}{9K_2 p_2} - K_2 p_2 \right) \sinh p_1 \sinh p_2$$

Unless K_1 and K_2 are much smaller than unity one may neglect terms involving the reciprocal of $K_1 p_1$ and $K_2 p_2$ and obtains for F the following accurate expression

$$F \approx (\cosh p_1 + K_1 p_1 \sinh p_1)(\cosh p_2 + K_2 p_2 \sinh p_2) -$$

$$- (a_2/a_1)^3 K_1 p_1 K_2 p_2 \sinh p_1 \sinh p_2$$

APPENDIX B
CALCULATION OF ψ_{OAB}

The magnetic field at the equatorial plane ($\theta \approx \pi/2$) can be found from Equation 1, namely,

$$\begin{aligned}\tilde{H}_\theta &= B + C a_1^3/r^3, & a_2 < r < a_1 \\ &= D & a_2 > r\end{aligned}$$

The magnetic flux ψ_{OAB} can then be calculated via (Fig. B1)

$$\begin{aligned}\psi_{OAB} &= -\mu_0 \iint_{OAB} \tilde{H}_\theta dS \\ &= -\mu_0 \left\{ \frac{a_2^2 \phi_0}{2} D + \int_{a_2}^{a_1} \int_0^{\phi'} \left(B + C \frac{a_1^3}{r^3} \right) r d\phi dr \right\} \\ &= -\mu_0 \left\{ \frac{a_2^2 \phi_0}{2} D + \int_{a_2}^{a_1} \left[\sin^{-1} \left(\frac{a_1 \sin \gamma}{r} \right) - \gamma \right] \left(B + C \frac{a_1^3}{r^3} \right) r dr \right\} \\ &= -\mu_0 \left\{ \frac{a_2^2 \phi_0}{2} D + B \left[\frac{a_1 a_2}{2} \sin \phi_0 - \frac{a_2^2}{2} \phi_0 \right] \right. \\ &\quad \left. + C a_1^3 \left[\frac{\phi_0}{a_2} - \frac{\cos \gamma - \cos(\gamma + \phi_0)}{a_1 \sin \gamma} \right] \right\} \\ &= \frac{1 + sT_0}{(1 + s\tau_1)(1 + s\tau_2) - \alpha^3 s^2 \tau_1 \tau_2} \frac{F \tilde{H}_0}{2}\end{aligned}$$

where

$$F = \mu_0 a_1 a_2 \sin \phi_0$$

$$T_0 = \tau_2 \left[(1 - \alpha) + \alpha \tan(\phi_0/2) (\cos \phi_0 - \alpha) / \sin \phi_0 \right]$$

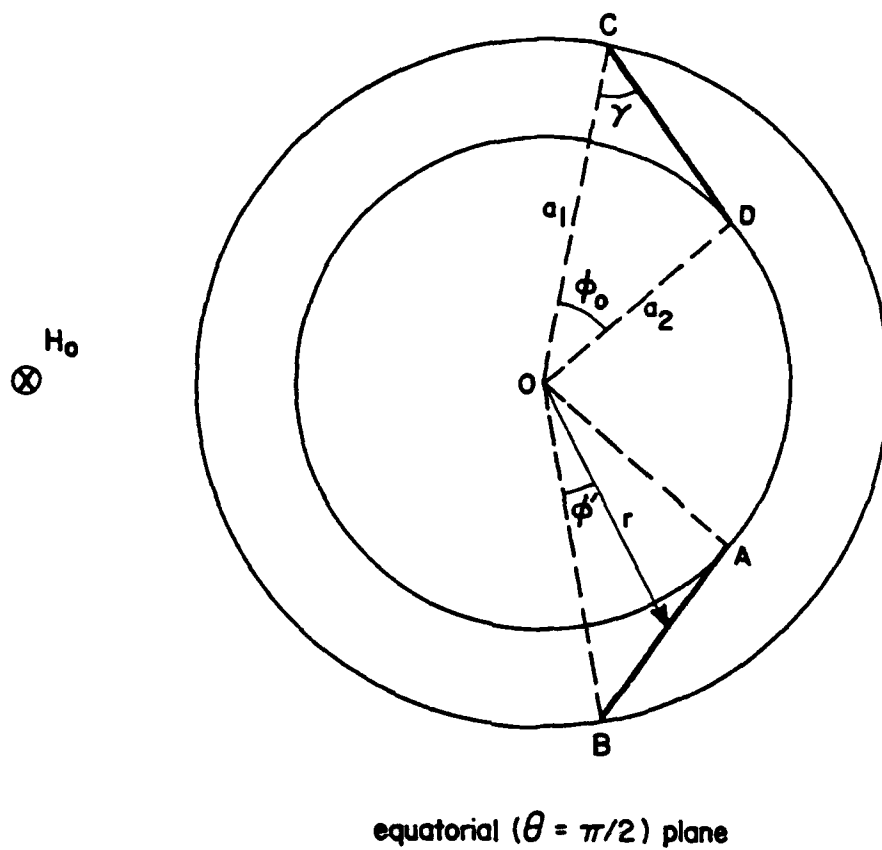


Figure B1. Geometry for calculating the flux ψ_{OAB} .

